IMPACT OF SEISMIC CODE PROVISIONS IN THE CENTRAL U.S.: A PERFORMANCE EVALUATION OF A REINFORCED CONCRETE BUILDING

A Thesis

by

ERIN KUEHT

Submitted to the Office of Graduate Studies of
Texas A&M University
in partial fulfillment of the requirements for the degree of

MASTER OF SCIENCE

August 2007

Major Subject: Civil Engineering

IMPACT OF SEISMIC CODE PROVISIONS IN THE CENTRAL U.S.: A PERFORMANCE EVALUATION OF A REINFORCED CONCRETE BUILDING

A Thesis

by

ERIN KUEHT

Submitted to the Office of Graduate Studies of
Texas A&M University
in partial fulfillment of the requirements for the degree of

MASTER OF SCIENCE

Approved by :

Chair of Committee, Mary Beth D. Hueste
Committee Members, Joseph M. Bracci
Paolo Gardoni
Walter Peacock
Head of Department, David Rosowsky

August 2007

Major Subject: Civil Engineering

ABSTRACT

Impact of Seismic Code Provisions in the Central U.S.:
A Performance Evaluation of a Reinforced Concrete Building.
(August 2007)
Erin Kueht, B.S. Texas A&M University
Chair of Advisory Committee: Dr. Mary Beth D. Hueste

The close proximity to the New Madrid Seismic Zone and the significant population and infrastructure presents a potentially substantial risk for central U.S. cities such as Memphis, Tennessee. However, seismic provisions in currently adopted Memphis building codes for non-essential structures have a lower seismic design intensity level than the 2003 *International Building Code* (IBC) with broader acceptance nationally. As such, it is important to evaluate structures designed with these local seismic provisions to determine whether they will perform adequately during two different design-level earthquakes in this region.

A four-story reinforced concrete (RC) moment frame with wide-module pan joists was designed according to current building codes relevant to the central U.S.: the 2003 IBC, the City of Memphis and Shelby County locally amended version of the 2003 IBC, and the 1999 *Standard Building Code* (SBC). Special moment frames (SMFs) were required for the IBC and SBC designs, but lower design forces in the amended IBC case study permitted an intermediate moment frame (IMF). However, the margin by which a SMF was required was very small for the SBC design. For slightly different conditions IMFs could be used.

Nonlinear push-over and dynamic analyses using synthetic ground motions developed for Memphis for 2% and 10% probabilities of exceedance in 50 years were conducted for each of the three designs. The FEMA 356 recommended Basic Safety Objective (BSO) is to dually achieve Life Safety (LS) for the 10% in 50 years earthquake and Collapse Prevention (CP) for the 2% in 50 years earthquake. For the

member-level evaluation, the SMF designs met the LS performance objective, but none of the designs met the CP performance objective or the BSO. However, the margin by which the SMF buildings exceeded CP performance was relatively small compared to that of the IMF building. Fragility curves were also developed to provide an estimate of the probability of exceeding various performance levels and quantitative performance limits. These relationships further emphasize the benefits of using an SMF as required by the IBC and, in this case, the SBC.

ACKNOWLEDGMENTS

This study was conducted at Texas A&M University and contributes to research conducted by the Mid-America Earthquake (MAE) Center within the consequence-based risk management paradigm. This material is based upon work supported under a National Science Foundation Graduate Research Fellowship. The opinions expressed in this paper are those of the author and do not necessarily reflect the views or policies of the sponsors.

I wish to thank my advisor, Dr. Mary Beth Hueste, for her guidance and encouragement throughout my undergraduate and graduate careers. She has been a first-rate mentor and I thoroughly appreciate the opportunities she has provided for outreach and presenting my research on a broader scope. I would also like to gratefully acknowledge Dr. Joseph Bracci for his help and advice in my research and career goals. I appreciate the support of my other committee members, Dr. Paolo Gardoni and Dr. Walter Peacock.

I would like to thank my fellow graduate student, Jong-Wha Bai, for his immense support in problem solving and gracious answering of my numerous questions, as well as my other civil engineering graduate student colleagues for their friendship and support throughout my graduate degree program. Another special thanks goes to my contacts in the structural engineering consulting industry who answered my technical questions with extreme patience. Lastly, I thoroughly appreciate the support of all my family and friends.

TABLE OF CONTENTS

Page

LIST OF FIGURES

Page

Page

Page

Page

LIST OF TABLES

Page

Page

Page

1 INTRODUCTION

1.1 Background

1.1.1 General

Seismic design has progressed significantly over the years due to contributions of practicing engineers as well as academic and government researchers. Lessons learned from structural failures in past earthquakes, such as the 1989 Loma Prieta earthquake in San Francisco and the 1994 Northridge earthquake in the Los Angeles area, combined with a growing theoretical understanding of earthquakes contributes to the continual progress of seismic design (Hamburger and Kircher 2000). However, this contemporary understanding can only improve structural performance in earthquakes if it is applied.

1.1.2 New Madrid Seismic Zone

The New Madrid Seismic Zone (NMSZ) is an intraplate seismic zone located in the central Mississippi valley extending into four states from northeastern Arkansas to southern Illinois (CUSEC 2007). It is most well known for three of the five largest earthquakes to occur in the continental United States in the winter of 1811-1812. From December 1811 to January 1812, three earthquakes with magnitudes larger than 7.0 on the Richter scale shook the town of New Madrid, Missouri, with such intensity that houses were thrown down, large areas sank into the earth, and lakes were permanently drained. Ground shaking effects were felt over the Eastern U. S., and as far away as Hartford, Connecticut (Street and Nuttli 1990). Despite the severe ground shaking, there was little structural damage due to the sparse population and the limited infrastructure in the region during the early nineteenth century. The population has dramatically increased since then, and the largest close metropolitan city is Memphis, Tennessee, with over 911,000 residents in the city and surrounding Shelby County (Census 2000).

This thesis follows the style and format of the *ASCE Journal of Structural Engineering*.

1.1.3 Seismic Hazards in Memphis, Tennessee

The close proximity to the NMSZ and the relatively large population in this area presents a potentially substantial risk for Central U.S. cities such as Memphis, Tennessee. Memphis has been the focus of several loss estimation studies for these reasons, and it has been shown that another strong New Madrid earthquake would cause substantial casualties and economic loss. A study conducted by FEMA (1985) estimated multi-billion dollar direct economic losses for the city of Memphis for an earthquake of moment magnitude M7.6. In the NCEER Memphis loss assessment report (Abrams and Shinozuka 1997), over $300 million dollars just in structural repair costs were estimated for reinforced concrete (RC) and unreinforced masonry (URM) buildings for a M7.5 event. According to the Shelby County building inventory developed by French and Muthukumar (2004), RC and URM buildings comprise approximately half of the total non single-family housing building inventory.

Regardless of this prospectively high risk, seismic provisions currently adopted in the Memphis building codes have a lower design seismic intensity level and building design category than the 2003 *International Building Code* (IBC) (ICC 2003), which has broader acceptance nationally. As such, it is important to evaluate structures designed according to these local seismic provisions to determine whether they will perform adequately during a major earthquake in this region. Although many studies have been conducted to examine the seismic performance of the existing building stock designed with earlier building codes, there has been little focus on new building construction with the current buildings codes in the Central U.S. for reinforced concrete joist structures.

1.2 Scope and Purpose

The objectives of this study are to compare the structural vulnerability of a typical RC frame structure designed according to the three building codes relevant to new design in the Central U.S.: the 2003 *International Building Code*, a locally amended version of the 2003 IBC (City of Memphis and Shelby County 2005), and the 1999 *Standard Building Code* (SBCCI 1999). Nonlinear push-over and dynamic analyses were conducted for each of the three designs. Synthetic ground motions for 2% and 10%

probabilities of exceedance in 50 years for Memphis, Tennessee, were used in the dynamic analysis. Fragility curves that link measures of earthquake intensity to the probability of exceeding specific performance levels were developed using FEMA 356 performance levels as well as quantitative performance criteria to compare the expected seismic performance of each case study building.

1.3 Methodology

The tasks used to accomplish the objectives are outlined in the following paragraphs.

1.3.1 Identification of Case Study Building

For a better understanding of current structural design in Memphis, phone interviews with structural engineers having substantial Memphis design experience were conducted to determine prevalent structural features and building types. Additionally, French and Muthukumar (2004) in collaboration with the Mid-America Earthquake (MAE) Center developed a database for the current building inventory in Shelby County, Tennessee, with a total of 287,057 building records categorized by building use, square footage, and year built. Using these sources, a four-story RC moment frame office building with wide-module joists was chosen as the case study structure.

1.3.2 Design of Case Study Buildings

Three models of the case study structure were designed according to the separate provisions of the current building codes adopted in Memphis and Shelby County for a site in downtown Memphis. Case Study 1 (CS1) was designed according to the provisions of the 2003 *International Building Code* (IBC), Case Study 2 (CS2) with the 2003 IBC with local amended seismic provisions, and Case Study 3 (CS3) with the design requirements of the 1999 *Standard Building Code* (SBC).

Each case study was economically designed in accordance with the corresponding building code and the American Concrete Institute (ACI) *Building Code Requirements for Reinforced Concrete* (ACI 318 1995; 2002). The commercial computer

software package ETABS (CSI 2002) was used for the analysis of the structures to determine member design forces and story deformations. The range of seismic demands required by each code created variations in structural member layout, member sizes, and reinforcement quantity and detailing.

1.3.3 Analysis of Case Study Buildings

Nonlinear push-over and dynamic response history analyses were performed using two-dimensional planar frame models developed with the nonlinear finite element analysis program, ZEUS-NL (Elnashai 2002). Two types of push-over analyses were conducted for each case study to capture the range of structural capacity: a rectangular push-over analysis with equal horizontal forces and a push-over analysis with a vertical distribution proportional to the fundamental mode shape. The nonlinear dynamic response history analysis was conducted using sets of synthetic ground motion records corresponding to 2% and 10% probabilities of exceedance in 50 years for Memphis, Tennessee. The push-over analysis results were compared to the response history results to evaluate how well the static analysis represented the dynamic response.

1.3.4 Evaluation and Comparison of Case Study Building Performance

The structural performance criteria provided in FEMA 356 were used for both global-level and member-level evaluations of the case study building response computed in the ZEUS-NL analysis. Interstory drifts from the dynamic analysis were compared to the global drift values suggested by FEMA 356, and plastic rotations at the beam-column joints from the median ground motion were checked with plastic rotation limits for the detailed FEMA 356 member-level evaluation. The FEMA 356 Basic Safety Objective was used to assess acceptable seismic performance for the case studies designed with the different code provisions.

1.3.5 Development of Fragility Curves

Fragility curves were developed using the approach outlined by Wen et al. (2004) for the three case studies. The relationship describing demand as a function of seismic

intensity was determined from a power law equation fitted to the interstory drift results of the dynamics analysis versus the corresponding spectral accelerations. To cover a larger range of seismic demands, the dynamic analysis was expanded to include results from twenty additional Memphis ground motion records for 2% and 10% probabilities of exceedance in 50 years, as well as the results from the twenty ground motions used in the FEMA 356 evaluation. Global-level and member-level performance criteria based on the FEMA 356 guidelines, as well as quantitative limit states derived using push-over analyses, were used to define the capacity limits for developing the fragility curves.

1.4 Outline

Section 1 of this thesis includes a brief background, scope, purpose and methodology. Section 2 summarizes the codes, standards and previous research studies that contribute and provide background to this investigation. The case study building description and design parameters are described in Section 3, and the analytical modeling procedure, assumptions and ground motion data are detailed in Section 4. Section 5 contains the results from the nonlinear static and dynamic analyses and FEMA 356 evaluation for the three case study buildings. The fragility analysis is discussed in Section 6. Finally, a summary of results, conclusions and recommendations based on this research are given in Section 7.

2 BACKGROUND

2.1 General

The relevant provisions and background information for the building codes analyzed in this study are presented in this Section. Literature reviews of research studies that contribute and correlate with this study are also included to provide additional background information.

2.2 Building Codes

2.2.1 History

2.2.1.1 General

The first known building code, the Laws of Hammurabi, was written during the reign of the Mesopotamian ruler Hammurabi in 2285-2242 B.C. Law 229: "If a builder has built a house for a man and has not made strong his work, and the house he built has fallen, and he has caused the death of the owner of the house, that builder shall be put to death." This was one of the first conditions of performance-based design. Even centuries later, few changes were made to this building philosophy (Francis and Stone 1998).

During the early twentieth century, the production of explicit model building codes expanded considerably. Three groups were formed to address structural safety concerns: the Building Officials and Code Administration (BOCA) in 1915, the International Conference of Building Officials (ICBO) in 1922, and the Southern Building Code Congress, International (SBCCI) in 1940. Each of these organizations established building codes in their particular geographic region. The *Uniform Building Code* (UBC) was used west of the Mississippi River, while the *National Building Code* (known as BOCA) was utilized in the upper Midwest and northeast. The *Standard Building Code* (SBC) was the building code of the South.

Each of these building codes reflected the philosophy and character of its geographic region. Differences in format, content, and appearance created difficulties for contractors and engineers who worked in more than one region. A call for a single set of national model codes was initiated by the American Architect's Association in the 1970s. The International Code Council (ICC) was formed in 1994 to accomplish this objective. After much collaboration and deliberation with representatives of the three building councils, the first *International Building Code* (IBC) was published in April 2000. With the development and publication of the IBC, the maintenance and updating of the three regional building codes was discontinued (Francis and Stone 1998).

2.2.1.2 Seismic Provisions

Due to the frequent number of damaging earthquakes in the Western region, the UBC was the first model building code to include written seismic regulations in 1927, although the regulations did not become mandatory until 1961. Elective seismic provisions did not appear in the SBC until 1976, and mandatory provisions were not adopted into the main body of the code until 1988 (Beavers 2002).

Natural hazard maps developed by the United States Geological Survey (USGS) and seismological investigations conducted on behalf of the nuclear power industry provided clear evidence that earthquakes were not just a problem in California. Following the 1971 San Fernando earthquake, a national policy for earthquake risk reduction was created: the National Earthquake Hazard Reduction Program (NEHRP) (Beavers 2002). In 1994, the SBC and BOCA codes adopted the 1991 NEHRP Provisions (see Fig. 2.1), in part to a federal executive order preventing federal agencies from taking space in new buildings that did not conform to the NEHRP Provisions (Hamburger and Kircher 2000).

In the development process of the IBC from the three regional building codes, it was decided to use the NEHRP Provisions utilized by BOCA and the SBC as the seismic provisions. However, the 1991 NEHRP Provisions adopted by the two codes would be out-of-date by the publication date. In collaboration with the ICC, Building Structural Safety Council, Structural Engineers Association of California, and American Society of

Civil Engineers, the 1997 NEHRP Provisions were developed for adoption into the 2000 IBC. The 2003 IBC seismic provisions were based on the 2000 NEHRP Provisions.

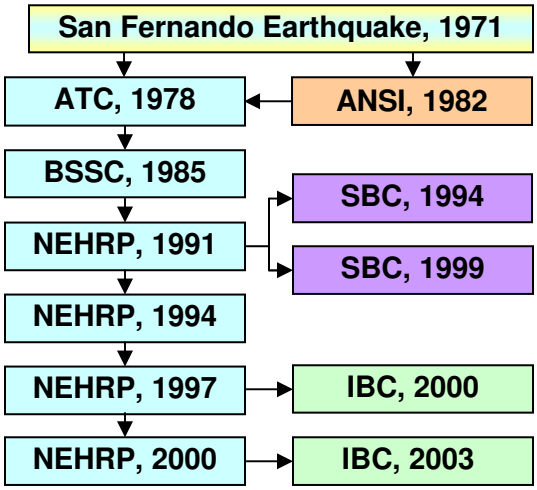

Fig. 2.1. Evolution of seismic design in building codes (adapted from Pezeshk 2004)

2.2.2 1999 SBC Seismic Provisions

2.2.2.1 Design Ground Motions

The seismic provisions in the 1999 *Standard Building Code* are based on the 1991 NEHRP Provisions (BSSC 1992). Two parameters, the Effective Peak Acceleration (EPV) and the Effective Peak Velocity (EPV), characterize the intensity of design ground-shaking, which are related to but not precisely equivalent to peak ground acceleration and peak ground velocity. The EPA and EPV are proportional to spectral ordinates for periods in the ranges of 0.1 - 0.5 s and 1 s, respectively.

In the SBC design procedure, the coefficients A_a and A_v replace the EPA and EPV parameters. The value of A_a is determined by dividing the EPA by the gravitational constant to give a dimensionless coefficient for computing lateral forces. Since EPV is a velocity with units of in/s the dimensionless coefficient A_v is obtained by dividing the EPV by a velocity-related acceleration coefficient of 0.4/12 in/s. Both quantities corresponded to a 475-year return period (10% probability of exceedance in 50 years)

earthquake with 5% damping. It has always been recognized by the BSSC that the maps and coefficients would be updated with time as design professionals reached a better understanding about structural performance, risk determination, and seismic hazards around the country (BSSC 1992).

2.2.2.2 Design Procedure

The Seismic Performance Category (SPC) is based on the building function (Seismic Hazard Exposure Group) and the peak velocity related acceleration, A_v. The SPC definitions are given in Table 2.1. Soil amplification for the site of a building is not included in the SPC determination. The SPC dictates seismic detailing requirements, as well as building height and lateral system limitations.

Table 2.1. SBC Seismic Performance Categories (adapted from SBCCI 1999)

Effective Peak Velocity-related Acceleration, A_v	Seismic Hazard Exposure Group		
	I	II	III
$A_v < 0.05$	A	A	A
$0.05 \leq A_v < 0.10$	B	B	C
$0.10 \leq A_v < 0.15$	C	C	C
$0.15 \leq A_v < 0.20$	C	D	D
$0.20 \leq A_v$	D	D	E

The most common analysis procedure to calculate seismic design forces in the SBC is the equivalent lateral force procedure. According to SBC Section 1607.4, the seismic base shear, *V*, is calculated using Eq. (2.1) with an upper limit of Eq. (2.2). Soil effects are not included in the upper limit base shear equation, which controls for buildings with very short periods. The SBC does not magnify the base shear for essential or hazardous buildings with an importance factor as in the IBC. A percentage of the base shear is distributed to each story based on the story mass and height.

$$V = \frac{1.2A_v S}{RT^{2/3}} W \quad (2.1)$$

$$V \leq \frac{0.5A_a}{R} W \quad (2.2)$$

where:

A_v = Coefficient representing effective peak velocity-related acceleration
A_a = Coefficient representing effective peak acceleration
S = Coefficient for the soil profile characteristics of the site
R = Response modification factor
T = Fundamental period of vibration of the structure in seconds in the direction under consideration
W = Seismic weight of the structure

There are four classifications of soil types in the SBC: rock, intermediate soil, soft soil, and very soft soil. These soil profile types correspond to site coefficients ranging from 1.0 to 2.0 (see Table 2.2) to amplify the base shear based on soil effects at the site. According to Dr. Glenn Rix of the Georgia Institute of Technology, a researcher for the Mid-America Earthquake Center, the soil deposits in Memphis are about 3,000 ft. deep and are generally stable deposits of sands, gravels, or stiff clays (personal communication, Feb. 24, 2006).

Table 2.2. SBC soil profiles (adapted from SBCCI 1999)

Soil type	Description	*S*
S_1	Rock of any characteristic, either shale-like or crystalline in nature, which has a shear wave velocity greater than 2,500 ft/s or stiff soil conditions where the soil depth is less than 200 ft. and the soil types overlaying rock are stable deposits of sands, gravel or stiff clays	1.0
S_2	Deep cohesionlesss or stiff clay conditions, where the soil depth exceeds 200 ft. and soil types overlaying rock are stable deposits of sands, gravels, or stiff clays.	1.2
S_3	20 to 40 ft. in thickness of soft to medium-stiff clays with or without intervening layers of cohesionless soils	1.5
S_4	Shear wave velocity of less than 500 ft/s containing more than 40 ft. of soft clay.	2.0

2.2.2.3 Fundamental Period

The upper limit for the period calculated using SBC Section 1607.4.1.2.1 is shown in Eq. (2.3) for a concrete moment-resisting frame. The code specifies an upper limit for the structural period (see Table 2.3) used in calculating the base shear to ensure a conservative design. The upper limit coefficient is based on the mapped effective peak velocity related coefficient, A_v.

$$T_{max} = C_a 0.03(h_n)^{3/4} \tag{2.3}$$

where:

C_a = Upper limit coefficient
h_n = Height from the base (ft.)

Table 2.3. Coefficient for upper limit on calculated period (adapted from SBCCI 1999)

A_v	Upper limit coefficient, C_a
0.4	1.2
0.3	1.3
0.2	1.4
0.15	1.5
0.1	1.7
0.05	1.7

2.2.3 2003 IBC Seismic Provisions

2.2.3.1 Design Ground Motion

In coordination with the development of the 2000 IBC, the 1997 NEHRP Provisions underwent significant changes including the development of new site factors, new USGS hazard mapping, and individual advances in design provisions for the major structural systems and materials (Holmes 2000). One of the most significant changes to the 1997 provisions is the updated seismic maps (BSSC 1998). Significant earthquake

data was discovered in the 20 or more years since the coefficient design maps in the earlier editions of the NEHRP Provisions were developed. These advances were incorporated into the new design procedure involving maps based on short-period and long-period response spectral accelerations.

The 1997 maps define the maximum considered earthquake (MCE) ground motion for use in design procedures to provide an approximate uniform margin against collapse (BSSC 1998). The MCE ground motions are based on a set of rules that depend on the seismicity of an individual region with a focus on ground motions rather than earthquake magnitude. The MCE ground motions are uniformly defined as the maximum level of earthquake ground shaking that is considered reasonable to design structures to resist. For most of the country, the MCE is based on a 2% probability of exceedance in 50 years ground motion. This design approach provides an approximate uniform margin against collapse throughout the U.S. (Leyendecker et al. 2000).

The goal of the new seismic maps was to provide for life safety during the design earthquake and collapse prevention for the MCE ground motion. To determine the difference between these two performance levels, an intensive study of actual building performance in earthquakes was conducted. A “seismic margin” was determined by the Seismic Design Provisions Group based on past structural performance in California earthquakes, which were designed for the 10% in 50 years earthquake. Structures were determined to have a low likelihood of collapse for a ground motion 1.5 times the design earthquake. Therefore, a factor of 2/3 (1/1.5) was multiplied by the MCE to design for life safety, but ensure collapse prevention at the MCE (Leyendecker et al. 2000).

2.2.3.2 Design Procedure

The 2003 IBC includes effects from local soil conditions using site classes categorized based on the average soil shear wave velocity, V_s, for the upper 100 ft. of the site profile. Table 2.4 lists the definition of each site class and the ranges of V_s in ft/s. Based on site specific and regional analyses conducted, Romero and Rix (2001) classified the soils around the Memphis area as Site Class D.

Table 2.4. Site class definitions (adapted from ICC 2003)

Site Class	Description	V_s (ft/s)
A	Hard rock	$V_s > 5{,}000$
B	Rock	$2{,}500 < V_s \leq 5{,}000$
C	Very dense soil and soft rock	$1{,}200 < V_s \leq 760$
D	Stiff soil profile	$600 \leq V_s \leq 760$
E	Soft soil profile	$V_s < 600$

The MCE response accelerations, S_s and S_1, are multiplied by site coefficients, F_a and F_v, to adjust for the soil amplification of seismic waves according to Eqs. (2.4) and (2.5). Values for F_a (for short period accelerations) in Table 2.5 range from 0.8 for hard rock to 2.5 for soft soil in low seismic areas, and values for F_v (for 1-sec. period accelerations) in Table 2.6 range from 0.8 to 3.5.

$$S_{MS} = F_a S_S \tag{2.4}$$

$$S_{M1} = F_v S_1 \tag{2.5}$$

where:

F_a = Site coefficient based on short period spectral acceleration
F_v = Site coefficient based on 1-sec. period spectral acceleration
S_S = Mapped short period spectral response acceleration
S_1 = Mapped 1-sec. period spectral response acceleration

Table 2.5. Values of Site Coefficient F_a (adapted from ICC 2003)

Site Class	Mapped spectral accelerations at short periods				
	$S_S \leq 0.25$	$S_S = 0.5$	$S_S = 0.75$	$S_S = 1.00$	$S_S \geq 1.25$
A	0.8	0.8	0.8	0.8	0.8
B	1.0	1.0	1.0	1.0	1.0
C	1.2	1.2	1.1	1.0	1.0
D	1.6	1.4	1.2	1.1	1.0
E	2.5	1.7	1.2	0.9	0.9
F	Site specific analysis needed				

Note: Use straight-line interpolation for intermediate values.

Table 2.6. Values of Site Coefficient F_v (adapted from ICC 2003)

Site Class	Mapped spectral accelerations at 1-sec. periods				
	$S_1 \leq 0.1$	$S_1 = 0.2$	$S_1 = 0.3$	$S_1 = 0.4$	$S_1 \geq 0.5$
A	0.8	0.8	0.8	0.8	0.8
B	1.0	1.0	1.0	1.0	1.0
C	1.7	1.6	1.5	1.4	1.3
D	2.4	2.0	1.8	1.6	1.5
E	3.5	3.2	2.8	2.4	2.4
F	Site specific analysis needed				

Note: Use straight-line interpolation for intermediate values.

The adjusted spectral accelerations are multiplied by the reciprocal of the seismic margin in Eqs. (2.6) and (2.7) to obtain the design spectral response accelerations, which are used to calculate V and the Seismic Design Category (SDC).

$$S_{DS} = \tfrac{2}{3} S_{MS} \tag{2.6}$$

$$S_{D1} = \tfrac{2}{3} S_{M1} \tag{2.7}$$

where:

S_{MS} = Adjusted MCE short period spectral response accelerations
S_{M1} = Adjusted MCE 1-sec. period spectral response accelerations

Seismic Design Categories determine detailing requirements, structural system restrictions, height limitations, and analysis procedures for irregular structures. The SDC is assigned based on the Seismic Use Group, which depends on the function of the building and how much damage is acceptable after an earthquake, as well as the amount of ground shaking expected at the site. Unlike the Seismic Performance Category in the SBC, the SDC includes the effect of soil amplification on the building performance during a seismic event. The maximum SDC value from Table 2.7 and Table 2.8 controls.

Table 2.7. Seismic Design Categories based on S_{DS} (adapted from ICC 2003)

Value of S_{DS}	Seismic Use Group		
	I	II	III
$S_{DS} < 0.167g$	A	A	A
$0.167g \le S_{DS} < 0.33g$	B	B	C
$0.33g \le S_{DS} < 0.50g$	C	C	D
$0.50g \le S_{DS}$	D	D	D

Table 2.8. Seismic Design Categories based on S_{D1} (adapted from ICC 2003)

Value of S_{D1}	Seismic Use Group		
	I	II	III
$S_{D1} < 0.067g$	A	A	A
$0.067g \le S_{D1} < 0.133g$	B	B	C
$0.133g \le S_{D1} < 0.20g$	C	C	D
$0.20g \le S_{D1}$	D	D	D

The equivalent lateral force procedure can be used for analysis of all structures except irregular structures in SDC D or higher. The 2003 IBC references *ASCE Minimum Design Loads for Buildings and Other Structures* (ASCE 7-02) (ASCE 2002) for seismic load analysis procedures. The seismic base shear, V, is determined using Eqs. (2.8) and (2.9) with the limitation of Eq. (2.10). A lower limit of $0.44S_{DS}IW$ is also imposed on V. The response modification factor, R, depends on the building type and is

intended to reduce the base shear for buildings with greater seismic detailing and ductility. An occupancy importance factor, I_E, is included in the base shear equations to provide for higher seismic performance for critical facilities.

$$V = C_s W \tag{2.8}$$

$$C_s = \frac{S_{DS}}{\left(R / I_E \right)} \tag{2.9}$$

$$C_s \leq \frac{S_{D1}}{T\left(R / I_E \right)} \tag{2.10}$$

where:

W = Effective seismic weight of the structure
C_s = Seismic response coefficient
S_{DS} = Design short period spectral response acceleration
I_E = Occupancy importance factor
R = Response modification factor
S_{D1} = Design 1-sec. period spectral response acceleration
T = Fundamental period of vibration of the building in the direction under consideration (s)

The combined effect of horizontal and vertical earthquake-induced forces, E, in the load combinations represents the ground acceleration in both directions shown in Eq. (2.11). The effect of horizontal seismic forces, Q_E, are the forces applied to each story as a percentage of the total base shear. In high seismic areas, these lateral loads are further amplified for structures without multiple lateral elements or without an equitable distribution of lateral elements throughout the structure by the redundancy coefficient, ρ.

$$E = \rho Q_E \pm 0.2 S_{DS} D \tag{2.11}$$

where:

D = Dead load
ρ = Redundancy coefficient
Q_E = Effect of horizontal seismic forces
S_{DS} = Design short period spectral response acceleration

The redundancy coefficient is determined by the ratio of the design shear resisted by the most heavily loaded single element to the total shear for a story and the tributary area of that element. For moment frames, this ratio is represented by the maximum of the sum of the shears in any two adjacent columns in the plane of a moment frame for a given direction of loading. The value of ρ is 1.0 for SDC A to C. For SDC D and higher, ρ is calculated using Eq. (2.12). The redundancy coefficient also affects the number of lateral resisting members in a particular direction. For concrete moment frame structures, if ρ is calculated to be greater than 1.25, additional moment frames are needed to distribute the lateral forces more evenly to reduce ρ to below 1.25.

$$\rho_x = 2 - \frac{20}{r_{\max_x}\sqrt{A_x}} \tag{2.12}$$

where:

$r_{\max_x}$ = Maximum sum of the shears in any two adjacent columns in the plane of a moment frame divided by the total story shear
A_x = Floor area of the diaphragm level immediately above the story

2.2.3.3 Fundamental Period

The upper limit for the fundamental period for an RC moment frames is calculated using Eq. (2.13) where the upper limit coefficient, C_u, depends on the 1-sec. spectral design acceleration (see Table 2.9), which is different for the 2003 IBC with and without the local amendments.

$$T_{max} = C_u(0.016)(h_n)^{0.9} \tag{2.13}$$

where:

C_u = Upper limit coefficient
h_n = Height from the base (ft.)

Table 2.9. Coefficient for upper limit on calculated period (adapted from ICC 2003)

S_{D1}	Upper limit coefficient, C_u
≥ 0.3	1.4
0.2	1.5
0.15	1.6
0.1	1.7
≤ 0.05	1.7

2.2.4 Amended 2003 IBC Seismic Provisions

For California and the rest of the west coast, the 2% in 50 years ground motion (the MCE used in the 2003 IBC) is approximately 1.5 times the 10% in 50 years ground motion. When the MCE is multiplied by seismic margin of 2/3 (1/1.5), the design earthquake becomes approximately a 10% in 50 years hazard for the western U.S. In the Central U.S., however, the 2% in 50 years earthquake is approximately 4 to 5 times larger than the 10% in 50 years earthquake (Dowty and Ghosh 2002). This comparison is shown in Fig. 2.2 for the short period spectral accelerations for the cities of Los Angeles, San Francisco, and Memphis. Therefore, the use of 2/3 of the MCE design earthquake in the IBC provisions led to a significantly greater demand for Memphis and the Central U.S. relative to the previous code provisions. This subject has been hotly debated in this region, and in the local seismic amendments, Memphis replaced the 2/3 MCE design earthquake with the 10% in 50 years ground motion.

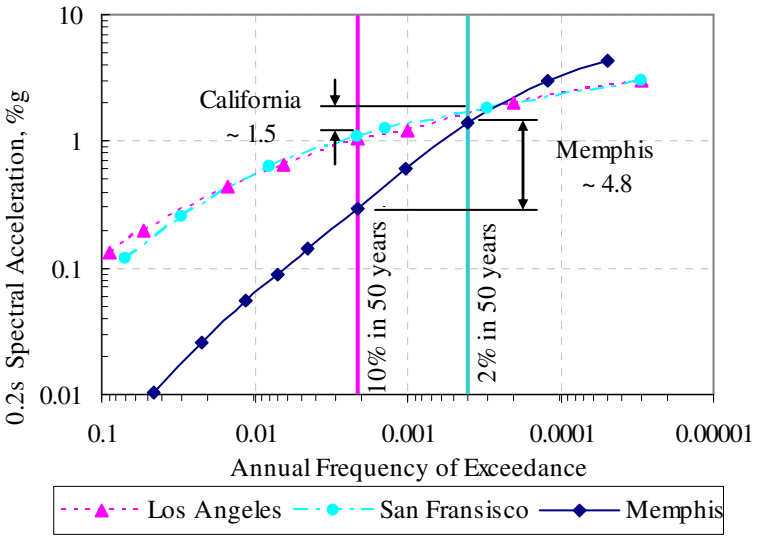

Fig. 2.2. Hazard curves for California and Memphis
(adapted from Leyendecker et al. 2000)

Applying the Memphis amended seismic provisions, Eqs. (2.4) and (2.5) become Eqs. (2.14) and (2.15). The prime symbol (′) denotes parameters that changed for the amended IBC. The spectral accelerations for Memphis are reduced by almost 75 percent from 0.28g to 0.07g for 1-sec. period accelerations and 0.93g to 0.29g for short period accelerations under the amendments.

$$S_{DS}' = S_{MS}' \tag{2.14}$$

$$S_{D1}' = S_{M1}' \tag{2.15}$$

where:

S_{MS}' = Maximum considered earthquake short period spectral response accelerations

S_{M1}' = Maximum considered earthquake 1-sec. period spectral response accelerations

The change in the mapped spectral accelerations for the local amendments also impacts the Seismic Design Category and has a major influence on the structural members and performance of a structure.

2.2.5 Summary of Seismic Provisions

The seismic design procedures outlined in each code are listed in Table 2.10. The seismic design coefficient, C_s, calculations for the 2003 IBC and 1999 SBC are shown in Table 2.11. The SBC calculations do not include the Importance Factor, I_E, which increases design forces for essential facilities such as hospitals and hazardous buildings to provide for better performance. There are no lower limits on the base shear for the SBC design. Amplification for soil conditions is also more detailed for the IBC design procedure.

Table 2.10. Summarized design procedure

Parameter	2003 IBC	Amended 2003 IBC	1999 SBC
Design map values	S_1, S_S	S_1', S_S'	A_a, A_v
Design hazard level	⅔ [2% in 50 years]	10% in 50 years	10% in 50 years
Adjusted for soils	F_a, F_v	F_a', F_v'	S
Base shear	$V = C_S W$		

Table 2.11. Seismic design coefficient, C_s, calculations

Parameter	Building Code	
	2003 IBC	1999 SBC
C_s	$\frac{S_{DS}}{R/I_E}$	$\frac{1.2A_v S}{RT^{2/3}}$
Upper limit C_s	$\frac{S_{D1}}{T\left(R/I_E\right)}$	$\frac{2.5A_a}{R}$
Lower limit C_s	$0.044 S_{DS} I_E$	None
Lower limit, High seismic	$\frac{0.5S_1}{R/I_E}$	None

Once the total base shear is determined for each code, it is distributed to each level through the lateral force, F_x, calculated as a percentage of the base shear using Eqs. (2.16) and (2.17).

$$F_X = C_{VX} V \tag{2.16}$$

$$C_{VX} = \frac{w_x h_x^{\,k}}{\sum_{i=1}^{n} w_i h_i^{\,k}} \tag{2.17}$$

where:

C_{VX} = Vertical distribution factor
V = Design seismic base shear
w_x, w_i = Portion of the total gravity load of the building, W, located or assigned to level i or x
h_x,h_i = Height from the base to level i or x (ft.)
k = Exponent related to the period of the building

The seismic lateral forces are applied both directly at the center of mass on the building and at a 5 percent eccentricity of the building length, L, or width, W, from the center of mass to account for accidental torsion. This results in the total of six seismic load cases shown in Fig. 2.3.

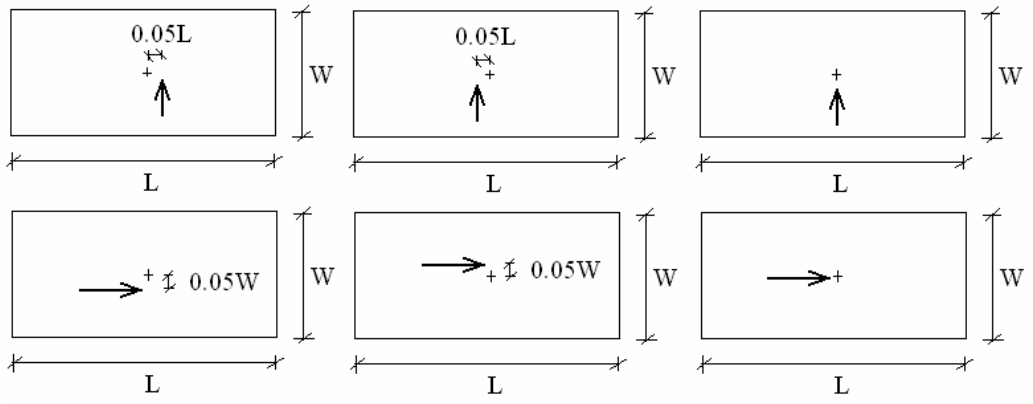

Fig. 2.3. IBC seismic load cases

An allowable drift limit of 2% is imposed in all three seismic code provisions on the design story drift, Δ, which is defined as the difference of the deflections of the center of the mass on the top and bottom of the story under consideration. The drift at level x, δ_x, is determined from Eq. (2.18).

$$\delta_x = \frac{C_d \delta_{xe}}{I_E} \tag{2.18}$$

where:

δ_{xe} = Diaphragm deflection from elastic analysis
I_E = Occupancy importance factor
C_d = Deflection amplification factor in 2003 IBC Table 1617.6

2.2.6 ACI 318 Concrete Provisions

Two different ACI 318 provisions were used in this study; the 2003 IBC references ACI 318-02 (ACI Committee 318 2002) as the concrete standard, while the 1999 SBC references ACI 318-95 (ACI Committee 318 1995). Most of the applicable design procedures are the same, except for load factors and moment redistribution procedures.

ACI 318 Chapter 21 specifies the special seismic detailing provisions for special moment frames (SMFs) and intermediate moment frames (IMFs). Sections 21.2 through 21.10 provide SMF detailing requirements to improve seismic performance and prevent the occurrence of story mechanisms in strong earthquakes. The IMF detailing requirements given in Section 21.12 are less stringent than the SMF requirements, but still provide for some ductility in an earthquake.

2.2.6.1 SMF Detailing Requirements

Special moment frames are required by the IBC and SBC for SDC D concrete frame structures and have the most detailed requirements for seismic performance. According to ACI 318 Section 21.3.2.2, flexural members of a SMF shall have a positive moment strength at the joint face that is not less than one-half the negative moment

strength. The minimum moment strength at any section shall not be less than one-fourth of the maximum moment strength. Two bars must be provided continuously both top and bottom for structural integrity.

Seismic hoops must be provided within twice the member depth from the column face, which is the approximate length of the plastic hinge zone (PHZ), and the first hoop must be placed within 2 in. of the column face. The spacing of the seismic hoops within the PHZ must be less than $d/4$, where d is the distance between the tension reinforcement and the compression face of the concrete. In this region, every other longitudinal bar must be supported by a cross-tie with a maximum spacing of 6 in. between transverse reinforcement. Outside the PHZ, the spacing of the seismic stirrups is determined by the shear demand with a maximum spacing of $d/2$. Two-legged stirrups are allowed in this region.

The SMF joint requirements are provided in ACI 318 Section 21.5. The column width must be greater than 20 times the diameter of the largest longitudinal bar. The shear demand of the joint is calculated based on the assumption that the stress in the flexural tensile reinforcement is $1.25f_y$. The shear strength depends only on the effective joint area, concrete compressive strength, and amount of joint confinement per ACI 318 Section 21.5.3. A joint is considered confined if the beam widths framing into it are at least three-fourths of the column width.

ACI stipulates a strong-column weak-beam design strategy to prevent story mechanisms from forming. In the vertical plane of the frame considered, the sum of the nominal flexural strength of the columns at the face of the joint is required to be at least 1.2 times the sum of the beam nominal flexural strength described in Eq. (2.19).

$$\sum M_{nc} \geq {}^{6}\!/_{5} \sum M_{nb} \tag{2.19}$$

where:

M_{nb} = Nominal flexural strength of beam including the slab in tension framing into a joint in a plane

M_{nc} = Nominal flexural strength of column framing into the joint for the factored axial load consistent with the lateral force direction

2.2.6.2 IMF Detailing Requirements

The IMF detailing requirements in ACI 318 Section 21.12 are less stringent than those for SMFs. The positive moment strength of beams at the face of the joint must be greater than one-third of the negative moment strength at the joint, and the minimum moment strength at any section shall not be less than one-fifth the maximum moment strength.

Joint confinement requirements do not apply to an IMF, which allows smaller columns and possily a lower concrete strength. The PHZ transverse beam reinforcement requirements are the same as the SMF, except that every other longitudinal bar does not have to be laterally supported. IMF column requirements allow larger transverse reinforcement spacing than SMF columns.

2.3 Structural Analysis

2.3.1 General

Out of the four seismic analysis procedures specified in *NEHRP Recommended Provisions for Seismic Regulations of New Buildings And Other Structures, Part 1: Provisions* (FEMA 450) (BSSC 2004), only the linear response history procedure and the nonlinear response history procedure predict the response of a structure subjected to ground motion records. Linear analysis procedures, however, are not capable of representing the inelastic responses predicted for buildings under large demands from earthquake loading. Therefore, nonlinear analysis procedures are used in this study to more accurately predict the seismic performance of the case study buildings.

2.3.2 Nonlinear Procedures

A nonlinear static procedure, commonly called a push-over analysis, involves monotonically applying lateral load to a structure until a specified displacement is reached or an instability occurs due to large inelastic deformations. The push-over analysis can be used to obtain the overall capacity of the structure including yield

displacement, peak base shear, as well investigating story mechanisms and the location of critical members (Jeong and Elnashai 2005).

In the nonlinear dynamic (response history) analysis, ground accelerations are applied at base of the structure in a finite element analysis to predict the structural response for the earthquake motions. The response history analysis is considered to be more accurate than a static analysis because it accounts for the dynamic response of the structure. However, the response can be highly sensitive to the characteristics of a particular ground motion. For a better estimate of the dynamic response for a particular magnitude event or recurrence interval, the median response of multiple ground motions should be used. FEMA 450 requires at least three ground motions for a response history analysis, and at least seven ground motion records are needed to use the median response instead of the maximum response.

Mwafy and Elnashai (2001) investigated the uniform, modal, and inverted triangular lateral load patterns in a push-over analysis compared with an incremental inelastic dynamic analysis for twelve RC buildings with different configurations. The findings indicated that push-over analyses provide insight on the inelastic response of buildings subjected to ground motions, especially for low rise RC buildings. The benefit of using more than one load pattern to capture a broader range of expected response was emphasized.

The basic concepts of the push-over analysis including lateral load patterns and practical applications were summarized by Krawinkler and Seneviratna (1998). Push-over drifts were compared with results from a response history analysis with nine ground motions for a four story steel moment frame building. It was concluded that push-over analyses can be helpful in exposing design weakness such as story mechanisms, especially in buildings that vibrate primarily in the first mode. However, additional evaluation procedures such as inelastic dynamic analysis should be conducted in conjunction with a push-over analysis for increased accuracy in predicting the dynamic response.

Kalkan and Kunnath (2006) evaluated four types of nonlinear static procedures using existing 6 and 13 story steel moment frames and 7 and 20 story RC moment frame buildings. A response history analysis with thirty ground motions was also used for comparison in the evaluation. The results showed that push-over analyses are more accurate in lower stories of taller buildings, but when higher modes contributions become significant, peak roof displacement and interstory drifts can be misrepresented.

Sadjadi et al. (2007) also used nonlinear response history and push-over analyses to investigate the seismic vulnerability of ductile, nominally-ductile, and gravity load designed RC moment frame buildings designed with Canadian building codes. Many other studies which are too numerous to mention have established the common practice of using both nonlinear static and response history analysis procedures to investigate the seismic vulnerability of buildings.

2.3.3 FEMA 356

2.3.3.1 General

The Prestandard and Commentary for the Seismic Rehabilitation of Buildings – FEMA 356 (ASCE 2000) proposed limits for the seismic evaluation of building structures. FEMA 356 uses target performance levels at certain recurrence intervals to define the Basic Safety Objective (BSO). Typical global interstory drift values are suggested as guidance for various building types and plastic rotation limits are provided for more detailed member-level evaluations.

2.3.3.2 Basic Safety Objective

Three target building performance levels are set based on the amount of damage a structure sustains during an earthquake:

(1) Immediate Occupancy (IO) – Very limited structural damage has occurred and the structure is safe and functional immediately following the earthquake

(2) Life Safety (LS) – Structural damage occurs, but a significant margin of safety against collapse still remains

(3) Collapse Prevention (CP) – Building will continue to support gravity loads, but without a margin against collapse

FEMA 356 defines the BSO as dually meeting the LS performance level under a 10% probability of exceedance in 50 years event and the CP performance level under a 2% probability of exceedance in 50 years event. This objective is intended to allow limited damage for frequent but moderate earthquakes, with significantly more damage for higher intensity, infrequent earthquakes.

2.3.3.3 Global and Member-Level Criteria

Intertory drift values are provided for the three structural performance levels to give an estimation of the global seismic performance for various concrete, steel and masonry building types. The interstory drifts associated with IO, LS and CP performance are 1%, 2% and 4%, respectively, for concrete frames. These drift values are suggested for structures that are designed and detailed for higher seismic demands, such as SMFs. For structures that are not specially detailed for seismic loading, smaller global drift values are more appropriate to meet the respective performance levels. Ramamoorthy et al. (2006) proposed using reduced interstory drift values of 0.5%, 1% and 2% for the IO, LS and CP performance levels, respectively, for gravity designed buildings with insufficient column-to-beam strength ratios and section detailing. These lower values are based on the FEMA 356 member plastic rotation limits, which are smaller for buildings without special detailing.

The primary evaluation measures in FEMA 356 are member-level acceptance criteria for concrete, steel, masonry, and wood and light metal framing construction for various types of elements. These limits are considered more accurate than the global drift values because they are refined to reflect member design details. Chapter 6 specifies plastic rotation limits for beams, columns, and beam-column joints for RC moment frames. Plastic rotation is defined as the inelastic rotation beyond the yield rotation of the member. Tables 2.12 and 2.13 provide the FEMA 356 plastic rotation

acceptance criteria to use with nonlinear procedures when evaluating RC beams and columns controlled by flexure.

Table 2.12. FEMA 356 acceptance criteria for nonlinear procedures – RC beams controlled by flexure (adapted from ASCE 2000)

Conditions			Plastic rotation acceptance criteria (rad.) [2]				
			Performance level				
			IO	Component type			
				Primary		Secondary	
				LS	CP	LS	CP
$\frac{\rho - \rho'}{\rho_{bal}}$	Transverse Reinforce-ment[1]	$\frac{V}{b_w d\sqrt{f'_c}}$					
≤ 0.0	C	≤ 3	0.01	0.02	0.025	0.02	0.05
≤ 0.0	C	≥ 6	0.005	0.01	0.02	0.02	0.04
≥ 0.5	C	≤ 3	0.005	0.01	0.02	0.02	0.03
≥ 0.5	C	≥ 6	0.005	0.005	0.015	0.015	0.02
≤ 0.0	NC	≤ 3	0.005	0.01	0.02	0.02	0.03
≤ 0.0	NC	≥ 6	0.0015	0.005	0.01	0.01	0.015
≥ 0.5	NC	≤ 3	0.005	0.01	0.01	0.01	0.015
≥ 0.5	NC	≥ 6	0.0015	0.005	0.005	0.005	0.01

Notes:

1. "C" and "NC" are abbreviations for conforming and nonconforming transverse reinforcement. A component is conforming if, within the flexural plastic hinge region, hoops are spaced at ≤ d/3, and if, for components of moderate and high ductility demand, the strength provided by the hoops (V_s) is at least three-fourths of the design shear. Otherwise, the component is considered nonconforming.
2. Linear interpolation between values listed in the table shall be permitted.

Table 2.13. FEMA 356 acceptance criteria for nonlinear procedures - RC columns controlled by flexure (adapted from ASCE 2000)

Conditions			Plastic rotation acceptance criteria (rad.) [2]				
			Performance level				
				Component type			
				Primary		Secondary	
			IO	LS	CP	LS	CP
$\frac{P}{A_g f'_c}$	Transverse reinforcement[1]	$\frac{V}{b_w d\sqrt{f'_c}}$					
≤ 0.1	C	≤ 3	0.005	0.015	0.02	0.02	0.03
≤ 0.1	C	≥ 6	0.005	0.012	0.016	0.016	0.024
≥ 0.4	C	≤ 3	0.003	0.012	0.015	0.018	0.025
≥ 0.4	C	≥ 6	0.003	0.01	0.012	0.013	0.02
≤ 0.1	NC	≤ 3	0.005	0.005	0.006	0.01	0.015
≤ 0.1	NC	≥ 6	0.005	0.004	0.005	0.008	0.012
≥ 0.4	NC	≤ 3	0.002	0.002	0.003	0.006	0.01
≥ 0.4	NC	≥ 6	0.002	0.002	0.002	0.005	0.008

Notes:

1. "C" and "NC" are abbreviations for conforming and nonconforming transverse reinforcement. A component is conforming if, within the flexural plastic hinge region, hoops are spaced at ≤ d/3, and if, for components of moderate and high ductility demand, the strength provided by the hoops (V_s) is at least three-fourths of the design shear. Otherwise, the component is considered nonconforming.
2. Linear interpolation between values listed in the table shall be permitted.

2.3.4 Fragility Curves

The fragility of a component or system is defined as "the conditional probability of attaining a performance limit state given the occurrence of a particular environmental demand," (Wen et al. 2003). Limit states represent a state of unsatisfactory performance, defined in terms of engineering parameters such as forces or deformations. The environmental demand in this study is expressed in terms of seismic intensity. The process for developing fragility curves is shown in Fig. 2.4. To capture a broad scope of earthquake demand, ground motions with a range of intensities reflecting the seismicity of the region are needed.

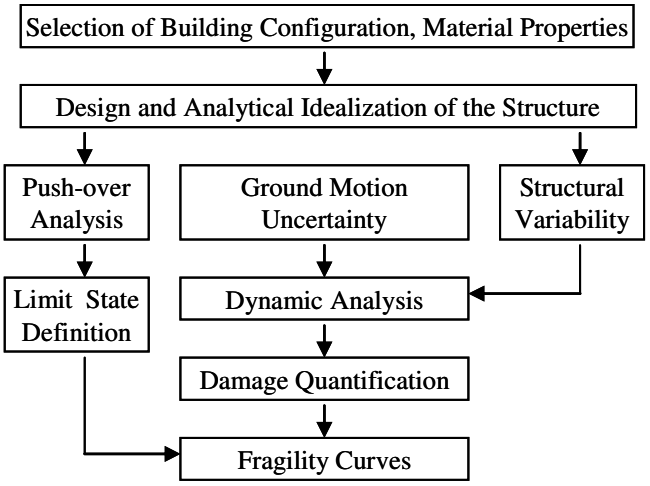

Fig. 2.4. Fragility curves methodology (adapted from Erberik and Elnashai 2004)

The probability of reaching a specified limit state (*LS*) is calculated using the following equation (Wen et al. 2004):

$$P[LS] = \Sigma\, P[LS|D=d]\; P[D=d] \tag{2.20}$$

where:

LS	=	Limit state
D	=	Spectrum of uncertain hazards
d	=	Control of interface variable, such as occurrence of a specific hazard intensity
$P[LS\|D=d]$	=	Fragility
$P[D=d]$	=	Seismic Hazard

Cornell et al. (2002) and Wen et al. (2004) used the power model in Eq. (2.21) to predict the seismic demand, *D*, in the fragility definition. Regression analysis of the response history results along with corresponding earthquake intensities is conducted to obtain the power equation parameters.

$$D = \alpha_0 (S_a)^{\alpha_1} e \tag{2.21}$$

where:

S_a	=	Spectral acceleration

α_0, α_1 = Parameters determined by regression analysis

e = Unit median error term that describes uncertainty in the relationship

According to Wen et al. (2004), limit states based on interstory drifts for RC buildings can be found either qualitatively using documented limits such as FEMA 356 performance limit guidelines or quantitatively using nonlinear push-over techniques. Quantitative limits are determined from the drifts at which yielding initiates in a nonlinear push-over analysis, expressed as First Yield (FY) and Plastic Mechanism Initiation (PMI). FY corresponds to the interstory drift at which the member of a story first begins to yield, and PMI is defined as the interstory drift at which a story mechanism initiates. PMI can occur when either both ends of a beam yield, as shown in Fig. 2.5, for all the beams in a story, or when yielding occurs at both ends of each column in a story.

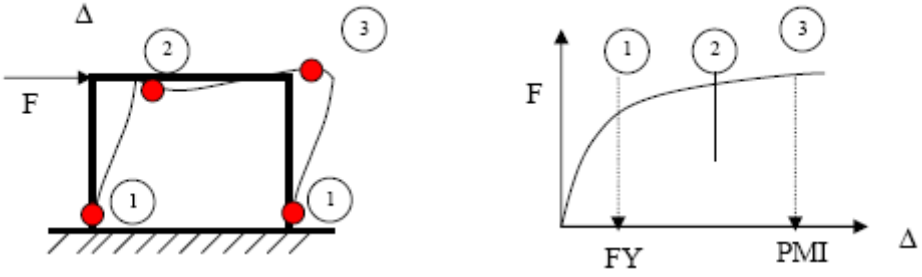

(a) Building response (b) Corresponding push-over curves

Fig. 2.5. Quantitative drift limit evaluation (Wen et al. 2004)

Estimating and incorporating uncertainty into fragility curves is an integral step of fragility analysis, as the levels of uncertainty can be quite large. Sources of uncertainties include ground motion determinations, building response, measures of performance, modeling material properties and other assumptions (Kinali and Ellingwood 2007), and can be categorized into three types of uncertainties: demand, capacity and modeling.

There have been many research studies conducted on methodologies for developing fragility curves to represent the seismic vulnerability of buildings. Only a few are mentioned here. Erbenik and Elnashai (2004) developed fragility curves for concrete flat slab buildings and compared them to fragility curves developed for concrete moment frames by Hwang and Huo (1997) and Singhal and Kiremidijian (1997). Fragility curves for low rise gravity load designed concrete frames were developed by Ramamoorthy et al. (2006).

2.4 Vulnerability of Central U.S. Buildings

Research on the seismic vulnerability of Central U.S. structures has primarily concentrated on the performance of existing buildings designed for older code requirements as well as retrofit options to improve the seismic performance. Ramamoorthy et al. (2006), as mentioned previously, assessed the seismic vulnerability of a low rise gravity load designed RC frame building in Memphis, Tennessee, representative of past construction. Hueste and Bai (2007) investigated the seismic performance of an unretrofitted five-story RC flat slab building designed with a 1980s regional building code prior to the inclusion of seismic provisions. The seismic response for ground motions for St. Louis, Missouri, and Memphis was compared with the building response after applying three different retrofit techniques. The seismic fragility of three different low to mid-rise steel frames designed with three different building codes adopted prior to 1993 was analyzed by Kinali and Ellingwood (2007) for Memphis ground motions.

3 CASE STUDY BUILDING

3.1 Introduction

To compare modern code provision in the Central U.S., current prevalent RC building types in this region were investigated. A building inventory database was compiled for Shelby County, Tennessee, by French and Muthukumar (2004), as part of the Mid-America Earthquake Center's research program. A total of 287,057 building records were categorized using county tax assessor information by building use, square footage, and year built. The results for post 1990 office buildings are summarized in Table 3.1. The data indicates that concrete moment resisting frames (MRF) are the second most prevalent structure type for office buildings constructed in Shelby County/ Memphis, Tennessee after 1990, comprising 4.4% of the total inventory for this category. Table 3.2 lists the structural characteristics of concrete moment frames in the Shelby County database. Parameters in bold were chosen for the case study building under investigation.

Table 3.1. Post 1990 Shelby County office building inventory (adapted from French and Muthukumar 2004)

Structure type	No. of office buildings	Percent of total office buildings
Light Metal Frame	955	86.1
Concrete MRF	**49**	**4.4**
Reinforced Masonry	42	3.8
Wood Frame	29	2.6
Concrete Tilt-up	25	2.3
Steel Frame	7	0.6
Concrete Shear Wall	1	0.1

Table 3.2. Concrete MRF parameters in Shelby County (adapted from French and Muthukumar 2004)

No. of stories	Percent of total		Square footage	Percent of total		Building use	Percent of total
01	27.1		≤ 2,500	8.9		**Office**	**36.4**
02	16.1		2,500 - 5,000	10.8		Multi-family residential	32.5
03 – 05	**41.4**		5000 - 10,000	9.1		Industrial	15.2
06 – 10	9.5		10,000 - 50,000	39.0		Retail/ Wholesale Trade	15.2
over 11	5.9		**≥ 50,000**	**32.1**		Single-family residential	0.7

For a better understanding of current structural design practices in this region, four of the largest structural engineering firms in Memphis, including the City of Memphis Engineering Department, were contacted. For each firm, a design engineer with between eight and twenty years of experience in the Memphis area was interviewed over the telephone. Most engineering firms agreed on the typical structure types for the various building categories (see Table 3.3). For multi-family residential construction (condos, hotels, etc.), wood/ composite deck and steel frame between three and five stories were the most popular buildings types. Steel frames between two and four stories were the main building types for office construction, and school buildings were usually one or two story reinforced masonry buildings. First floor story heights of 14 to 16 ft. and upper story heights of 10 to 12 ft. were common. Typical span lengths were between 30 and 40 ft.

Table 3.3. Typical Memphis buildings based on engineers' input

Building category	No. of stories	Structure type
Multi-family residential	3-5	Wood/ composite deck, Steel frame
Office	2-4	Steel frame
School (K-12)	1-2	Reinforced masonry

Although Memphis engineers stated that steel frame construction is more popular for office buildings at this time due to steel and concrete market costs, the Memphis test bed inventory shows that there has been a significant number of reinforced concrete MRFs constructed since 1990. In addition, research involving the seismic vulnerability of Memphis steel frames is being conducted by other MAE center institutions.

3.2 Building Description

The case study building is a four story RC moment frame with an overall height of 51 ft. The first story height is 15 ft., with the upper stories of 12 ft. The rectangular foot print of the building is 150 ft. by 90 ft. with five 30 ft. bays in the East-West (E-W) direction and three 30 ft. bays in the North-South (N-S) direction.

Wide-module pan joists run in the E-W direction, and the number of moment frames in this direction depends on the seismic design requirements. While each case study has interior moment frames in the N-S direction and exterior moment frames in both directions, CS1 is the only structure with interior moment frames in the E-W directions. The exterior E-W frames in CS2 and CS3 met the design provision lateral demand without requiring additional interior moment frames. However, drift limits and 2003 IBC redundancy constraints for the higher lateral forces required N-S interior and exterior moment frames for CS1. This is explained in more detail later. Figs. 3.1 and 3.2 show the plan and elevation views of the structure.

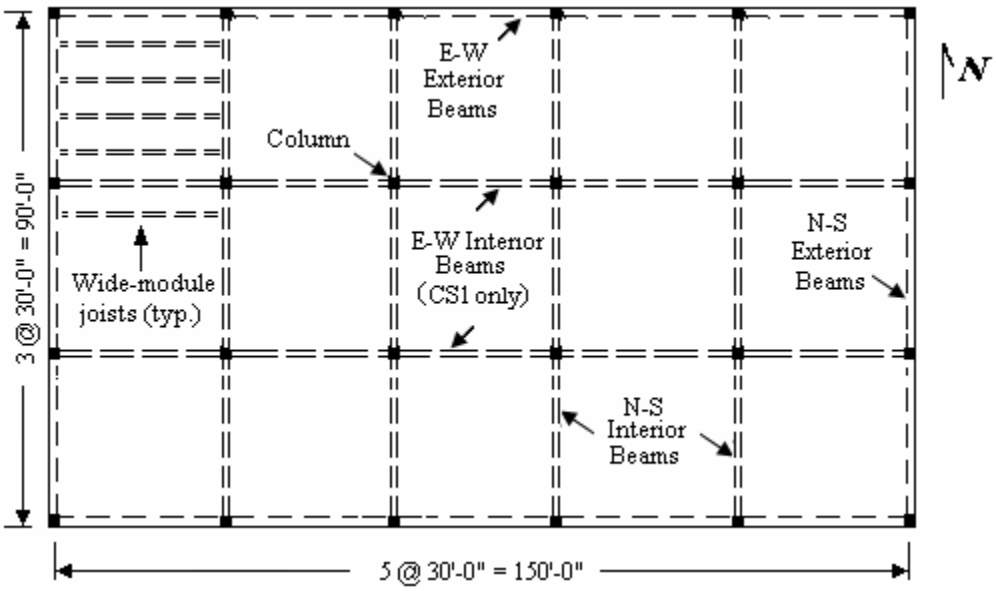

Fig. 3.1. Case study building plan view

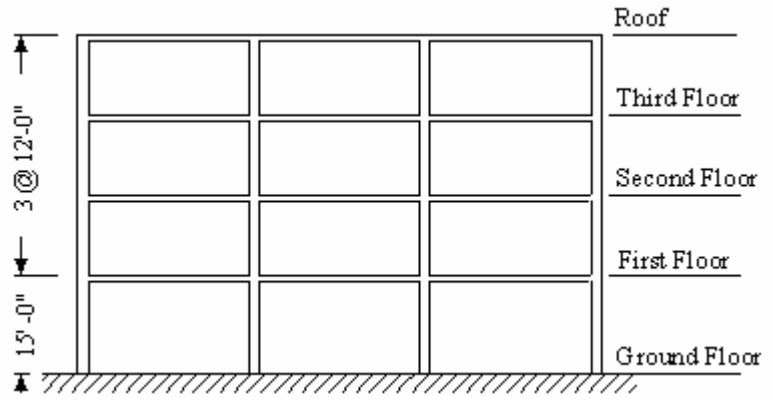

Fig. 3.2. Case study building elevation view

3.3 Building Design

Three case study buildings were designed with the requirements of three different buildings codes and modeled in ETABS, a 3-D structural analysis software program (CSI 2002), to determine the member forces and story displacements. Member sizes and reinforcement were designed based on these demands.

3.3.1 General

According to the Memphis and Shelby County Office of Construction and Code Enforcement, Memphis and Shelby County adopted the 2003 *International Building Code* (IBC) (ICC 2003) effective January 1, 2006, with local seismic amendments: Appendix L, Alternate Seismic Protection Calculations and Procedures (City of Memphis and Shelby County 2005). However, the structural requirements of the 1999 *Standard Building Code* (SBC) (SBCCI 1999) are still permitted for all structures with the exception of essential facilities. Essential facilities, such as hospitals and fire stations, must be designed according to the more stringent design provisions of the 2003 IBC without local amendments (Allen Medlock, Interim director, personal communication, Feb. 2, 2006).

Case Study 1 (CS1) was designed according to the load requirements of the 2003 IBC, without local amendments. Case Study 2 (CS2) was designed according to the 2003 IBC with the local seismic amendments. The design of structural components for each of these case studies was carried out according to the provisions of the American Concrete Institute (ACI) *Building Code Requirements for Reinforced Concrete*, ACI 318-02 (ACI Committee 318 2002). Case Study 3 (CS3) was designed according to the load requirements of the 1999 SBC, which references ACI 318-95 (ACI Committee 318 1995) as the concrete design standard. Table 3.4 lists the case study buildings and their respective building codes.

Table 3.4. Case study buildings and design codes

Case study	Building code	Concrete standard
CS1	2003 IBC	ACI 318-02
CS2	2003 IBC (w/ local amendments)	ACI 318-02
CS3	1999 SBC	ACI 318-95

3.3.2 Non-seismic Loads

Non-seismic loads were calculated from Chapter 16 of the 2003 IBC for CS1 and CS2 and Chapter 16 of the 1999 SBC for CS3. The gravity and wind load provisions were identical for each case study; the only differences between the three sets of code provisions applied to the seismic design requirements and the load combinations.

3.3.2.1 Gravity Loads

The design gravity loads were determined as follows. The weight of concrete was assumed to be 150 pcf when computing the self weight of the RC members. A super-imposed dead load of 15 psf was applied to account for the service equipment, including electrical, mechanical, and plumbing. Glass cladding, a common exterior for office buildings, was chosen with an assumed cladding load of 20 psf over the vertical tributary area of the perimeter beam members. A 20 psf partition load was applied as live load for CS1 and CS2 but as dead load for CS3, per SBC specifications. The roof live load of 12 psf for the 13,500 sq. ft. tributary area controlled over snow and rain load. The design live load of 50 psf was reduced for the columns and the N-S interior beams, which have the largest tributary due to the framing direction of the wide-module joists. The gravity loads are summarized in Table 3.5.

Table 3.5. Gravity loads

Load category	Load type	SBC value (psf)	IBC value (psf)
Dead, *D*	Cladding	20	20
	Partition	20	-
	Superimposed	15	15
Live, *L*	Design Live	50	50
	Partition	-	20
Roof live, L_r	Roof live	12	12

Live loads were applied on selected spans in addition to a uniform load to produce the greatest effect at each location under consideration. The same live load

patterns were applied to each case study. In accordance with ACI 318 Section 8.9, live load patterns include factored dead load on all spans and full factored live load on adjacent spans and full factored live load on alternate spans. Fig. 3.3 shows the alternating live load patterns used in the design model. Variations of these patterns were used to capture all the critical loadings.

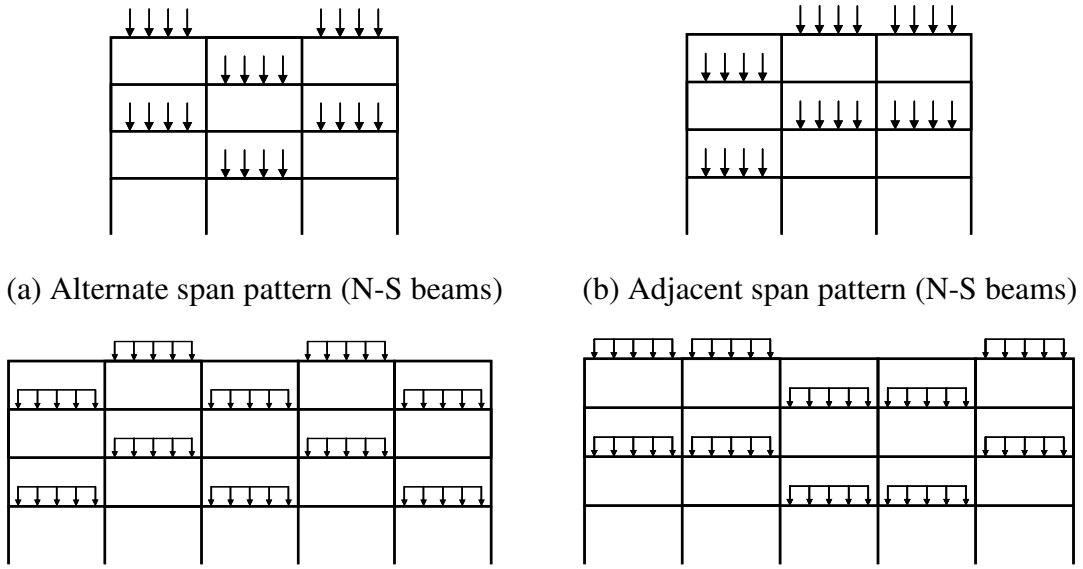

(a) Alternate span pattern (N-S beams) (b) Adjacent span pattern (N-S beams)

(c) Alternate span pattern (E-W beams) (d) Adjacent span pattern (E-W beams)

Fig. 3.3. Live load patterns

3.3.2.2 Wind Loads

The design wind load was applied as a lateral force to each story diaphragm combining the load effects from the windward and leeward sides of the building. The 2003 IBC references ASCE 7-02 (ASCE 2002) for wind load calculations, and the 1999 SBC references ASCE 7-95 (ASCE 1995). The wind provisions match for these two standards. The four wind load cases required from ASCE 7 are illustrated in Fig. 3.4. A total of 12 wind cases were modeled to capture the effects of the different wind cases for both the N-S and E-W directions.

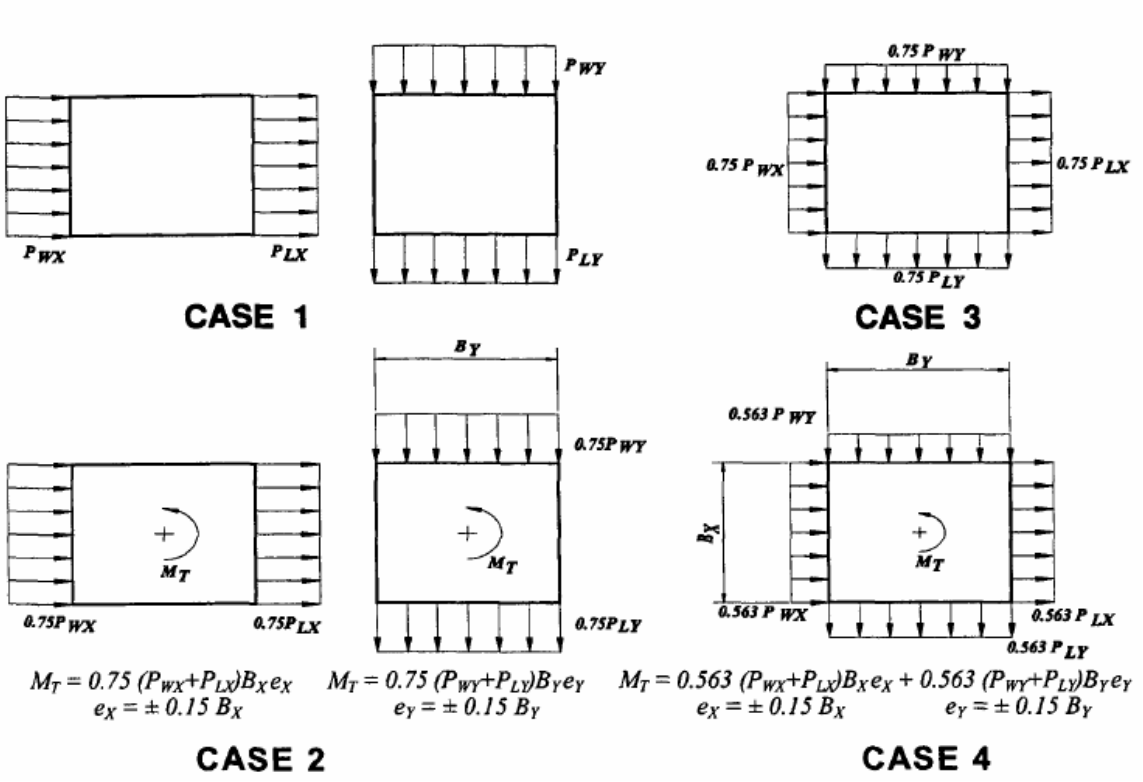

Fig. 3.4. ASCE 7 wind load cases (ASCE 2002)

The wind loads were calculated from the pressure load multiplied by the vertical tributary area to each floor and roof level for each side of the building. An additional uniform uplift pressure was applied to the roof, as shown in Fig. 3.5. The point loads applied to the center of mass of each diaphragm for ASCE 7 Wind Case 1 are summarized in Table 3.6. These loads were adapted for the other cases to model torsion and cross-wind effects. After the analysis, it was determined that wind did not control for lateral design.

Table 3.6. ASCE 7 Case 1 wind loads

Story level	E-W direction (kips)	N-S direction (kips)
4	23.5	39.2
3	45.6	75.9
2	43.0	71.6
1	45.1	75.1

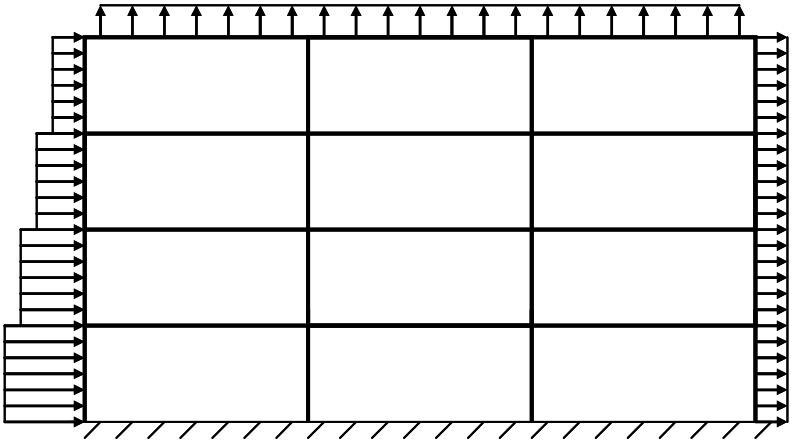

Fig. 3.5. Typical wind load distribution

3.3.2.3 Load Combinations

The following 2003 IBC factored load combinations were used in the required strength design for gravity and wind loads for CS1 and CS2. These combinations include the different live load patterns and twelve wind cases. The seismic load combinations are discussed in the following sections.

(i) $1.4D$ (3.1)

(ii) $1.2D + 1.6L + 0.5L_r$ (3.2)

(iii) $1.2D \pm 1.6W + 0.5L + 0.5L_r$ (3.3)

(iv) $0.9D \pm 1.6W$ (3.4)

where:

D = Dead load
L = Live load
L_r = Roof live load
W = Wind load

The ACI 318-95 factored strength design load combinations listed in Eqs. (3.5) through (3.7) were used in SBC calculations to compute the factored gravity and wind effects for CS3. In the SBC, the live load, L, includes roof live loads.

(i) $U = 1.4D + 1.7L$ (3.5)

(ii) $U = 0.75\ (1.4D + 1.7L + 1.7W)$ (3.6)

(iii) $U = 0.9D \pm 1.3W$ (3.7)

3.3.3 CS1 Seismic Loads

The CS1 mapped spectral accelerations for short (0.2 sec.) and 1-sec. periods, S_s and S_1 ($S_s = 1.398g$, $S_1 = 0.423g$), were determined using the USGS zip code earthquake ground motion hazard look-up website (http://eqint.cr.usgs.gov/eq/html/zipcode.shtml) for the zip code 38103 for downtown Memphis. The physical location of the building's site in the city has a large impact on the S_a.

Fig. 3.6 shows the location of selected Memphis zip codes and Table 3.7 shows the corresponding spectral accelerations for short and 1-sec. periods determined from the USGS website. For CS1, spectral accelerations for a 2% probability of exceedance in 50 years are used. The S_1 values range from $0.987g$ in southeast Memphis to almost 1.5 times this value for downtown Memphis and the surrounding areas. The zip code used in this investigation is circled in Fig. 3.6 and bolded in Table 3.7

Fig. 3.6. Memphis zip codes

Table 3.7. Spectral accelerations for various Memphis zip codes

Zip code	0.2-sec. S_a, S_s (%g)		1-sec. S_a, S_1 (%g)	
	10% in 50 years	2% in 50 years	10% in 50 years	2% in 50 years
38115	0.239	0.987	0.061	0.287
38118	0.245	1.056	0.061	0.303
38138	0.261	1.101	0.063	0.312
38117	0.266	1.169	0.064	0.337
38114	0.272	1.235	0.064	0.372
38134	0.284	1.267	0.068	0.388
38109	0.275	1.300	0.065	0.407
38127	0.292	1.398	0.069	0.423
38103	**0.292**	**1.398**	**0.069**	**0.423**

Site Class D was chosen for the soil site conditions, based on recommendations by Romero and Rix (2001). Taking into account soil amplification, the design spectral accelerations, S_{DS} and S_{D1} were calculated as $0.923g$ and $0.451g$, respectively, and S_{D1} controlled in the calculation of the base shear, V. The design base shear for CS1 was determined to be 620 kips using the equivalent lateral force procedure outlined in ASCE 7-02. An office building is classified as Seismic Use Group I (IBC Table 1604.5) with an importance factor of 1.0. The Seismic Use Group and design spectral accelerations, S_{DS} and S_{D1}, classify CS1 as Seismic Design Category (SDC) D. For SDC D, a special moment frame (SMF) is required for the lateral resisting system of an RC frame.

The following 2003 IBC factored load combinations include horizontal seismic effects as well as a vertical seismic component based on the value of S_{DS} to account for ground shaking in both directions.

$$\text{(v)} \quad (1.2 + 0.2\,S_{DS})D \pm \rho Q_E + 0.5L = 1.39D \pm 1.0Q_E + 0.5L \tag{3.8}$$

$$\text{(vi)} \quad (0.9 - 0.2\,S_{DS})D \pm \rho Q_E = 0.71D \pm 1.0Q_E \tag{3.9}$$

where:

D = Dead load

L = Live load
Q_E = Effect of horizontal seismic forces
ρ = Redundancy coefficient

The redundancy coefficient, ρ, was calculated for the controlling seismic load combination in the N-S and E-W directions without considering accidental torsion. The maximum shear from the ETABS seismic load combination for a single column was doubled and divided by the total shear to obtain r_{max} at each story. The equation to calculate ρ is given in Section 2. The ρ_x values for the controlling E-W direction are shown in Table 3.8. The code lower limit of 1.0 controlled over the maximum computed ρ_x. When only E-W exterior moment frames were included in the CS1 model, ρ was greater than 1.25, which is not allowed for RC moment frames. Therefore, interior moment frames were added in the final model to calculate the values in Table 3.8.

Table 3.8. Calculation of redundancy coefficient for seismic forces in E-W direction

Story	Story shear (k)	Max. column shear (k)	r_{max}	ρ_x
1	531.6	28.2	0.106	0.259
2	514.6	30.1	0.117	0.424
3	397.3	22.1	0.130	0.341
4	208.0	13.6	0.111	0.585

3.3.4 CS2 Seismic Loads

For clarity in this study, the IBC seismic parameters that changed due to the amendments in CS2 are marked with a prime symbol (i.e. S_s'). The main specifications of Appendix L modify the design earthquake from the IBC recommendation of 2/3 of the maximum considered earthquake (MCE) (2% in 50 years) to the 10% in 50 years event. As discussed in Section 2, these design events are similar on the west coast, but not for Memphis and other cities in the Central U.S. The S_s' and S_1' values for the Memphis local amendments change from 1.398g to 0.29g and 0.423g to 0.069g,

respectively. The 10% in 50 years S_s' and S_1' were also taken from the USGS zip code earthquake ground motion hazard look-up website for zip code 38103.

The modified spectral accelerations for soil effects are not multiplied by 2/3 as they are in CS1, and $S_{D1}' = S_{M1}' = 0.166g$, and $S_{DS}' = S_{MS}' = 0.464g$. The CS1 and CS2 seismic parameters are compared in Table 3.9. The final design values S_{DS}' and S_{D1}' of $0.464g$ and $0.166g$ are reduced by 50 and 63 percent relative to the 2003 IBC values for CS1 when Appendix L is applied.

The reductions of S_{DS}' and S_{D1}' also change the SDC from D to C. As a result, an IMF can be used as the lateral resisting system instead of a SMF for SDC C, reducing the seismic detailing requirements. However, this increases the seismic design forces by decreasing the response modification coefficient, R. From IBC Table 1617.6.2, R' is 5.0 for an IMF instead of 8.0 for a SMF. The seismic coefficient increases from 2.4 percent for SDC D to 3.8 percent for SDC C. The total base shear for the IMF in CS2 was 358 kips. The 1-sec. period design spectral acceleration controlled in the base shear calculation.

Table 3.9. Comparison of seismic design parameters for CS1 and CS2

Parameter	CS1 (IBC)	CS2 (IBC amend.)
S_S	$1.398g$	$0.290g$
S_1	$0.423g$	$0.069g$
Site Class	D	D
F_a	1.0	1.6
F_v	1.6	2.4
S_{MS}	$1.398g$	0.464g
S_{M1}	$0.677g$	$0.166g$
S_{DS}	$0.932g$	$0.464g$
S_{D1}	$0.451g$	$0.166g$
R	8.0	5.0
SDC	D	C

The IBC amendments also affect the seismic load combinations. The factored effect on dead load due to seismic forces decreases with the lower S_{DS}' changing the load

factors from 1.39 to 1.29 for the strength load combination and from 0.71 to 0.81 for the uplift load combination.

$$\text{(iv)} \quad (1.2 + 0.2S_{DS}')D \pm \rho 1.0Q_E + 0.5L = 1.29D \pm 1.0Q_E + 0.5L \tag{3.10}$$

$$\text{(v)} \quad (0.9 - 0.2\,S_{DS}')D \pm \rho 1.0Q_E = 0.81D \pm 1.0Q_E \tag{3.11}$$

For SDC C, the seismic redundancy coefficient, ρ, is equal to 1.0. Without upper limit restrictions on ρ and a smaller drift demand, exterior moment frames were adequate to resist the lateral seismic demand in the E-W direction in CS2.

3.3.5 CS3 Seismic Loads

For the 1999 SBC design for CS3, A_a and A_v values were each taken as 0.203 based on recommendations from engineers with design experience in downtown Memphis. The soil profile type S_2 was chosen for Memphis based on the recommendation from Dr. Glenn Rix of the Georgia Institute of Technology, a researcher for the Mid-America Earthquake Center (personal communication, Feb. 24, 2006).

The total design base shear was calculated as 358 kips, which is 4.2 percent of the total dead weight of the building. Seismic Hazard Exposure Group I for an office building and A_v value of 0.203 classified CS3 as Seismic Performance Category (SPC) D. Seismic Performance Categories are the SBC equivalent of Seismic Design Categories in the IBC with some slight modifications discussed in Section 2. To ease confusion, the SPC is referred to as SDC in the performance evaluation of this report. For the SPC seismic classifications, the minimum value for SPC D is A_v = 0.20, and the design A_v of 0.203 was just above this value. In design practice this number might be rounded down to SPC C; however, in this study CS3 was designed as a SMF for SPC D. It is recognized that rounding down to a lower SPC would have had a significant impact on the design and performance of the structure.

Eqs. (3.12) and (3.13) are taken from SBC Section 1609.2 for seismic factored load combinations. Similar to the IBC load combinations, the earthquake effects are divided into a vertical and horizontal component.

(iv) $U = (1.1 + 0.5A_v)D + 1.0L \pm 1.0E = 1.2D + 1.0L \pm 1.0E$ (3.12)

(v) $U = (0.9 - 0.5A_v)D \pm 1.0E = 0.8D \pm 1.0E$ (3.13)

where:

D	=	Dead load
L	=	Live load (includes roof live loads)
E	=	Earthquake load
A_v	=	Seismic coefficient representing effective peak-velocity related acceleration

3.3.6 Seismic Load Summary

The difference in the seismic design level for each case study is clearly illustrated in the comparison of the design response spectra in Fig. 3.7. The design spectra plot the seismic response coefficient, C_s, as a function of period. The coefficient C_s is the value multiplied by the building seismic weight to obtain the seismic base shear for design. The fundamental period for each case study building, based on the upper limit for the design period for each code, is also shown. The SBC design base shear (CS3) was almost half of the IBC value (CS1), and the amended IBC design base shear (CS2) was almost one-third of the IBC value when comparing the same type of lateral system. CS2 was designed as an IMF, which increased the design forces to almost the level of CS3. The SMF spectrum for CS2 is provided for reference.

Table 3.10 compares the seismic design parameters for each case study. The IBC base shear was 7.2% of the seismic weight, W, and the SBC base shear was 4.2% W. The amended IBC base shear was 3.8% W and was calculated using a smaller response modification coefficient corresponding to a less ductile lateral system. In addition to the expected level of ground shaking, differences in the structural period, amplification due to soil conditions, and the level of ductility in the building contributed to the variation in these values.

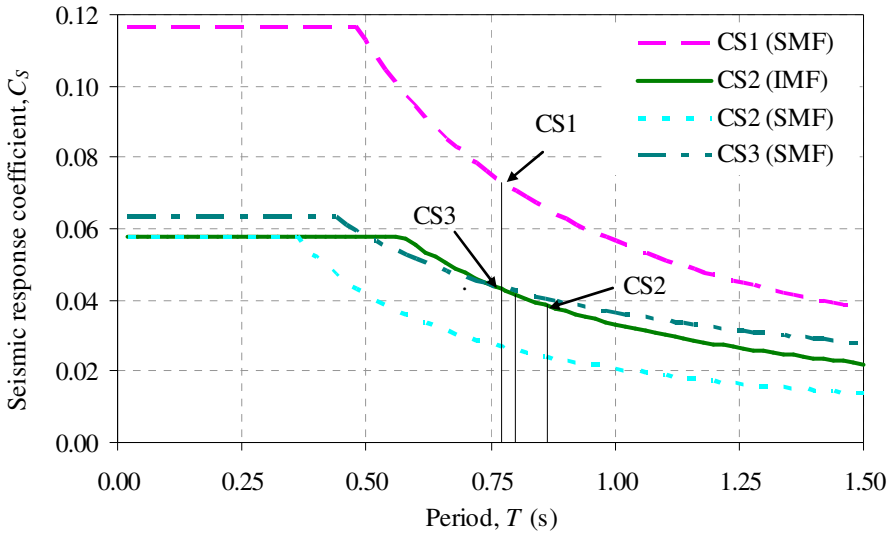

Fig. 3.7. Comparison of seismic design coefficients, C_s

Table 3.10. Summary of seismic design parameters

Case study	Structural period, T (s)	Building weight, W (k)	C_s	Base shear, V (k)	SDC	Lateral system
CS1	0.771	8598	0.072	619.9	D	SMF
CS2	0.864	8438	0.038	323.4	C	IMF
CS3	0.802	8458	0.042	358.0	D	SMF

3.4 Analysis for Design Loads

3.4.1 General

To design each case study building, the finite-element-based structural analysis program ETABS (CSI 2002), was used to determine member forces based on gravity and lateral loads. The 3-D models are shown in Fig. 3.8. The only difference between the models is the presence of interior beams in the long direction for CS1. Gravity and lateral loads were applied per the requirements of each design code to each of the three models. A total of 93 load combinations were used for the IBC design and 100 load combinations were used for the SBC design.

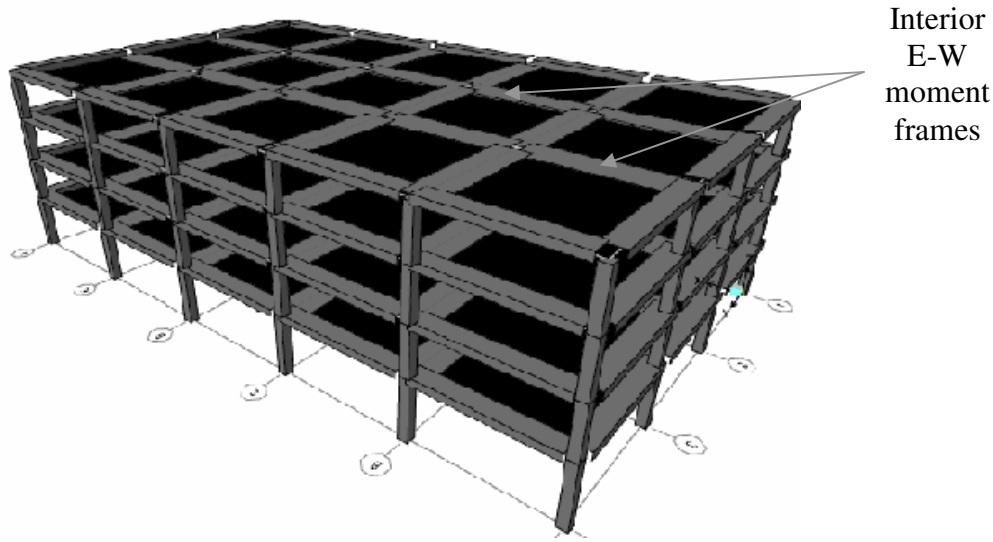

(a) CS1

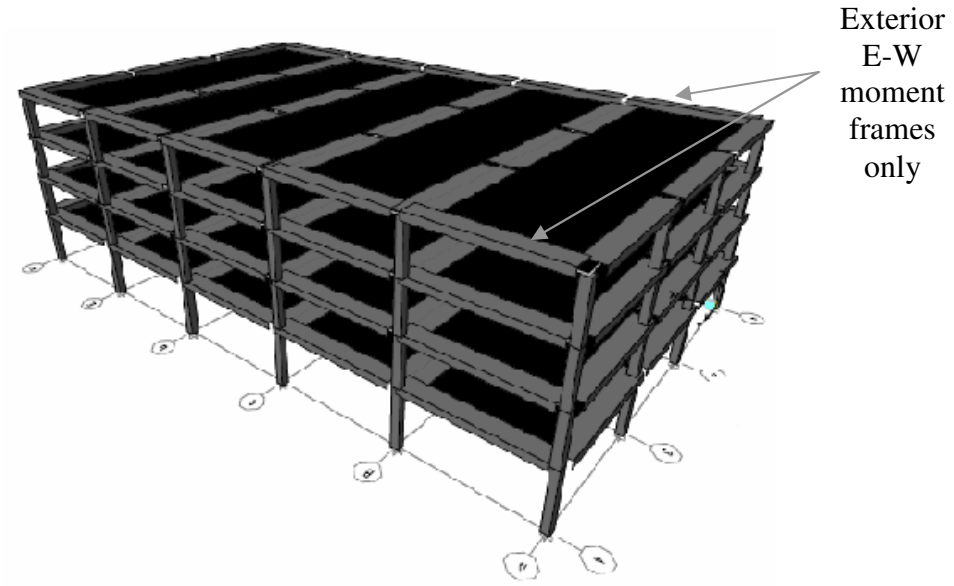

(b) CS2 and CS3

Fig. 3.8. ETABS 3-D models

3.4.2 Modeling Assumptions

Rigid diaphragms were assigned at each floor level, typical for modeling cast-in-place slabs. Rigid end offsets were defined at the ends of the horizontal and vertical

members so that the member end forces correspond to values at the support face. The concrete moment frame joints were assigned a rigid zone factor of 1.0, corresponding to zero joint deformation. The member stiffness properties were defined using estimates of the effective moment of inertia, I_{cr}. Per ACI 318-02 Section 10.11.1, the following reduced section properties were used, where I_g is the gross moment of inertia based on the overall concrete dimensions:

- Beams: $I_{cr} = 0.35I_g$
- Columns: $I_{cr} = 0.7I_g$

Beams were modeled as T-sections with effective flange widths calculated using ACI 318 Section 8.10. Lateral loads were applied as point loads to the center of the mass. Seismic and wind accidental torsional effects were modeled as additional torsional moments applied to the structure.

The wide-module joists were not included in the ETABS model since they are not part of the lateral resisting system. Point loads based on the joist tributary area were applied to the N-S beams to model the wide-module joist framing, and a uniform gravity load was applied to the E-W beams for the smaller tributary width of the adjacent slab.

3.4.3 Design Fundamental Period

The period of each structure, *T,* was determined from the ETABS analysis to be larger than the upper limit in the code provisions. Therefore, the design periods for CS1, CS2 and CS3 were 0.771, 0.864, and 0.803 s, respectively, using the code empirical equations. The E-W fundamental periods were longer than the N-S periods and therefore control in the determination of the design code upper limits for each case study in Table 3.11. The variability in the ETABS periods reflects the different levels of flexibility in the case studies due to column size and number of moment frames.

Table 3.11. Controlling E-W design fundamental periods

Case study	Period, T (s)	
	ETABS	Code upper limit
CS1	1.154	0.771
CS2	1.804	0.864
CS3	1.478	0.802

3.5 Member Design

3.5.1 General

The range of seismic demands required by the different code provisions creates variation in the structural member layout, member sizes, and reinforcement quantity and detailing. These differences were mainly dependent on the lateral frame type. CS1 and CS3 were designed with SMF lateral systems, which must meet the requirements of Sections 21.2-21.7 in ACI 318-02 and ACI 318-95. CS2 was designed with an IMF lateral system to meet the requirements of Section 21.12 in ACI 318-02. The only applicable changes between ACI 318-95 and ACI 318-02 are the shear and flexure reduction factors and the load combinations. Moment redistribution was practiced in all case study structures to reduce rebar congestion in the columns.

The case study buildings have the same number of moment frames in the short direction, but the magnitude of the earthquake loads and the code provisions created differences in the long direction. Lateral frames were not required along the two interior column lines in the long direction, and the modified wide-module joist layout increased the loading on the N-S interior beams for CS2 and CS3.

3.5.2 Member Dimensions

Beam and column dimensions are summarized in Table 3.12. The beam sizes are the same for the two SMF case studies (CS1 and CS3). The beams depth is the same as the wide-module joists to reduce forming costs, a common practice in design. N-S interior SMF beams were 22 x 21 in., perimeter beams were 18 x 21 in. and columns were 24 x 24 in. The CS1 interior E-W beams were also 18 x 21 in. SMF beams widths

for CS1 and CS3 were kept smaller than the columns to maintain the strong-column, weak-beam SMF requirements. Strong-column weak-beam requirements do not apply to IMF structures, and the smaller design story drift permitted a smaller column size for CS2 (20 x 20 in.). CS2 N-S interior beams were widened to 24 x 21 in. to maintain a compressive strength of 4000 psi concrete throughout the structure. Forming costs are also reduced when the beams are wider than the columns.

Table 3.12. Typical member sizes

Lateral system	Frame member	b_w (in.)	h (in.)	b_{eff} (in.)
SMF (CS1 and CS3)	Column	24	24	-
	N-S Exterior Beam	22	21	48
	N-S Interior Beam	18	21	90
	E-W Beam	18	21	48
IMF (CS2)	Column	20	20	-
	N-S Exterior Beam	24	21	48
	N-S Interior Beam	18	21	90
	E-W Beam	18	21	48

For the CS1 interior columns, the shear demand from the N-S beam reinforcement exceeded the shear strength for a column confined on all four sides per ACI 318 Chapter 21 SMF requirements. To increase the shear capacity without expanding the joint size, the compressive strength (f'_c) for the interior SMF columns was increased to 6000 psi through the second story in CS1. The same SMF requirements applied to CS3 for the bottom three stories, and the interior column strength was also increased to 6000 psi. Exterior columns had less shear demand, but still required 5000 psi for the lower stories to meet the demand for the SMF case studies. The confinement requirements did not apply to the IMF structure, and 4000 psi concrete strength was used for columns in all stories. The f'_c values for each case study is given in Table 3.13.

For the CS1 and CS3 N-S interior beams, heavier seismic and gravity demands increased the f'_c to 5000 psi on the lower floors, while 4000 psi concrete was sufficient

for the upper floors. CS3 had one additional level where 5000 psi concrete was needed due to the higher gravity demands from the joist reconfiguration without interior frames. The same compressive strength was maintained for all slabs, beams, and wide-module joists on the same floor. The f'c values for each member is given in Table 3.13.

Table 3.13. Compressive strength of elements

Case study	Element	Story level	f'_c (ksi)
CS1	Interior Columns	1 – 2	6
		3 - 4	5
	Exterior Columns	1 – 2	5
		3 - 4	4
	Beams	1 – 2	5
		3 - 4	4
CS2	All	1 - 4	4
CS3	Interior Columns	1 - 3	6
		4	5
	Exterior Columns	1 - 3	5
		4	4
	Beams	1 - 3	5
		4	4

Grade 60 reinforcement was used for the transverse and longitudinal reinforcement in all structural members. The practice of using only odd numbered rebar for longitudinal reinforcement (#5, 7, 9) to easier differentiate between rebar in the field was also employed. Transverse reinforcement in ties, stirrups, and hoops consists of #3 or #4 US bars. Cover between the edge of the concrete and the transverse steel was kept at 1.5 in. for all members.

Wide-module joists span in the E-W direction with a 5 in. one-way slab reinforced with WW10 mesh (#3@12 in. each way). The slab thickness was determined based on the minimum thickness for fire rating, which also works for the deflection requirements of ACI-318 Section 9.5.2.1. The wide-module joists have a 6 in. nominal

web width and are formed from 16 in. deep by 66 in. pans, giving a total depth of 21 in. as shown in Fig. 3.9.

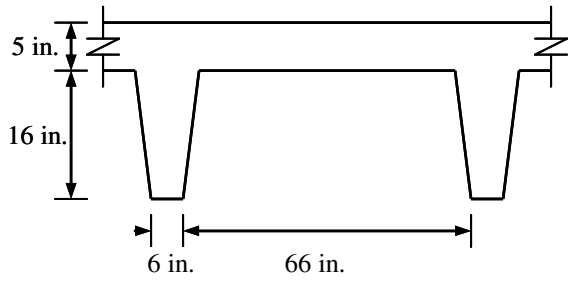

Fig. 3.9. Typical wide-module joist cross-section

3.5.3 Reinforcement

3.5.3.1 Beams

Gravity demand from the wide-module joists controlled the design of the N-S interior beams. The E-W beams had a much smaller tributary area and the design was controlled by lateral loads. The E-W interior and exterior beams have the same reinforcement. The CS2 and CS3 N-S beams carry slightly more load than CS1 due to the absence of interior E-W moment frames.

Top (T) and bottom (B) longitudinal and transverse reinforcement (stirrups) are shown in Tables 3.14 and 3.22 for the case study structures. The N-S exterior beams have additional skin reinforcement for torsion placed at the middle (M) of the section. Sections A and C are in the plastic hinge zone (PHZ) near the column face, and section B is at midspan as shown in Fig. 3.10.

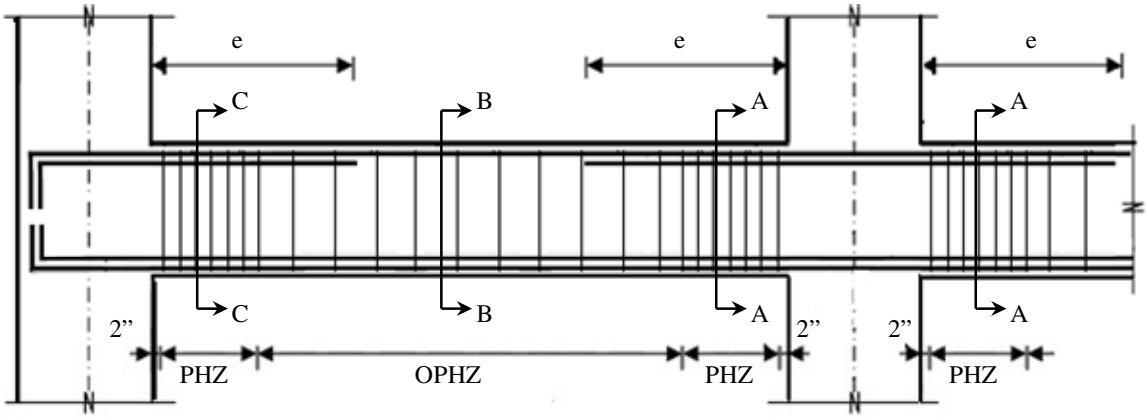

Legend: PHZ = Plastic Hinge Zone = 42 in. from each face of column
OPHZ = Outside Plastic Hinge Zone
e = Negative steel cut-off bar length

Fig. 3.10. Typical beam detailing

Table 3.14. CS1 N-S interior beam reinforcement

Story level	f'_c (ksi)	No. of bars- Bar size (US)				Stirrups (US) PHZ, OPHZ[1]
			A[1]	B[1]	C[1]	
4	4	T	5-#9	2-#9	5-#9	11-#4@4” 3-Leg Hoops, #4@8” 2-Leg Stirrups
		B	3-#9			
3	4	T	6-#9	2-#9	6-#9	11-#4@4” 4-Leg Hoops, #4@7” 2-Leg Stirrups
		B	5-#7			
2	5	T	7-#9	2-#9	7-#9	11-#4@4” 4-Leg Hoops, #4@7” 2-Leg Stirrups
		B	4-#9			
1	5	T	7-#9	2-#9	7-#9	11-#4@4” 4-Leg Hoops, #4@7” 2-Leg Stirrups
		B	4-#9			

[1] See Fig. 3.10 for definition

Table 3.15. CS1 N-S exterior beam reinforcement

Story level	f'_c (ksi)	No. of bars- Bar size (US)				Stirrups (US) PHZ, OPHZ[1]
			A[1]	B[1]	C[1]	
4	4	T	6-#7	2-#7	6-#7	11-#3@4" 4-Leg Hoops, #3@8" 2-Leg Stirrups
		M	2-#5			
		B	4-#7			
3	4	T	7-#7	2-#7	6-#7	11-#4@4" 4-Leg Hoops, #4@9" 2-Leg Stirrups
		M	2-#5			
		B	4-#7			
2	5	T	5-#9	2-#9	5-#9	11-#4@4" 3-Leg Hoops, #4@9" 2-Leg Stirrups
		M	2-#5			
		B	5-#7			
1	5	T	5-#9	2-#9	5-#9	11-#4@4" 3-Leg Hoops, #4@9" 2-Leg Stirrups
		M	2-#5			
		B	5-#7			

[1] See Fig. 3.10 for more details

Table 3.16. CS1 E-W beam reinforcement

Story level	f'_c (ksi)	No. of bars- Bar size (US)				Stirrups (US) PHZ, OPHZ[1]
			A[1]	B[1]	C[1]	
4	4	T	4-#7	2-#7	4-#7	11-#3@4" 4-Leg Hoops, #3@9" 2-Leg Stirrups
		B	4-#5			
3	4	T	4-#7	2-#7	4-#7	11-#3@4" 4-Leg Hoops, #3@9" 2-Leg Stirrups
		B	4-#5			
2	5	T	4-#7	2-#7	4-#7	11-#3@4" 4-Leg Hoops, #3@9" 2-Leg Stirrups
		B	2-#7/ 2-#5			
1	5	T	4-#7	2-#7	4-#7	11-#3@4" 4-Leg Hoops, #3@9" 2-Leg Stirrups
		B	2-#7/ 2-#5			

[1] See Fig. 3.10 for more details

Table 3.17. CS2 N-S interior beam reinforcement

Story level	f'_c (ksi)		No. of bars- Bar size (US)			Stirrups (US) PHZ (Hoops), OPHZ (Seismic Stirrups)
			A[1]	B[1]	C[1]	
4	4	T	6-#9	2-#9	5-#9	11-#4@4" 2-Leg Hoops, #4@8" 2-Leg Stirrups
		B	4-#9			
3	4	T	7-#9	2-#9	6-#9	11-#4@4" 2-Leg Hoops, #4@7" 2-Leg Stirrups
		B	3-#9/ 2-#7			
2	4	T	7-#9	2-#9	6-#9	11-#4@4" 2-Leg Hoops, #4@7" 2-Leg Stirrups
		B	3-#9/ 2-#7			
1	4	T	7-#9	2-#9	6-#9	11-#4@4" 2-Leg Hoops, #4@7" 2-Leg Stirrups
		B	3-#9/ 2-#7			

[1] See Fig. 3.10 for more details

Table 3.18. CS2 N-S exterior beam reinforcement

Story level	f'_c (ksi)		No. of bars- Bar size (US)			Stirrups (US) PHZ, OPHZ[1]
			A[1]	B[1]	C[1]	
4	4	T	6-#7	2-#7	6-#7	11-#3@4" 2-Leg Hoops, #3@9" 2-Leg Stirrups
		M	2-#5			
		B	4-#7			
3	4	T	5-#9	2-#9	5-#9	11-#3@4" 2-Leg Hoops, #3@9" 2-Leg Stirrups
		M	2-#5			
		B	5-#7			
2	4	T	5-#9	2-#9	5-#9	11-#3@4" 2-Leg Hoops, #3@9" 2-Leg Stirrups
		M	2-#5			
		B	5-#7			
1	4	T	5-#9	2-#9	5-#9	11-#3@4" 2-Leg Hoops, #3@9" 2-Leg Stirrups
		M	2-#5			
		B	5-#7			

[1] See Fig. 3.10 for more details

Table 3.19. CS2 E-W beam reinforcement

Story level	f'_c (ksi)		No. of bars- Bar size (US)			Stirrups (US) PHZ, OPHZ[1]
			A[1]	B[1]	C[1]	
4	4	T	3-#7	2-#7	3-#7	11-#3@4" 2-Leg Hoops, #3@9" 2-Leg Stirrups
		B	4-#5			
3	4	T	3-#7	2-#7	3-#7	11-#3@4" 2-Leg Hoops, #3@9" 2-Leg Stirrups
		B	3-#7			
2	4	T	4-#7	2-#7	4-#7	11-#3@4" 2-Leg Hoops, #3@9" 2-Leg Stirrups
		B	3-#7			
1	4	T	4-#7	2-#7	4-#7	11-#3@4" 2-Leg Hoops, #3@9" 2-Leg Stirrups
		B	3-#7			

[1] See Fig. 3.10 for more details

Table 3.20. CS3 N-S interior beam reinforcement

Story level	f'_c (ksi)		No. of bars- Bar size (US)			Stirrups (US) PHZ, OPHZ[1]
			A[1]	B[1]	C[1]	
4	4	T	6-#9	2-#9	5-#9	11-#3@4" 4-Leg Hoops, #4@8" 2-Leg Stirrups
		B	4-#9			
3	5	T	7-#9	2-#9	6-#9	11-#3@4" 4-Leg Hoops, #4@8" 2-Leg Stirrups
		B	2-#9/ 4-#7			
2	5	T	7-#9	2-#9	6-#9	11-#3@4" 4-Leg Hoops, #4@8" 2-Leg Stirrups
		B	2-#9/ 4-#7			
1	5	T	7-#9	2-#9	6-#9	11-#3@4" 4-Leg Hoops, #4@8" 2-Leg Stirrups
		B	2-#9/ 4-#7			

[1] See Fig. 3.10 for more details

Table 3.21. CS3 N-S exterior beam reinforcement

Story level	f'_c (ksi)	No. of bars- Bar size (US)				Stirrups (US) PHZ, OPHZ[1]
			A[1]	B[1]	C[1]	
4	4	T	6-#7	2-#7	6-#7	11-#3@4" 4-Leg Hoops, #3@9" 2-Leg Stirrups
		M	2-#5			
		B	4-#7			
3	5	T	5-#9	2-#9	5-#9	11-#3@4" 4-Leg Hoops, #3@9" 2-Leg Stirrups
		M	2-#5			
		B	5-#7			
2	5	T	5-#9	2-#9	5-#9	11-#3@4" 4-Leg Hoops, #3@9" 2-Leg Stirrups
		M	2-#5			
		B	5-#7			
1	5	T	5-#9	2-#9	5-#9	11-#3@4" 4-Leg Hoops, #3@9" 2-Leg Stirrups
		M	2-#5			
		B	5-#7			

[1] See Fig. 3.10 for more details

Table 3.22. CS3 E-W beam reinforcement

Story level	f'_c (ksi)	No. of bars- Bar size (US)				Stirrups (US) PHZ, OPHZ[1]
			A[1]	B[1]	C[1]	
4	4	T	3-#7	2-#7	3-#7	11-#3@4" 4-Leg Hoops, #3@9" 2-Leg Stirrups
		B	3-#7			
3	5	T	3-#7	2-#7	3-#7	11-#3@4" 4-Leg Hoops, #3@9" 2-Leg Stirrups
		B	3-#7			
2	5	T	4-#7	2-#7	4-#7	11-#3@4" 4-Leg Hoops, #3@9" 2-Leg Stirrups
		B	4-#5			
1	5	T	4-#7	2-#7	4-#7	11-#3@4" 4-Leg Hoops, #3@9" 2-Leg Stirrups
		B	4-#5			

[1] See Fig. 3.10 for more details

Two continuous bars must run through the entire beam for the top and bottom reinforcement. However, the additional negative steel needed near the column face can be cut-off near the midspan. The number of bars discontinued and the cut off lengths for CS1, CS2, and CS3 are shown in Tables 3.23 and 3.25.

Table 3.23. CS1 negative bar cutoff lengths

Beam location	Story level	Cut off bars	e[1] (in.)
N-S Interior	1 – 2	5-#9	110
	3	4-#9	96
	4	3-#9	74
N-S Exterior	1 – 3	3-#9	122
	4	4-#7	96
E-W	1 – 3	2-#7	108
	4	1-#7	90

[1] See Fig. 3.10 for definition

Table 3.24. CS2 negative bar cutoff lengths

Beam location	Story level	Cut off bars	e[1] (in.)
N-S Interior	1 – 3	5-#9	100
	4	4-#9	78
N-S Exterior	1 – 3	3-#9	106
	4	4-#7	72
E-W	1 – 3	2-#7	66
	4	1-#7	42

[1] See Fig. 3.10 for definition

Table 3.25. CS3 negative bar cutoff lengths

Beam location	Story level	Cut off bars	e[1] (in.)
N-S- Interior	1 – 3	5-#9	105
	4	4-#9	90
N-S- Exterior	1 – 3	3-#9	92
	4	4-#7	68
E-W	1 – 2	2-#7	82
	3 – 4	1-#7	75

[1] See Fig. 3.10 for definition

Typical PHZ first floor interior and exterior cross sections at the midspan and column face are shown in Figs. 3.11 and 3.12 for CS1 and CS3 and Figs. 3.13 and 3.14 for CS2. The torsional reinforcement is shown in the exterior beam cross sections.

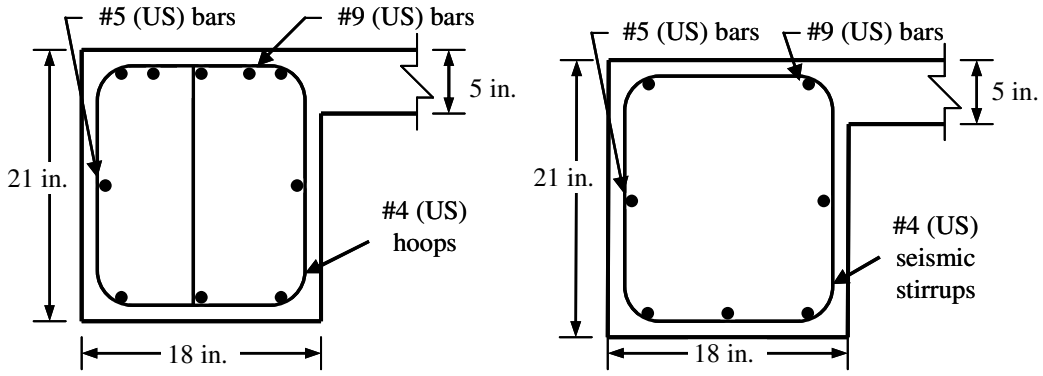

(a) Column face (b) Midspan

Fig. 3.11. Typical SMF 1st floor N-S exterior beam cross sections

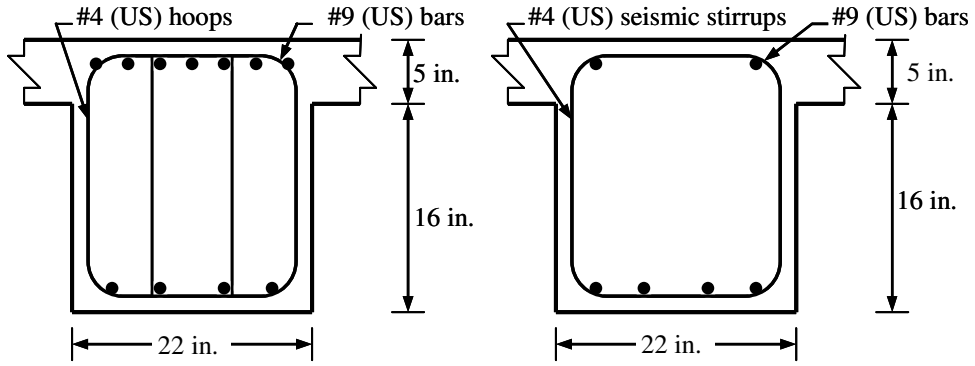

(a) Column face (b) Midspan

Fig. 3.12. Typical SMF 1st floor N-S interior beam cross sections

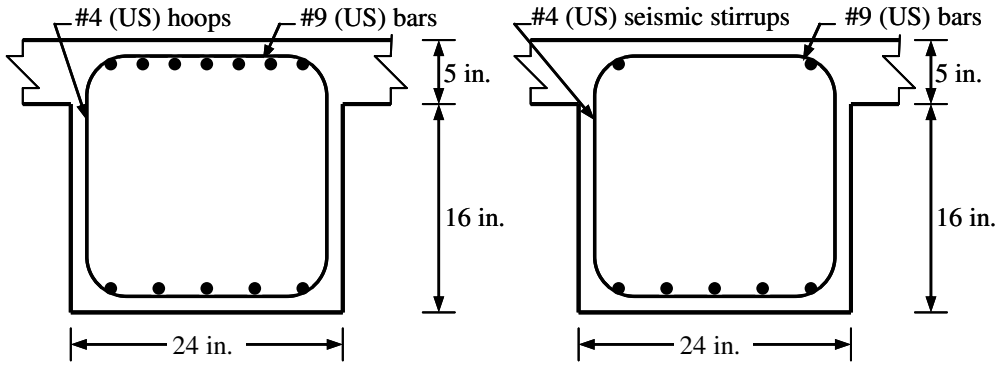

(a) Column face (b) Midspan

Fig. 3.13. Typical IMF 1st floor N-S interior beam cross sections

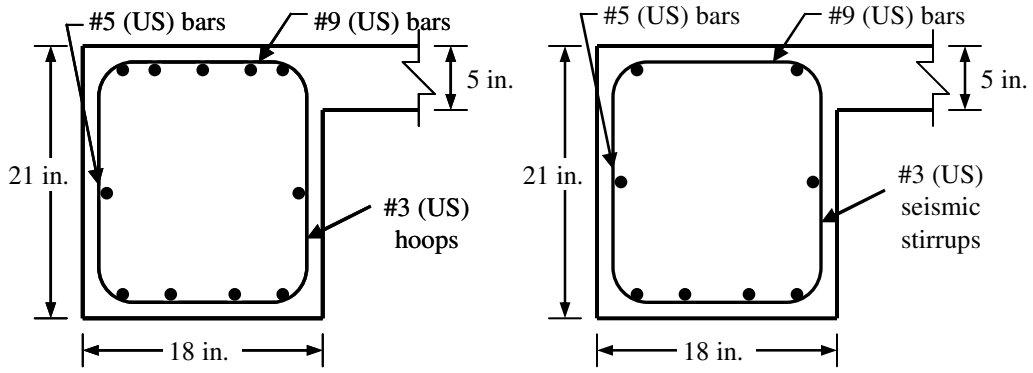

(a) Column face (b) Midspan

Fig. 3.14. Typical IMF 1st floor N-S exterior beam cross sections

3.5.3.2 Columns

The column reinforcement for each case study is shown in Fig. 3.15 and Tables 3.26 through 3.28. For the interior columns, the spacing within 24 in. from the joint face (per ACI 318 Section 21.4.4.4) is given, along with the reinforcement for the remaining length of the column. The longitudinal column reinforcement was the same for the columns of the same size. For CS1 and CS3, 12-#8 longitudinal bars provided a reinforcement ratio, ρ, of 1.4 percent, which is within the allowable range of 1 to 6 percent for SMF structures. The differences in the shear strength reduction factor, ϕ, from 0.75 to 0.85 and the load combinations did not have a significant effect. Enough strength was provided for CS2 by 8-#8 bars for both interior and exterior columns, with a reinforcement ratio, ρ, of 1.6 percent, as shown in Table 3.27. The interior columns carried higher axial load, while the exterior columns carried higher moments. The columns were determined to be non-slender according to ACI 318 Section 10.12.2.

The transverse hoop spacing for CS1 and CS3 was determined by the minimum cross-sectional area of rectangular hoop reinforcement for SMFs, which depends on hoop spacing, f'_c, and the confinement area in the column. Higher strength concrete requires smaller transverse hoop spacing. Within the zone where flexural yielding is likely to occur (24 in. from each joint face as defined by ACI 318), the minimum transverse spacing was 4 in. for 6000 psi concrete, 5 in. for 5000 psi concrete and 6 in.

for 4000 psi concrete. Outside this zone, the minimum spacing increases to 6 in., but was kept at 5 in. for consistency in the 5000 psi columns. The upper stories did not meet the strong-column weak-beam requirements; therefore, the flexural yield confinement reinforcement (#4 bars @ 4 in.) was provided throughout the length of the column per ACI 318 Section 21.4.2.3. The transverse reinforcement needed for confinement also provided enough strength for the shear demand. IMF columns have less strict confinement detailing requirements, and the spacing was increased to 8 in. throughout the entire column height in CS2.

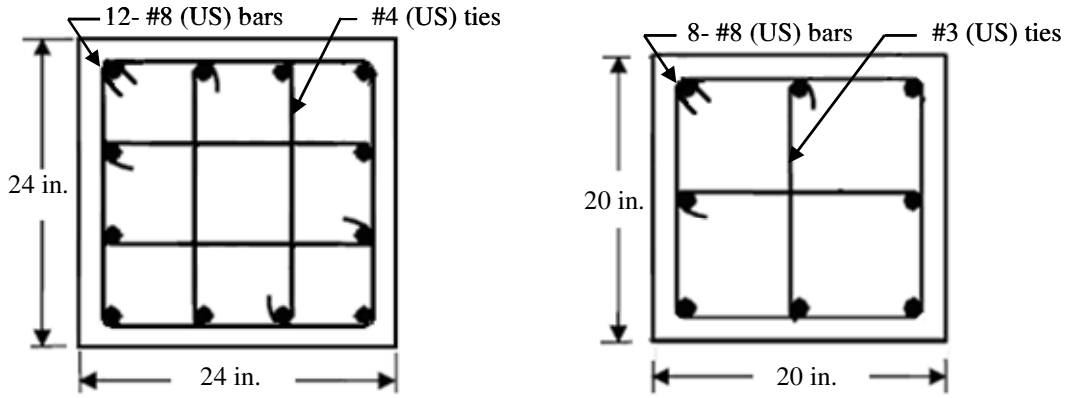

(a) CS1 and CS3 (b) CS2

Fig. 3.15. Column cross-sections

Table 3.26. CS1 column reinforcement

Column location	Story level	No. of bars Bar size (US)	ρ	f'_c (ksi)	Tie bar size (US) and spacing
Exterior	1 – 2	12-#8	0.014	5	#4@5”
	3 - 4	12-#8	0.014	4	#4@6”
Interior	1 – 2	12-#8	0.014	6	7-#4@4”/ #4@6”
	3 - 4	12-#8	0.014	5	#4@5”

Table 3.27. CS2 column reinforcement

Column location	Story level	No. of bars-Bar size (US)	ρ	f'_c (ksi)	Tie bar size (US) and spacing
Exterior	1 - 4	8-#8	0.016	4	#3@8”
Interior	1 - 4	8-#8	0.016	4	#3@8”

Table 3.28. CS3 column reinforcement

Column location	Story level	No. of bars-Bar size (US)	ρ	f'_c (ksi)	Tie bar size (US) and spacing
Exterior	1 – 3	12-#8	0.014	5	#4@5”
	4	12-#8	0.014	4	#4@4”
Interior	1 – 2	12-#8	0.014	6	7-#4@4”/ #4@6”
	3	12-#8	0.014	6	#4@4”
	4	12-#8	0.014	5	#4@5”

3.5.4 Column-to-Beam Strength Ratios

One of the most important factors in a building’s structural performance under seismic loading is the column-to-beam strength ratio (Dooley and Bracci 2001). For a SMF, the column-to-beam strength ratio must be greater than 1.2 according to ACI 318 Section 21.4.2.2 (discussed in Chapter 2). The N-S interior beams control for calculating the column-to-beam strength ratios to meet this requirement, as they are the strongest beams. The column-to-beam strength ratios for the first story are summarized in Table 3.29 for use in the performance analysis. The column-to-beam strength ratios are higher in the E-W direction because the beams are weaker in this direction. For strength contribution of the beams in the interior frames for CS2 and CS3, the nominal strength from a single joist was used.

Table 3.29. Column-to-beam strength ratios

Model direction	Case study	Column-to-beam strength ratio	
		Interior frame	Exterior frame
E-W	CS1	3.02	3.02
	CS2	4.98	1.13
	CS3	2.91	3.02
N-S	CS1	1.44	1.97
	CS2	0.80	1.13
	CS3	1.43	1.97

3.6 Lateral Frame Cost Estimate Comparisons

There are additional costs such as material, labor, and formwork associated with using a SMF over an IMF. Material costs estimates were taken from the *2007 RS Means Building Construction Cost Data* (RS Means 2007) for the different concrete compressive strengths as well as reinforcement (see Table 3.30). Concrete costs ranged from $108 to $130 per cubic yard (cyd) for the different compressive strengths in this study. Reinforcing steel costs for construction jobs with greater than 100 tons of steel was estimated at $1,310 per ton.

Table 3.30. RS Means material cost data

Material	Cost/ unit quantity
6 ksi concrete	$130/ cyd
5 ksi concrete	$114/ cyd
4 ksi concrete	$108/ cyd
Reinforcing steel	$1,310/ ton

Material quantities were determined for each of the case study buildings. The concrete quantities (in cubic yards) and associated costs using the RS material cost data are given in Table 3.31. CS1, designed as an SMF with interior beams in the E-W direction, had the highest concrete cost, not including labor. The concrete cost for CS1 was only about 10 percent higher than the IMF for CS2.

Since the reinforcement quantities were very similar for the SMF buildings (CS1 and CS3), the comparison only includes CS1 and CS2 (designed as an IMF). Reinforcement quantities include longitudinal bars and transverse hoops and ties. As shown in Table 3.32, the SMF buildings had more than twice as much column reinforcement as the IMF building due to the larger column area and smaller transverse reinforcement spacing. The beam reinforcement was similar between the two lateral frame types. The total cost increase for reinforcement quantities, not including placement, for a SMF versus an IMF was about 15 percent.

Table 3.31. Concrete quantities and costs

f'_c	Quantity (cyd)			Cost		
	CS1	CS2	CS3	CS1	CS2	CS3
6 ksi	32	-	32	$4,160	-	$4,160
5 ksi	811	-	778	$92,450	-	$88,690
4 ksi	776	1,501	742	$83,810	$162,110	$80,140
Total	**1,619**	**1,501**	**1,552**	**$180,420**	**$162,110**	**$172,990**

Table 3.32. Reinforcement quantities and costs

Location	Quantity (tons)		Cost	
	SMF	IMF	SMF	IMF
Columns	39	18	$51,090	$24,570
Beams	102	101	$133,620	$137,870
Total	**141**	**119**	**$184,710**	**$162,440**

Some additional structural costs that were not computed include forming and labor costs, which would vary for the type of lateral system. According to the *RS Means Construction Cost Data* (2007), forming can be one of the most expensive costs in construction. Beams with the same depth as the wide-module joists reduces forming costs uniformly for each case study; however, there is an additional cost in forming around the interior E-W beams for CS1, as well as the intersection area of the smaller

beams into the columns for the SMF buildings. The additional labor to place the smaller column tie spacing as well as the greater number of ties within the cross section should also be taken into consideration.

Professional cost estimates for constructing an ordinary moment frame (OMF) building and an SMF building were used in a study by Hayes et al. (2005), and the costs were determined to be 30 percent higher for the SMF. An OMF does not have any detailing requirements for seismic loading, while an IMF does have some detailing requirements. The difference in costs for an IMF compared to an SMF should be smaller than an OMF to an SMF. These costs, however, only include structural costs, which are generally a small portion of the overall cost of the building. The professional structural cost estimate in Hayes et al. (2005) was estimated to be about 10 percent of the total building costs.

4 NONLINEAR MODELING

4.1 Introduction

This section presents the modeling procedures for the case study buildings. The ZEUS-NL program developed by Elnashai et al. (2002) was used for the nonlinear analysis. The synthetic ground motion records developed by Rix and Fernandez (2006) for the Memphis, Tennessee, Lowlands for 2% and 10% probabilities of exceedance in 50 years were used in the nonlinear dynamic analysis. The following sections describe the analytical modeling assumptions and synthetic ground motions.

4.2 Analytical Models

4.2.1 General

ZEUS-NL is a finite element structural analysis program developed for eigenvalue, push-over, and nonlinear dynamic analysis. The program uses a fiber element model capable of representing the spread of inelasticity within the member cross-section and along the member length to model two-dimensional and three-dimensional steel, reinforced concrete (RC), and composite structures. Effects of geometric and material nonlinear behavior are taken into account through inelastic cyclic specified material constitutive relationships. Hueste and Bai (2007), Erbenik and Elnashai (2004), and Jeong and Elnashai (2005) have also investigated the seismic vulnerability of RC structures using ZEUS-NL.

The fiber element approach in ZEUS-NL divides the cross section of the material into individual layers as shown in Fig. 4.1. Each fiber is classified by an appropriate material stress-strain relationship (Karayannis 1994). The cubic element, used for modeling members, evaluates the element forces through numerical integration at the two Gauss points shown in Fig. 4.2.

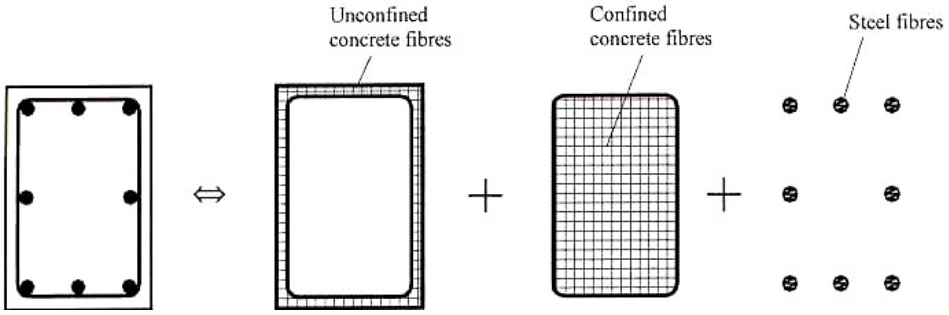

Fig. 4.1. Decomposition of a rectangular RC section (Elnashai et al. 2000)

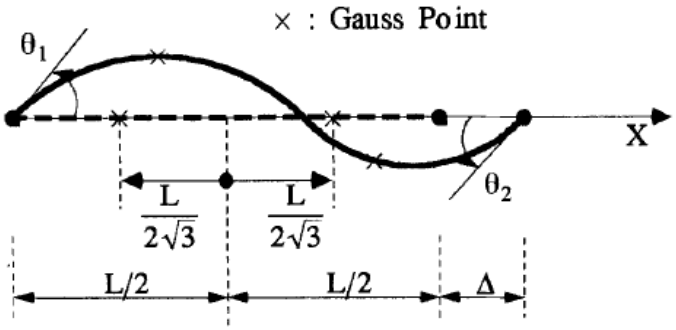

Fig. 4.2. Degrees of freedom and Gauss points of cubic formulation (Karayannis 1994)

In this study, the constant-average acceleration method (γ=0.5, β=0.25) for the Newmark integration scheme was used. A time step of 0.005 was used for the dynamic response history analysis, which matches the time interval for the synthetic ground motion records.

4.2.2 Building Model

Due to the symmetrical configuration and lack of irregularities, one-half of each case study structure was modeled as a two-dimensional frame. Both directions (N-S and E-W) were analyzed in ZEUS-NL to examine effects from the differences in structural member layout between the case studies. In the long direction (E-W), one exterior and one interior frame were linked with rigid truss elements that only allow lateral force and

displacement transfer between frames. In the short direction (N-S), one exterior and two interior frames were linked with rigid truss elements. The overall geometry of the frames modeled in each direction is shown in Fig. 4.3.

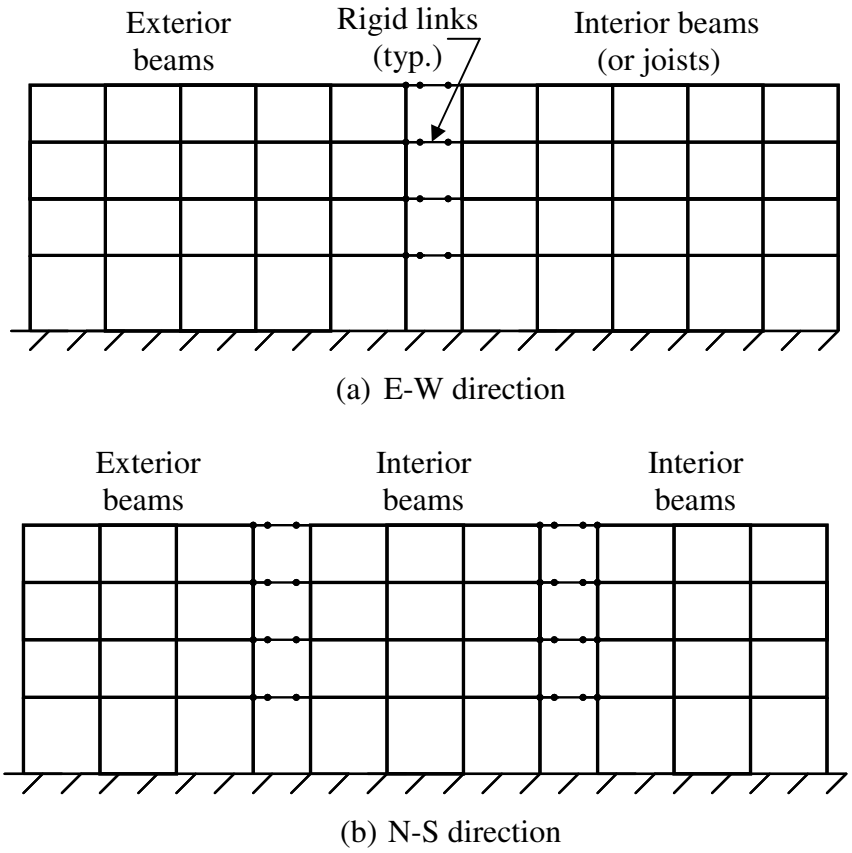

Fig. 4.3. ZEUS-NL 2-D frame models

The effective flange widths for the beams were determined from ACI 318 Section 8.10. Uncracked section properties were used because ZEUS-NL updates the member properties at each time step interval during the analysis as cracking occurs under loading. Modeling the 5 in. thick slab without the wide-module pan joists led to convergence problems in the finite element model. Therefore, single wide-module joists were included along the E-W interior frames in the CS2 and CS3 models to represent the additional stiffness contribution of the joists to the lateral system. The actual 6 in. web

width and 6 ft. effective flange width were used to model the joists based on the reasonable and conservative assumption that either a single joist would frame into the column or two joists would contribute half their stiffness if the column fell between the joists.

Beams were divided into 10 sub elements in the model, with three equally spaced nodes to apply loads. A node was placed at the column face to model the rigid zone, and additional nodes were placed near the joints to calculate the forces at the critical sections more accurately. Column elements were divided into nine elements with more elements concentrated near the joints. The global node locations for a typical frame are shown in Fig. 4.4, and a detailed view of the area in the rectangle is shown in Fig. 4.5. Rigid elements placed at beam-column joints (see Fig. 4.6) prevent joint distortion and moves inelastic behavior outside the joint region.

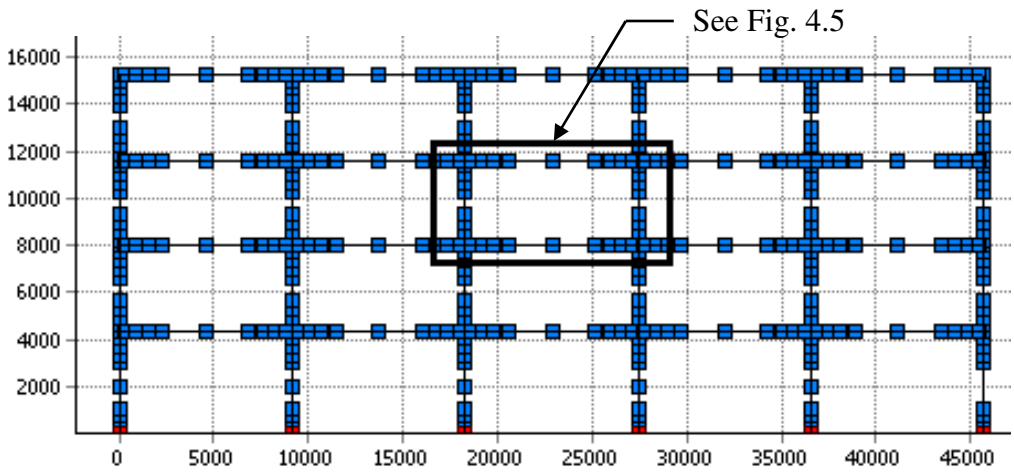

Note: 1 in. = 25.4 mm

Fig. 4.4. Typical frame geometry in ZEUS-NL (units in mm)

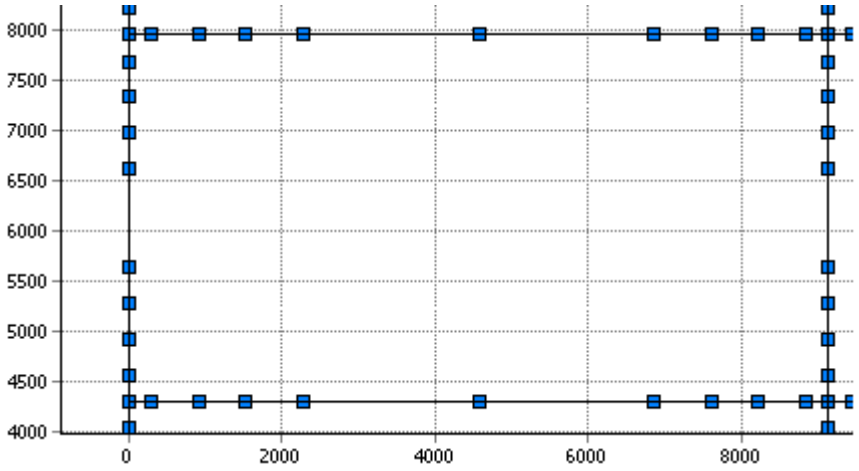

Note: 1 in. = 25.4 mm

Fig. 4.5. Typical node locations for modeling frame members (units in mm)

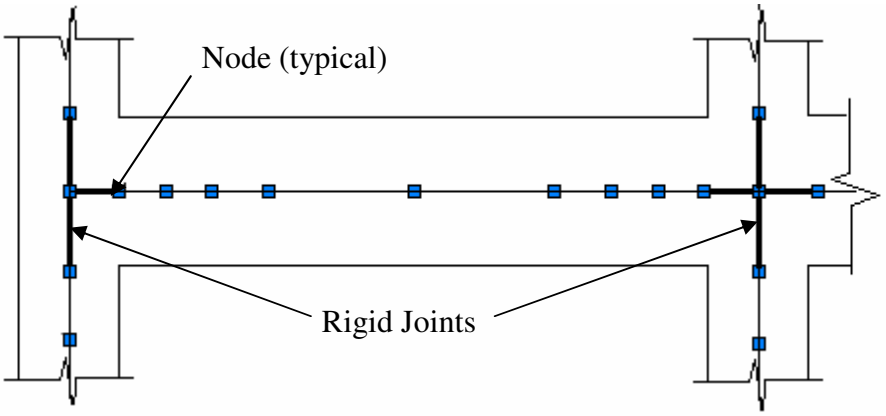

Fig. 4.6. Rigid joint definition

4.2.3 Individual Member Modeling

The structural members (beams, joists, columns, and rigid connections) were modeled using a cubic plastic three-dimensional element (cubic). To model the rigid joints, the joint element (joint) was used. Column cross-sections were defined using the RC rectangular section (rcrs), and the beam and wide-module joist cross-sections were defined using the RC T-section (rcts). The rigid joints were modeled with the rectangular solid section (rss) with high axial stiffness. The ZEUS-NL sections used in this study are

shown in Fig. 4.7. To model the reinforcing steel and rigid connections, the bilinear elasto-plastic material model with kinematic strain hardening (stl1) was used, while the uniaxial constant confinement concrete material model (conc2) was used to model the concrete. The material models for stl1 and conc2 are shown in Fig. 4.8.

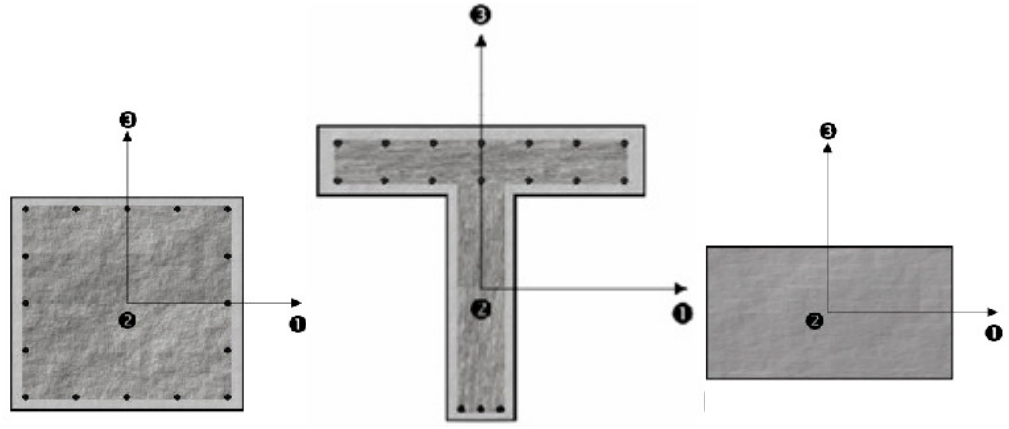

(a) RC retangular (rcrs) (b) RC flanged (rcts) (c) Rectangular solid (rss)

Fig. 4.7. ZEUS-NL element cross-sections (adapted from Elnashai et al. 2002)

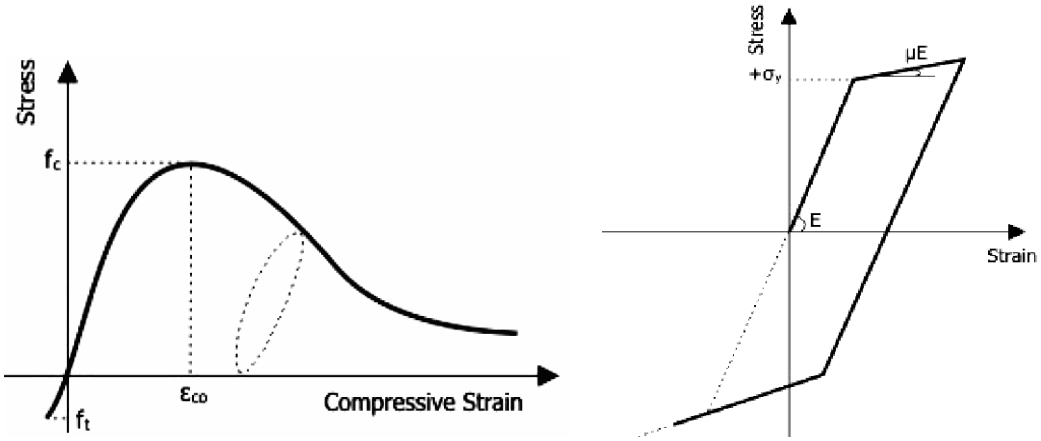

(a) Concrete (con2) (b) Steel (stl1)

Fig. 4.8. ZEUS-NL material models (Elnashai et al. 2002)

The stl1 parameters are Young's modulus (E), yield strength (σ_y), and a strain-hardening parameter (μ). Input parameters for the conc2 model include compressive strength (f'_c), tensile strength (f_t), maximum strain (ε_{co}) and a confinement factor (k). The material modeling parameters and values are shown in Table 4.1. Confinement factors are discussed in the following section. The material properties for the rigid connections had very high values of E and σ_y to prevent yielding. Three sets of conc2 properties were used to model the three different concrete compressive strengths.

Table 4.1. ZEUS-NL material modeling parameter values

Material type	Parameter	Values
stl1 (Reinforcing steel)	E	200,000 N/mm^2 (29,000 ksi)
	σ_y	413 N/mm^2 (60,000 psi)
	μ	0.02
stl1 (Rigid connection)	E	6,890,000 N/mm^2 (1,000,000 ksi)
	σ_y	34,500 N/mm^2 (5,000,000 psi)
	μ	0.02
conc2 (4 ksi concrete)	f'_c	27.6 N/mm^2 (4000 psi)
	f_t	2.76 N/mm^2 (400 psi)
	ε_{co}	0.002
conc2 (5 ksi concrete)	f'_c	34.5 N/mm^2 (5000 psi)
	f_t	3.45 N/mm^2 (500 psi)
	ε_{co}	0.002
conc2 (6 ksi concrete)	f'_c	41.4 N/mm^2 (6000 psi)
	f_t	4.14 N/mm^2 (600 psi)
	ε_{co}	0.002

Note: See Fig. 4.8 for graphical description of variables.

4.2.4 Confinement Factors

ZEUS-NL uses a constant confinement factor, k, to model the effects of transverse confinement in the members based on the model by Mander et al. (1988). This factor is dependent on the transverse and longitudinal reinforcement, concrete

strength, and member dimensions. The confinement factor provides additional strength past the initial compressive strength, f'_c, and less steep stiffness degradation after the initiation of yielding in the stress-strain curve in Fig. 4.8. The confinement factor for a rectangular concrete section with axial compression forces is calculated as the ratio of the confined concrete compressive strength, f'_{cc}, to the unconfined concrete compressive strength, f'_{co}, and is calculated using the following equations (Mander et al. 1988).

$$f'_{cc} = f'_{co}\left(-1.254 + 2.254\sqrt{1+\frac{7.94 f'_l}{f'_{co}}} - 2\frac{f'_l}{f'_{co}}\right) \tag{4.1}$$

$$f'_l = k_e \rho f_{yh} \tag{4.2}$$

$$k_e = \frac{A_e}{A_{cc}} \tag{4.3}$$

$$A_e = \left(b_c d_c - \sum_{i=1}^{n}\frac{(w_i')^2}{6}\right)\left(1-\frac{s'}{2b_c}\right)\left(1-\frac{s'}{2d_c}\right) \tag{4.4}$$

$$A_{cc} = A_c\left(1-\rho_{cc}\right) \tag{4.5}$$

where:

f'_{co} = Unconfined concrete compressive strength
f'_l = Effective lateral confining stresses
k_e = Confinement effectiveness coefficient
f_{yh} = Yield strength of transverse reinforcement
A_e = Area of effectively confined core concrete
A_{cc} = Area of core within center lines of perimeter spiral or hoops excluding area of longitudinal steel
A_c = Area of core of section within center lines of perimeter spiral
b_c = Concrete core dimension to center line of perimeter hoop in x-direction
d_c = Concrete core dimension to center line of perimeter hoop in y-direction
w_i' = i^{th} clear transverse spacing between adjacent longitudinal bars
s' = Clear spacing between spiral or hoop bars
ρ_{cc} = Ratio of area of longitudinal steel to area of core of section

The type of moment frame had the largest effect on the value of *k*. The SMF case studies, CS1 and CS3, had confinement factors ranging from 1.27 to 1.43 for the different f'_c values and transverse reinforcement (TR) spacing in the columns as shown in Table 4.2. The CS2 columns had a smaller *k* value of 1.12 predominantly due to the larger TR spacing. These *k* values applied in both model directions. The beam confinement factors are shown in Tables 4.3 and 4.4 for the E-W and N-S directions. The *k* values changed for the different f'_c values, reinforcement, and beam sizes. The N-S beams were more heavily loaded and reinforced, and correspondingly had higher *k* values than the E-W beams. The concrete outside the transverse reinforcement was considered unconfined with a *k* equal to 1.0.

Table 4.2. ZEUS-NL column confinement factors

Case study	f'_c (ksi)	TR bar size (US) and spacing	Confinement factor, *k*
CS1 CS3	4	#4@6”	1.39
	5	#4@5”	1.40
	6	#4@4”	1.43
	6	#4@6”	1.27
CS2	4	#3@8”	1.12

Table 4.3. ZEUS-NL beam confinement factors (E-W)

Case study	Location	f'_c (ksi)	Story level	Confinement factor, *k*	
				Interior	Exterior
CS1	PHZ	5	1 – 2	1.16	1.16
		4	3 – 4	1.21	1.21
	OPHZ	5	1 – 2	1.00	1.00
		4	3 – 4	1.00	1.00
CS2	PHZ	4	1 – 4	1.12	-
	OPHZ	4	1 – 4	1.00	-
CS3	PHZ	5	1 – 3	1.16	-
		4	4	1.21	-
	OPHZ	5	1 – 3	1.00	-
		4	4	1.00	-

Table 4.4. ZEUS-NL beam confinement factors (N-S)

Case study	Location	f'_c (ksi)	Story level	Confinement factor, k	
				Interior	Exterior
CS1	PHZ	5	1 – 2	1.33	1.28
		4	3	1.40	1.41
		4	4	1.35	1.41
	OPHZ	5	1 – 2	1.10	1.05
		4	3	1.10	1.05
		4	4	1.10	1.05
CS2	PHZ	4	1 – 4	1.31	1.19
	OPHZ	4	1 – 4	1.14	1.00
CS3	PHZ	5	1 – 3	1.33	1.18
		4	4	1.40	1.20
	OPHZ	5	1 – 3	1.06	1.00
		4	4	1.06	1.00

4.2.5 Loads, Masses and Damping

The gravity loads were applied as point loads to the beams based on the tributary seismic weight (member self-weight, superimposed dead, and partition loads) using the approximate load path. ZEUS-NL cannot model distributed loads; therefore, equivalent point loads based on the concentrated load factors in Table 3-22a of the *AISC Steel Construction Manual* (2005) were used for the E-W floor members with a distributed tributary load, w (see Fig. 4.9). For the N-S beams, the tributary loads from the joists were applied directly as point loads. In the dynamic analysis, tributary masses were lumped at the beam-column joints using a lumped mass element (Lmass) to represent the seismic dead weight.

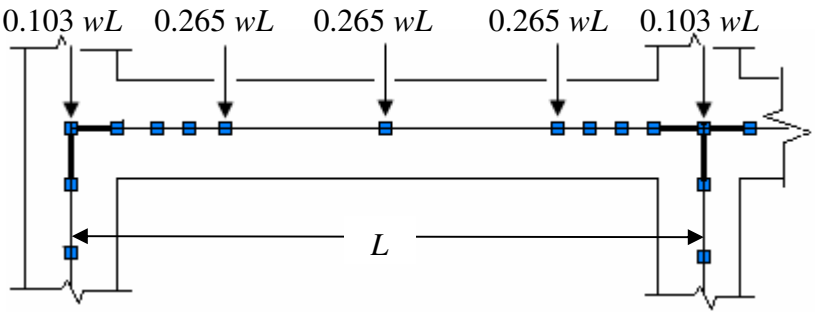

Fig. 4.9. Equivalent point loads applied to E-W members and joists

4.3 Synthetic Ground Motions

Representative strong ground motions for the New Madrid Seismic Zone are not available due to the lack of recorded strong motion data in this region. Therefore, synthetic ground motions developed by Rix and Fernandez (2006) for 2% and 10% probabilities of exceedance in 50 years earthquake scenarios were used in the dynamic analysis. These ground motions reflect attenuation relationships for soil sites in the Upper Mississippi Embayment with incorporated effects of epistemic and aleatory uncertainties in source, path, and site processes, as well as the effect of non-linear soil behavior. Spectral accelerations for five percent damping for each suite of ten ground motions are shown in Fig. 4.10. The acceleration time histories are given in Appendix A.

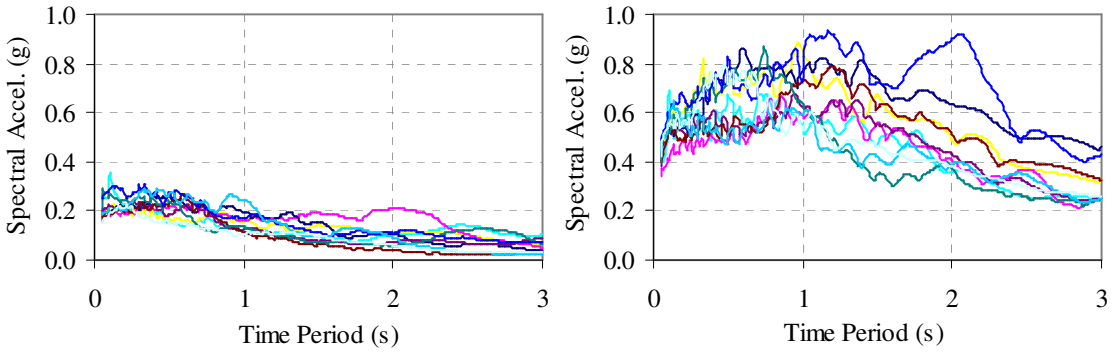

(a) 10% in 50 years (b) 2% in 50 years

Fig. 4.10. Spectral accelerations for Rix-Fernandez ground motions

To reduce computational time, the ground motions were truncated at the time point where the energy reached 95 percent of the total energy. This procedure was based on recommendations by Trifunac and Brady (1975) that the duration of the strong ground motion be the time interval remaining between the low and high 5 percent cut-off of the total energy. The equation to compute the total energy of a strong ground motion record is given in Eq. (4.6). Tables 4.5 and 4.6 show the ground motion record details.

$$E_{Total} = \int_0^t a^2(t)dt \tag{4.6}$$

where :

E_{Total} = Total energy of a ground motion record

$a(t)$ = Acceleration at time, t

Table 4.5. 10% in 50 years Rix-Fernandez ground motions

Ground motion	Peak ground acceleration (g)	Duration (s)	Duration of 95% energy (s)
475_01	0.1565	55.645	47.260
475_02	0.1235	55.390	46.490
475_03	0.1047	58.670	50.500
475_04	0.1309	85.770	74.035
475_05	0.1219	71.660	64.285
475_06	0.1046	71.710	64.320
475_07	0.1610	59.730	51.455
475_08	0.1710	60.095	51.795
475_09	0.1143	43.710	35.840
475_10	0.0975	44.530	37.785

Table 4.6. 2% in 50 years Rix-Fernandez ground motions

Ground motion	Peak ground acceleration (*g*)	Duration (s)	Duration of 95% energy (s)
2475_01	0.3139	55.365	46.200
2475_02	0.3352	54.800	45.320
2475_03	0.2748	58.945	51.970
2475_04	0.3266	84.245	72.615
2475_05	0.2915	73.355	67.145
2475_06	0.3076	72.330	65.670
2475_07	0.3380	59.530	51.540
2475_08	0.3734	57.975	49.400
2475_09	0.3298	43.595	35.045
2475_10	0.3390	43.565	36.815

5 ANALYSIS AND EVALUATION

5.1 Nonlinear Analysis

5.1.1 General

The building models were analyzed in both the N-S and E-W directions. The case studies have the most variation in the E-W direction due to the weaker gravity designed interior frames in CS2 and CS3. The main distinction in the N-S direction is between the special (CS1 and CS3) and intermediate (CS2) moment frames. Nonlinear static push-over analysis was conducted to obtain the overall capacity of each structure. Nonlinear dynamic response history analysis was also conducted for two sets of synthetic ground motion records.

5.1.2 Fundamental Periods

ZEUS-NL initially models members using uncracked section properties and updates the member section properties as cracking occurs under loading according to the relationships describing the material properties. As a result, the eigenvalue analysis for each case study produced uncracked fundamental periods. To determine more representative cracked fundamental periods, the displacement responses were used from an impulse load of 0.4g corresponding to the maximum peak ground acceleration (PGA) of the median 2% in 50 years ground motion.

The fundamental periods determined from the ZEUS-NL analysis were compared to those from the ETABS models with uncracked cracked section properties and cracked sections properties based on ACI 318 recommendations. The E-W fundamental periods are summarized in Table 5.1. The CS2 and CS3 ETABS models are more flexible in the long (E-W) direction because the ETABS models (used for design) only include the elements designed to resist lateral loads, whereas the ZEUS-NL models (used for nonlinear analysis) contain all structural members including gravity designed elements.

The differences in building stiffness can be seen by comparing the fundamental periods of each case study.

Table 5.1. Comparison of fundamental periods, T (s) (E-W)

Case Study	ZEUS-NL		ETABS	
	Cracked	Uncracked	Cracked	Uncracked
CS1	1.27	0.72	1.15	0.77
CS2	1.30	0.96	1.80	1.25
CS3	1.29	0.82	1.48	1.00

The fundamental periods for the ZEUS-NL models in the N-S direction are given in Table 5.2. The structures are slightly stiffer in this direction, as indicated by the shorter periods. The smaller columns with a lower f'_c in CS2 produced a more flexible structure and longer periods than CS1 and CS3 in this direction.

Table 5.2. ZEUS-NL fundamental periods, T (s) (N-S)

Case study	Cracked	Uncracked
CS1	1.13	0.68
CS2	1.25	0.82
CS3	1.08	0.66

5.1.3 Push-over Analysis

Two vertical distributions of lateral loads were used in the static push-over analysis: a vertical distribution proportional to the fundamental mode shape and a rectangular uniform distribution (see Fig. 5.1). These load patterns were intended to produce a lateral response envelope for the structures. The load percentages based on the first mode shape from the eigenvalue analysis shown in Fig. 5.1(a) vary slightly by case study and analysis direction. Each modal pattern resembles an inverted triangular shape and is referred to as the triangular push-over in the following sections. A load control

phase was used in the push-over analysis to develop the load deflection curve until convergence difficulties emerged and the ZEUS-NL analysis automatically switched to a displacement control phase to capture the post-yield behavior of the structure.

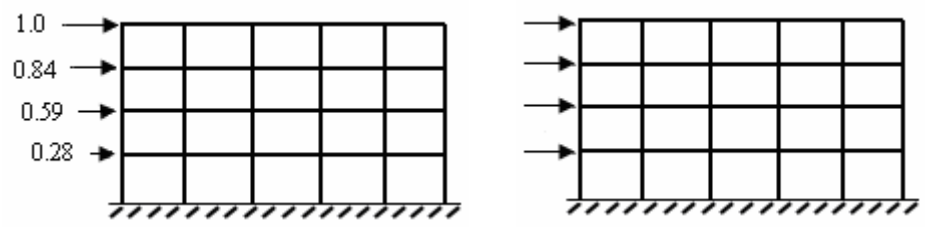

(a) Modal (inverted triangular) pattern (b) Rectangular pattern

Fig. 5.1. Load patterns for push-over analysis

The push-over curves for the E-W direction are shown in Fig. 5.2. The horizontal axis displays the building drift, defined as the top story displacement divided by the total building height. The vertical axis is the base shear ratio, *V/W*, where *V* is the total base shear force and *W* is the seismic weight of the building. The rectangular pattern shows more strength capacity for each case study than the triangular pattern. In each case, CS1 with interior moment frames, showed greater initial stiffness and strength than CS2 and CS3. Although CS2 and CS3 had the same interior gravity designed wide-module joists, the larger columns with special seismic detailing in CS3 exhibited more ductility.

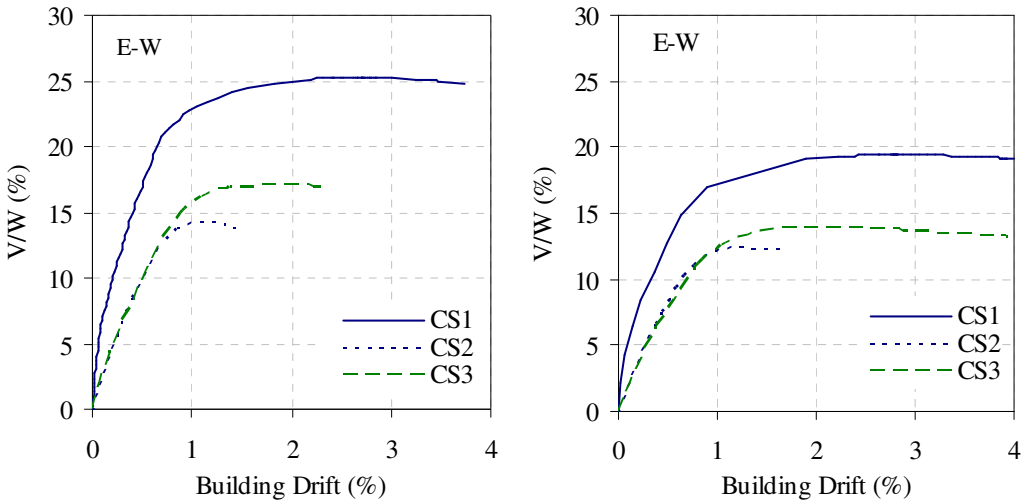

(a) Rectangular push-over (b) Triangular push-over

Fig. 5.2. Push-over results (E-W)

Fig. 5.3 shows the push-over curves for the case studies in the N-S direction. The similarity in the push-over curves of CS1 and CS3 is due to the same beam and column sizes in the N-S frames. CS3 had slightly different f'_c values and reinforcement, which may explain the difference in performance past the yield point. The negative slope after initial yielding in the CS2 push-over curve signifies a soft first story mechanism. The cut-off points of the CS2 curves corresponds to a strength degradation of twenty percent.

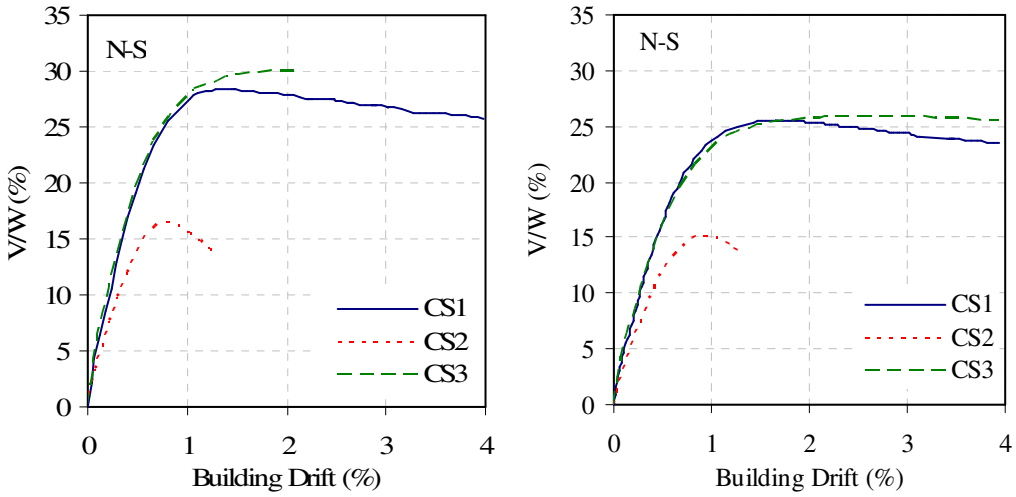

(a) Rectangular push-over (b) Triangular push-over

Fig. 5.3. Push-over results (N-S)

5.1.4 Dynamic Analysis

The nonlinear dynamic analysis was conducted with two suites of synthetic ground motions developed by Rix and Fernandez (2006) for 2% and 10% probabilities of exceedance in 50 years hazard levels. Each suite contained 10 ground motions, and the median response from each ground motions suite was used to compare the case study responses. The same trends noted for the static analysis were observed when comparing the case study dynamic response values.

Table 5.3 gives the maximum dynamic response for each case study for the 10% in 50 years ground motion records in the E-W direction, and Table 5.4 gives the maximum dynamic response for the 2% in 50 years ground motion records. The median response is provided in the tables for the median maximum base shear ratio, *V/W*, and median maximum building drift for each case study.

Table 5.3. E-W maximum building drift and base shear ratio (10% in 50 years)

Ground motion	*V/W* (%)			Max. building drift (%)		
	CS1	CS2	CS3	CS1	CS2	CS3
475_01	12.80	11.50	14.78	0.54	0.94	0.96
475_02	13.21	9.61	12.27	0.62	0.56	0.67
475_03	16.44	9.04	15.42	1.22	1.10	1.22
475_04	16.16	9.99	14.47	0.98	1.06	1.15
475_05	12.91	10.38	11.24	0.51	0.59	0.62
475_06	10.38	5.76	10.47	0.34	0.36	0.39
475_07	13.07	7.61	11.04	0.49	0.51	0.50
475_08	15.26	9.76	12.65	0.71	0.63	0.87
475_09	14.43	8.63	12.69	0.60	0.61	0.72
475_10	10.62	7.28	11.83	0.44	0.57	0.60
Median	**13.14**	**9.32**	**12.46**	**0.57**	**0.60**	**0.69**

Table 5.4. E-W maximum building drift and base shear ratio (2% in 50 years)

Ground motion	*V/W* (%)			Max. building drift (%)		
	CS1	CS2*	CS3	CS1	CS2*	CS3
2475_01	19.59	12.79	16.64	2.35	2.34	2.56
2475_02	20.46	16.74	17.83	2.20	1.12	2.94
2475_03	18.50	11.32	16.45	2.85	2.35	3.01
2475_04	21.82	20.90	18.23	6.34	3.09	5.67
2475_05	18.60	13.73	17.89	2.64	2.81	2.53
2475_06	19.04	12.50	16.76	2.67	1.91	2.34
2475_07	21.88	23.53	20.45	1.85	1.33	1.86
2475_08	19.99	12.30	19.78	2.33	1.78	2.92
2475_09	19.07	10.60	18.18	2.47	1.26	2.68
2475_10	20.28	24.75	18.72	3.51	3.59	3.96
Median	**19.79**	**13.26**	**18.03**	**2.55**	**2.13**	**2.80**

*Reported results are values immediately before model became unstable

The median E-W responses for the 10% in 50 years motions show that CS1 had greater shear demands and lower drifts than CS2 and CS3. The CS3 shear demand was close to that of CS1, while the CS2 shear demand was significantly lower. For the 2% in 50 years motions, the CS2 nonlinear analysis stopped when the demands exceeded the capacity of the wide-module joists and large plastic rotation demands occurred leading

to instability. Only one of the ten ground motion records ran completely through. The reported E-W 2% in 50 years results for CS2 are the values computed immediately before the instabilities. The wide-module joists in CS3 withstood the 2% in 50 years ground motions without exceeding their capacity, which can be attributed to the higher ductility and strength in the SMF columns. The 2% in 50 years performance response showed a similar trend for the case studies to that of the 10% in 50 years response. However, the wide-module joists exceeded their capacity at lower maximum drifts in CS2 than the maximum response for CS1 or CS3.

The dynamic results for the 10% in 50 years ground motion records are given in Table 5.5 for the N-S direction and in Table 5.6 for the 2% in 50 years ground motion records. As in the push-over analysis, the N-S direction showed greater shear demands than the E-W direction for each case study.

Table 5.5. N-S maximum building drift and base shear ratio (10% in 50 years)

Ground motion	*V/W* (%)			Max. building drift (%)		
	CS1	CS2	CS3	CS1	CS2	CS3
475_01	15.86	15.63	13.73	0.42	0.68	0.38
475_02	16.44	12.75	16.08	0.46	0.47	0.49
475_03	19.68	16.59	19.76	0.78	0.95	0.66
475_04	20.08	16.03	20.78	0.75	0.78	0.77
475_05	14.39	12.12	16.94	0.42	0.41	0.45
475_06	15.69	10.64	15.89	0.40	0.37	0.48
475_07	17.34	12.16	17.67	0.53	0.49	0.52
475_08	20.58	14.47	21.01	0.77	0.61	0.75
475_09	19.27	14.12	20.49	0.69	0.59	0.79
475_10	18.83	11.05	15.69	0.59	0.34	0.44
Median	**18.08**	**13.43**	**17.31**	**0.56**	**0.54**	**0.50**

Table 5.6. N-S maximum building drift and base shear ratio (2% in 50 years)

Ground motion	*V/W* (%)			Max. building drift (%)		
	CS1	CS2	CS3	CS1	CS2	CS3
2475_01	26.64	17.04	25.24	1.96	1.62	1.48
2475_02	26.22	16.79	26.87	2.69	2.27	2.25
2475_03	25.87	16.51	27.55	2.07	1.95	1.91
2475_04	28.43	17.39	28.43	3.14	7.75	2.31
2475_05	26.84	16.55	27.52	2.96	3.00	1.77
2475_06	27.87	16.47	27.78	2.12	2.61	1.85
2475_07	25.78	16.47	25.16	1.55	1.41	1.45
2475_08	25.66	17.02	28.21	3.30	2.89	3.02
2475_09	25.85	16.90	26.22	1.46	2.08	1.38
2475_10	26.08	17.01	26.15	1.48	4.87	1.33
Median	**26.15**	**16.85**	**27.20**	**2.10**	**2.44**	**1.81**

With moment frames along each bay in the N-S direction, the ground motion records ran completely in the CS2 2% in 50 years analysis and can be more directly compared with the other case studies. The N-S 10% in 50 years median responses were similar to the E-W direction. For the 2% in 50 years median response, however, CS3 showed slightly higher median base shear demands and lower drifts than CS1.

5.1.5 Comparison of Push-over and Dynamic Results

The push-over response curves along with the maximum dynamic responses for each ground motion for the E-W direction are provided in Fig. 5.4. Each discrete data point represents the maximum dynamic response (maximum base shear and the maximum building drift) for a ground motion record. The median ground motion responses for both the 10% and 2% in 50 years motions are circled in each of the figures. The legend for CS1 in Fig. 5.4. also applies to CS2 and CS3.

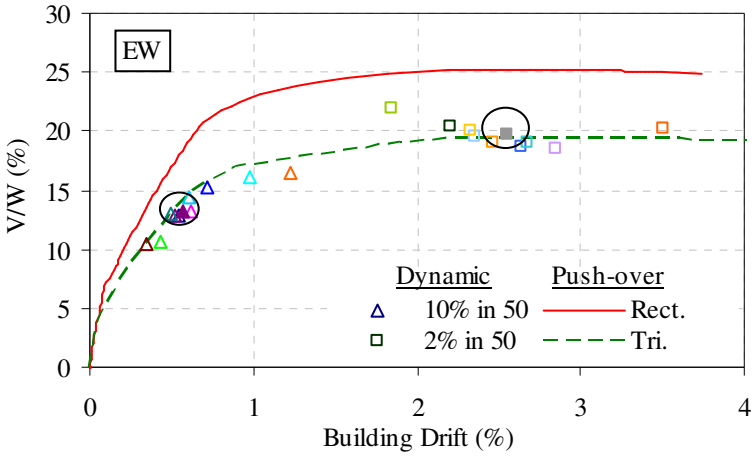

(a) CS1

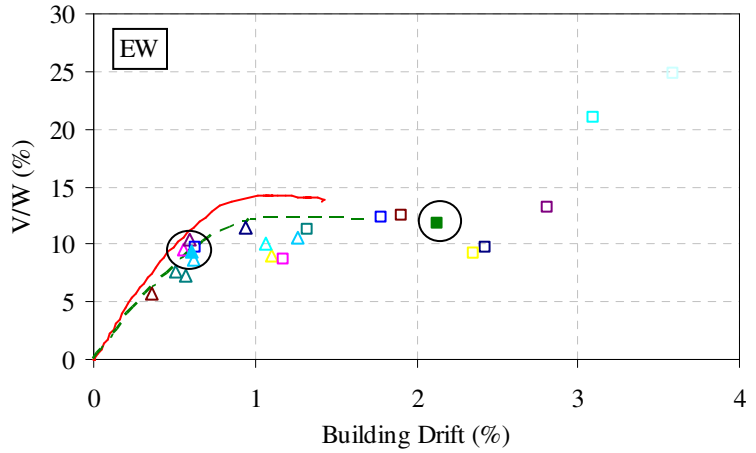

(b) CS2

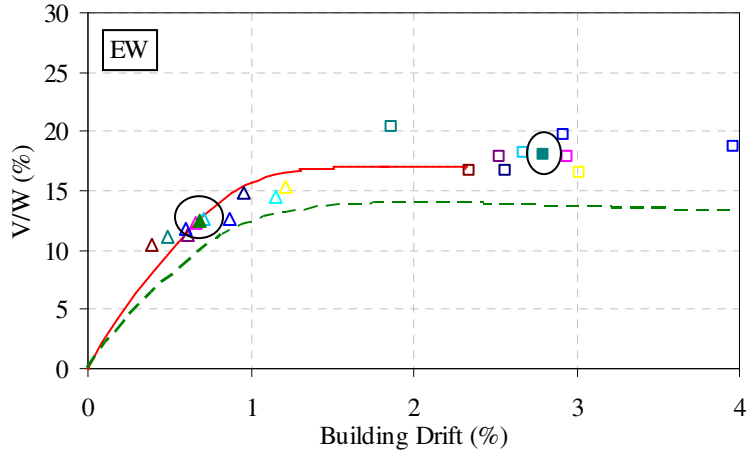

(c) CS3

Fig. 5.4. Comparison of push-over and dynamic analyses (E-W)

The dynamic results generally fell between the triangular and rectangular push-over curves, giving an approximate envelope of the structural response. While the CS3 push-over curve in the E-W direction showed a similar initial trend to CS2, the dynamic results indicated that with stronger columns and special seismic detailing, CS3 actually had additional lateral resistance for a given drift demand under earthquake loading.

In the N-S direction, the dynamic response is more consistent with the static response. Fig. 5.5 shows the comparison of the push-over curves in the N-S direction with the maximum dynamic response for each of the twenty ground motion records. The push-over analysis shows a story mechanism forming in the N-S direction for CS2, but the dynamic results do not follow the strength reduction observed in the push-over analysis. For this particular structure, the maximum drift response for the 2% in 50 years hazard occurred at lower shear values following the story mechanism, while the maximum shear occurred directly before the story mechanism occurred. This is not shown in the plots of maximum drift versus maximum base shear, but would be reflected by a plot of maximum drift versus the corresponding base shear.

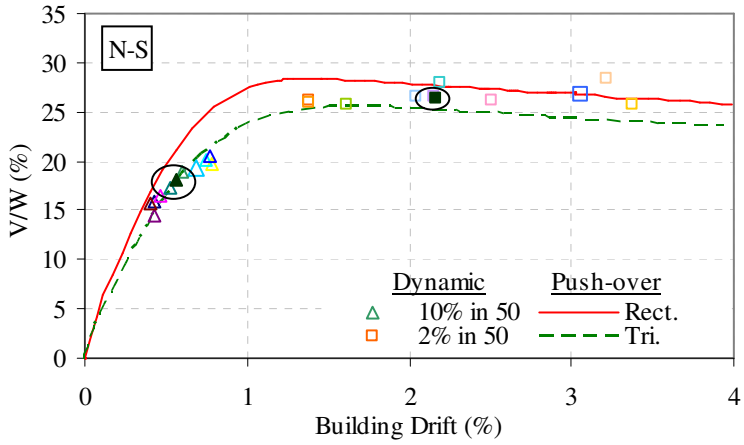

(a) CS1

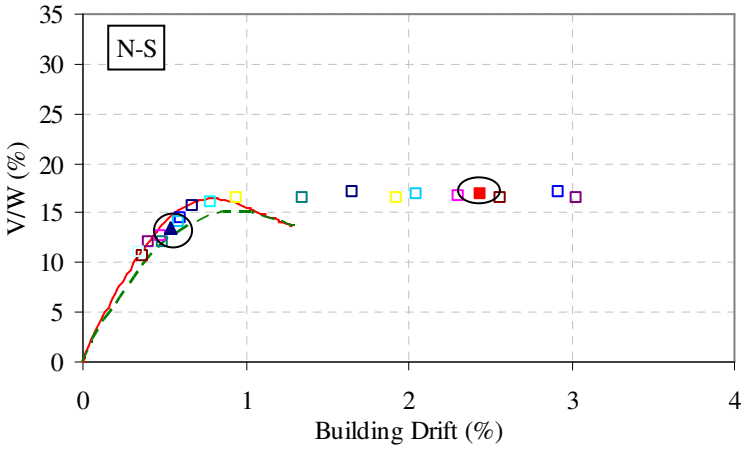

(b) CS2

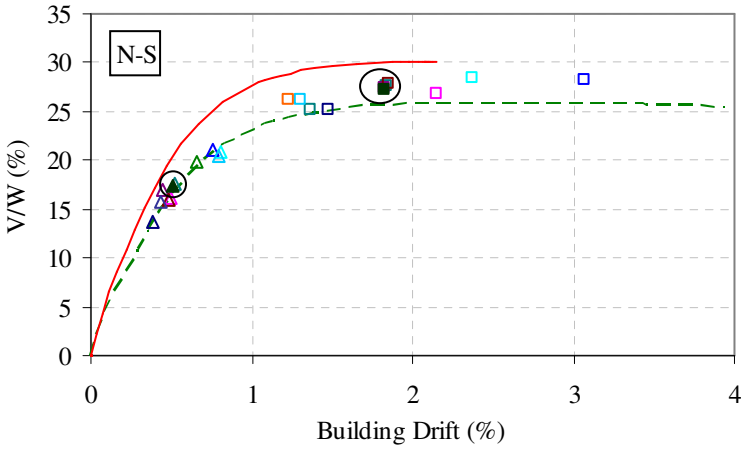

(c) CS3

Fig. 5.5. Comparison of push-over and dynamic analyses (N-S)

5.2 Performance Evaluation

5.2.1 General

The structural performance criteria provided in FEMA 356 (ASCE 2000) were used for both global-level and member-level evaluations of the case study buildings. FEMA 356 provides suggested interstory drift values as a guideline for assessing global structural performance, while recommended plastic rotation limits specify criteria for more detailed member-level evaluations.

FEMA 356 safety objectives are designated to meet a target performance level at a specific hazard level. Performance levels are used to describe the maximum damage to a structure. The performance levels included in this study are Life Safety (LS) and Collapse Prevention (CP). LS performance is defined as significant damage has occurred, but there is still some margin against structural collapse. CP performance is when a structure does not have a margin against collapse after an earthquake and can just barely support gravity loads. The Basic Safety Objective (BSO) suggested by FEMA 356 is LS performance for the 10% in 50 years hazard level and CP performance for the 2% in 50 years hazard level. Meeting either of these performances without the other is considered a Limited Objective.

5.2.2 Global-level Limits

5.2.2.1 General

FEMA 356 suggests a typical value of 2% interstory drift associated with LS performance level and 4% drift for CP performance for concrete frames. These drift values are suggested for structures that are properly designed for seismic loadings, such as SMFs. The IMF case study, with a column-to-beam strength ratio of less than 0.8, would not necessarily qualify. Ramamoorthy et al. (2006) proposed using reduced interstory drift values of 1% and 2% interstory drift for the LS and CP performance levels, respectively, for buildings with insufficient column strength and section detailing, based on the FEMA 356 member-level rotations. These interstory drift limits (see Table

5.7) were compared to the maximum interstory drifts from the ZEUS-NL response history analysis using the median ground motion records for both hazard levels, shown in Appendix B.

Table 5.7. Global interstory drift values for concrete frame elements

Structural performance level	Drift (%)		
	CS1	CS2	CS3
Life Safety (LS)	2	1	2
Collapse Prevention (CP)	4	2	4

5.2.2.2 E-W Direction

A comparison of the E-W maximum interstory drifts for the median 2% and 10% in 50 years ground motions with the global drift limits is shown in Fig. 5.6. The median maximum interstory drifts for the 10% in 50 years hazard were less than 1% for each case study, meeting both the suggested FEMA 356 2% drift value as well as the modified 1% drift value for LS performance. The CP drift value of 4% was also met for the CS1 and CS3 2% in 50 years response.

The dynamic analysis for the CS2 model using the median 2% in 50 years motion did not complete due to model instability when the capacities of the wide-module joists were exceeded and large plastic rotations occurred. The response of the building prior to the instability did not meet the modified CP drift value of 2%. Because the analysis was not completed for the entire 2% in 50 years ground motion record, the CS2 response is denoted by a dotted line in Fig. 5.6. CS1 and CS3 met both the LS and CP global drift values for the respective hazard levels, satisfying the BSO for the global response evaluation, while CS2 only met the limited performance objective of LS for the 10% in 50 years hazard.

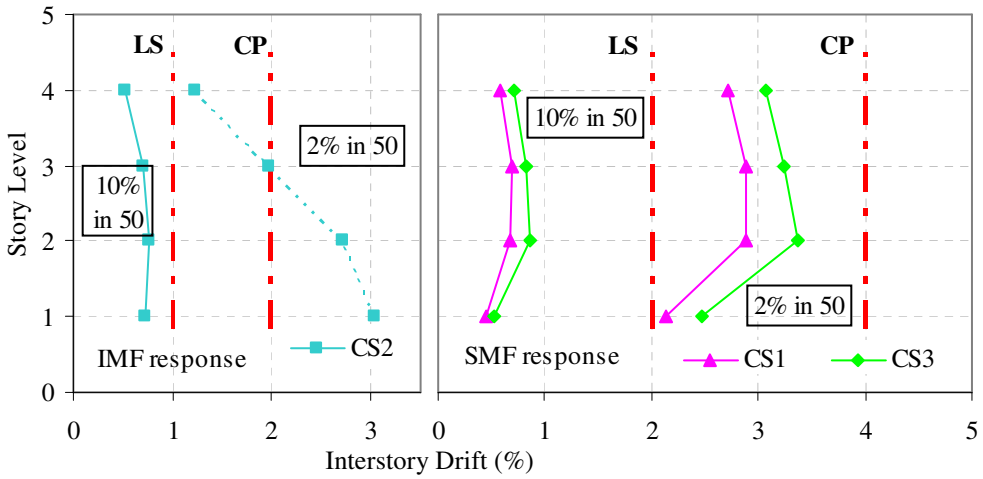

Fig. 5.6. Median maximum interstory drifts (E-W)

5.2.2.3 N-S Direction

Fig. 5.7 shows the maximum interstory drifts for the median 2% and 10% in 50 years ground motions for the N-S frames, along with the FEMA 356 global drift values. The median 10% in 50 years maximum interstory drifts were also less than 1% for each case study in the N-S direction, achieving LS performance for all case studies. The story mechanism that formed at the first story of CS2 resulted in a predicted maximum median interstory drift of more than 7%, exceeding the CP performance limit. However, the median maximum interstory drifts were less than 3% for CS1 and CS3, and satisfied the suggested 4% CP drift value for well-detailed RC frames. The N-S global results matched the E-W results for the BSO evaluation with only CS2 not satisfying CP performance for the 2% in 50 years hazard.

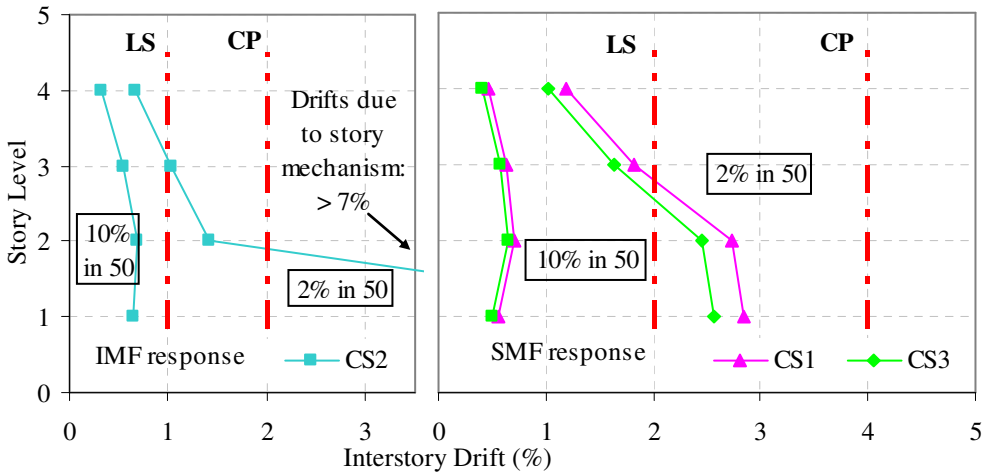

Fig. 5.7. Median maximum interstory drifts (N-S)

5.2.3 Member-level Limits

5.2.3.1 General

The FEMA 356 member-level evaluation is based on plastic rotation limits for RC moment frames. This more detailed evaluation uses rotation acceptance criteria determined for the LS and CP performance levels based on member reinforcement ratios, confinement, and shear demand-to-strength ratios for beam and columns controlled by flexure. The ZEUS-NL plastic rotations for the ground motion record nearest the median response for each story were used in the evaluation. Plastic rotation, θ_p, is determined as the inelastic rotation beyond the yield rotation. The yield rotation is based on the moment-area theorem. The following expressions are used to determine these values.

$$\theta_p = \theta_{\max} - \theta_y \tag{5.1}$$

$$\theta_y = \frac{M_y L}{6 E_c I_{cr}} \tag{5.2}$$

where:

θ_p = Plastic rotation (rad.)
θ_{max} = Maximum rotation (rad.)

θ_y = Yield rotation (rad.)
M_y = Design moment (kip-in.)
E_c = Modulus of elasticity of concrete (ksi)
I_{cr} = Cracked section moment of inertia (in.^{4})
L = Length of member (in.)

FEMA 356 has stricter acceptance criteria for members with poor seismic detailing based on the transverse reinforcement (TR) spacing. If the plastic hinge zone TR spacing is less than $d/3$ (where d is the effective member depth) and the strength provided by the hoops is at least three-fourths of the design shear, then the member is considered conforming (C). If a member does not meet this classification, it is nonconforming (NC) with significantly smaller rotation limits for each limit state.

Members are also classified as primary or secondary for rotation acceptance limits. The main lateral resisting elements such as the moment frame beams and columns are primary elements, whereas the interior gravity designed wide-module joists are secondary elements. Secondary elements have larger rotation limits than elements originally designed for lateral resistance, although the increase is usually offset if the members are also nonconforming.

5.2.3.2 E-W Direction

The FEMA 356 plastic rotation limits are summarized in Tables 5.8 through 5.10 for the columns and exterior and interior floor members in the E-W frames. These tables also contain the median maximum plastic rotation for each case study and story level for both the 10% and 2% in 50 years hazards. The bolded rotations exceeded the corresponding limit state member rotation limits, and the CS2 rotations in italics were the last computed values before the model became unstable. The column rotation limits depended on the TR spacing, f'_c and the axial load. The CS2 columns were classified as NC due to the larger TR spacing, with smaller rotation limits than the CS1 and CS3 limits. The interior wide-module joists in CS2 and CS3 were also classified as NC; however, as secondary members, the rotation limits were not always lower than the CS1 moment frame interior floor member limits.

Table 5.8. Column plastic rotations (E-W)

Case study	Story level	TR	FEMA 356 limit (rad.)		Max. plastic rot. (rad.)	
			LS	CP	10% in 50 yrs	2% in 50 yrs
CS1	1	C	0.0150	0.0200	0.0060	**0.0334**
	2	C	0.0150	0.0200	0.0062	**0.0273**
	3	C	0.0150	0.0200	0.0054	**0.0242**
	4	C	0.0150	0.0200	0.0050	**0.0223**
CS2	1	NC	0.0031	0.0041	**0.0074**	***0.0784***
	2	NC	0.0038	0.0048	**0.0067**	***0.0319***
	3	NC	0.0046	0.0056	**0.0063**	***0.0259***
	4	NC	0.0050	0.0060	0.0034	***0.0186***
CS3	1	C	0.0150	0.0200	0.0068	**0.0401**
	2	C	0.0150	0.0200	0.0064	**0.0390**
	3	C	0.0150	0.0204	0.0055	**0.0336**
	4	C	0.0150	0.0200	0.0052	**0.0306**

Note: 1. Rotation in bold exceeded the corresponding limit state limits
2. Rotations in italics were the last computed values before the model became unstable

Table 5.9. Exterior frame floor member plastic rotations (E-W)

Case study	Story level	TR	FEMA 356 limit (rad.)		Max. plastic rot. (rad.)	
			LS	CP	10% in 50 yrs	2% in 50 yrs
CS1	1	C	0.0190	0.0247	0.0036	**0.0334**
	2	C	0.0190	0.0247	0.0027	**0.0273**
	3	C	0.0188	0.0247	0.0013	0.0242
	4	C	0.0188	0.0247	0.0004	0.0223
CS2	1	C	0.0187	0.0244	0.0040	**0.0249**
	2	C	0.0187	0.0244	0.0027	0.0197
	3	C	0.0200	0.0250	0.0013	0.0155
	4	C	0.0200	0.0250	0.0004	0.0091
CS3	1	C	0.0190	0.0245	0.0047	**0.0274**
	2	C	0.0190	0.0245	0.0032	**0.0292**
	3	C	0.0190	0.0245	0.0036	0.0216
	4	C	0.0188	0.0244	0.0027	0.0216

Table 5.10. Interior frame floor member plastic rotations (E-W)

Case study	Story level	TR	FEMA 356 limit (rad.)		Max. plastic rot. (rad.)	
			LS	CP	10% in 50 yrs	2% in 50 yrs
CS1	1	C	0.0193	0.0247	0.0050	**0.0262**
	2	C	0.0193	0.0247	0.0045	**0.0280**
	3	C	0.0194	0.0247	0.0036	**0.0257**
	4	C	0.0194	0.0247	0.0026	0.0235
CS2	1	NC	0.0180	0.0271	0.0041	***0.0733***
	2	NC	0.0180	0.0271	0.0037	***0.0273***
	3	NC	0.0180	0.0271	0.0030	*0.0226*
	4	NC	0.0180	0.0271	0.0000	*0.0157*
CS3	1	NC	0.0171	0.0257	0.0024	**0.0357**
	2	NC	0.0171	0.0257	0.0014	**0.0342**
	3	NC	0.0171	0.0257	0.0005	0.0190
	4	NC	0.0160	0.0240	0.0000	0.0169

For the 10% in 50 years hazard, the CS1 and CS3 median maximum response values were within the beam and column plastic rotation limits for LS performance. However, CS2 did not meet the stricter NC column rotation limits for LS performance for the 10% in 50 years ground motions. The locations in CS2 where the column LS performance limits were exceeded for the median 10% in 50 years motion are shown in Fig. 5.8.

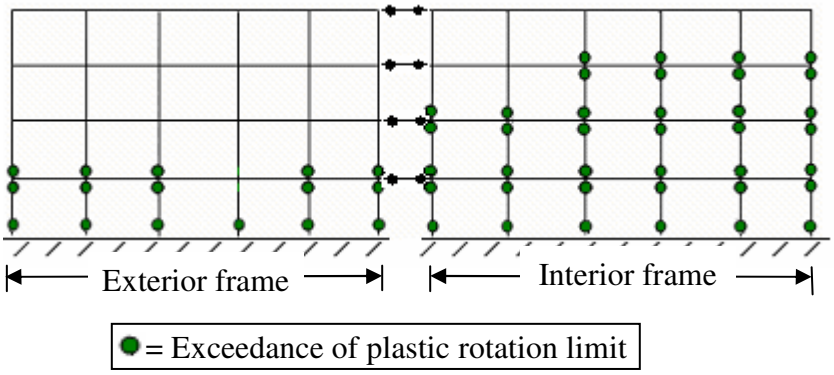

Fig. 5.8. Locations where LS plastic rotation limits are exceeded in CS2 (E-W)

All the case studies exceeded the CP performance level for the 2% in 50 years motions; however, the degree of exceedance varied significantly between the SMF and IMF buildings. The column plastic rotations of the SMF case studies were at most twice as large as the corresponding CP rotation limits, compared to up to 18 times the CP limits for the CS2 columns. As a result, none of the case studies met the BSO in the E-W direction, and only CS1 and CS3 met the LS limited performance objective. Fig. 5.9 shows the locations where the CP rotation limits were exceeded for the median 2% in 50 years ground motion in each of the case studies.

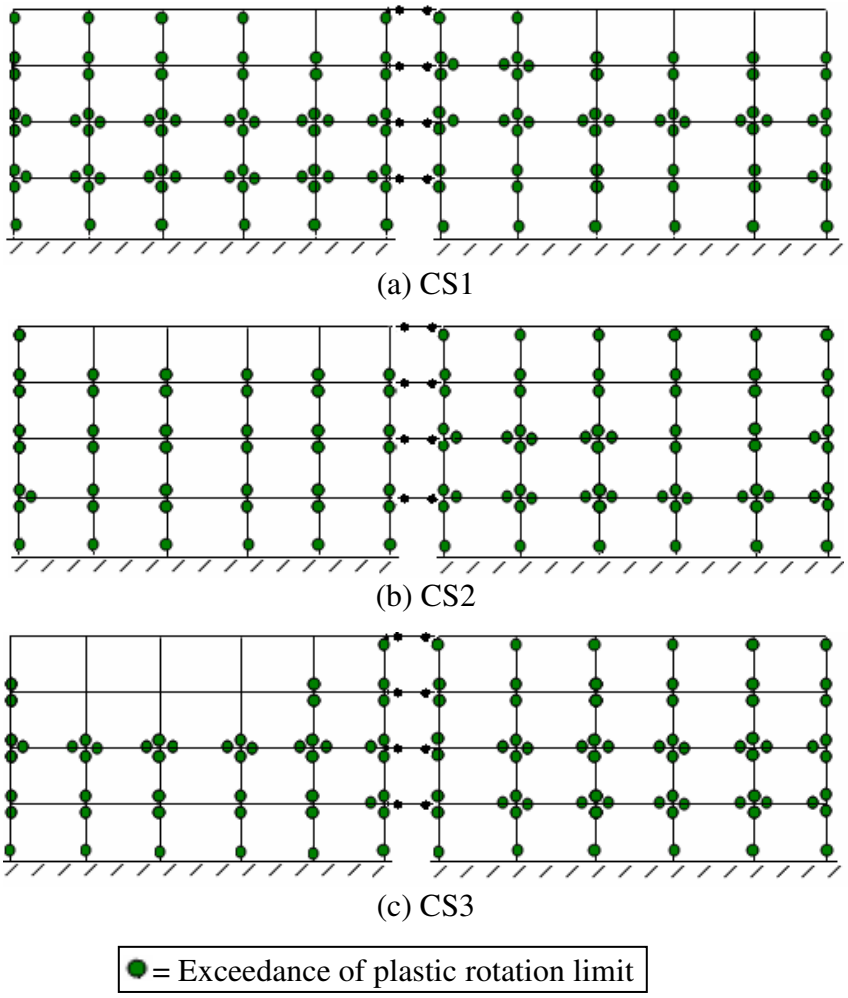

Fig. 5.9. Locations where CP plastic rotation limits are exceeded (E-W)

5.2.3.3 N-S Direction

The N-S evaluation produced similar results to the E-W direction. However, there were fewer instances of plastic rotation limits being exceeded, indicating that the E-W direction is more vulnerable. Tables 5.11 through 5.13 give FEMA 356 plastic rotation limits and the median maximum plastic rotations for each suite of ground motions in the N-S direction. The column rotation limits were the same as in the E-W direction, and similarly the only LS plastic rotation limits exceeded for the 10% in 50 years hazard were the CS2 column rotations shown in Fig. 5.10.

Table 5.11. Column plastic rotations (N-S)

Case study	Story level	TR	FEMA 356 limit (rad.)		Max. plastic rot. (rad.)	
			LS	CP	10% in 50 yrs	2% in 50 yrs
CS1	1	C	0.0150	0.0200	0.0063	**0.0340**
	2	C	0.0150	0.0200	0.0052	**0.0248**
	3	C	0.0150	0.0200	0.0044	0.0192
	4	C	0.0150	0.0200	0.0040	0.0149
CS2	1	NC	0.0031	0.0041	**0.0058**	**0.0303**
	2	NC	0.0038	0.0048	**0.0051**	**0.0122**
	3	NC	0.0046	0.0056	0.0031	**0.0062**
	4	NC	0.0050	0.0060	0.0028	**0.0060**
CS3	1	C	0.0150	0.0200	0.0058	**0.0301**
	2	C	0.0150	0.0200	0.0046	**0.0239**
	3	C	0.0150	0.0204	0.0032	0.0158
	4	C	0.0150	0.0200	0.0029	0.0102

Note: Rotation in bold exceeded the corresponding performance limits

Table 5.12. Exterior frame floor member plastic rotations (N-S)

Case study	Story level	TR	FEMA 356 limit (rad.)		Max. plastic rot. (rad.)	
			LS	CP	10% in 50 yrs	2% in 50 yrs
CS1	1	C	0.0183	0.0241	0.0012	**0.0308**
	2	C	0.0183	0.0241	0.0006	0.0223
	3	C	0.0189	0.0244	0.0030	0.0143
	4	C	0.0194	0.0247	0.0022	0.0088
CS2	1	C	0.0153	0.0226	0.0014	**0.0265**
	2	C	0.0153	0.0226	0.0003	0.0074
	3	C	0.0153	0.0226	0.0000	0.0011
	4	C	0.0168	0.0234	0.0000	0.0023
CS3	1	C	0.0148	0.0223	0.0010	**0.0253**
	2	C	0.0148	0.0223	0.0000	0.0194
	3	C	0.0148	0.0223	0.0000	0.0150
	4	C	0.0164	0.0231	0.0000	0.0085

Table 5.13. Interior frame floor member plastic rotations (N-S)

Case study	Story level	TR	FEMA 356 limit (rad.)		Max. plastic rot. (rad.)	
			LS	CP	10% in 50 yrs	2% in 50 yrs
CS1	1	C	0.0162	0.0232	0.0024	**0.0268**
	2	C	0.0168	0.0232	0.0011	0.0206
	3	C	0.0163	0.0228	0.0003	0.0153
	4	C	0.0169	0.0233	0.0000	0.0108
CS2	1	C	0.0138	0.0217	0.0033	**0.0224**
	2	C	0.0138	0.0217	0.0006	0.0065
	3	C	0.0138	0.0217	0.0000	0.0020
	4	C	0.0152	0.0225	0.0000	0.0016
CS3	1	C	0.0131	0.0211	0.0014	**0.0256**
	2	C	0.0131	0.0211	0.0004	0.0186
	3	C	0.0131	0.0211	0.0000	0.0110
	4	C	0.0125	0.0208	0.0000	0.0054

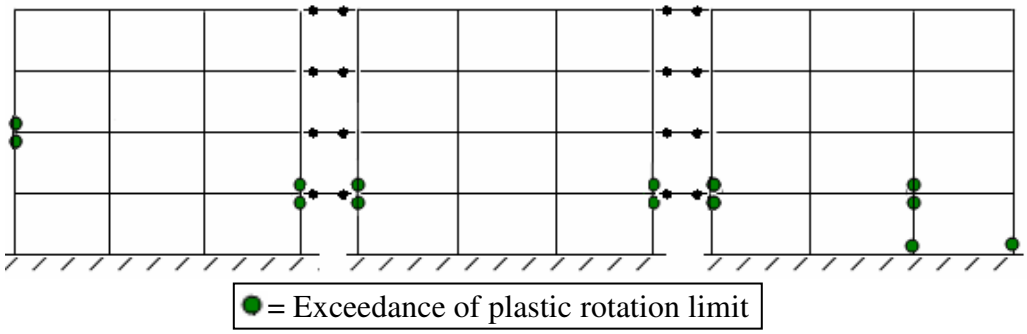

Fig. 5.10. Locations where LS plastic rotation limits are exceeded in CS2 (N-S)

The N-S frame plastic rotations were not as large, and each case study achieved the same performance objectives as the E-W direction. CS1 and CS3 met the limited performance objective for the 10% in 50 years motions but not for the 2% in 50 years motions. CS2 did not meet either limited performance objective. To compare the amount of exceedance between the case studies for the 2% in 50 years, the maximum median column plastic rotations for the CS1 and CS3 frames were at most 1.7 times larger the CP rotation limits compared to 7 times larger for CS2. The locations where the CP plastic rotation limits were exceeded for the N-S direction are shown in Fig. 5.11. The first story of CS2 is highlighted to indicate the presence of a first story mechanism.

A summary of the FEMA 356 evaluation is given in Table 5.14. CS1 and CS3 met the BSO for the global-level analysis. The LS limited performance objective was met for the CS2 global-level analysis and the member-level analysis for CS1 and CS3. No performance objectives were achieved for the CS2 member-level analysis.

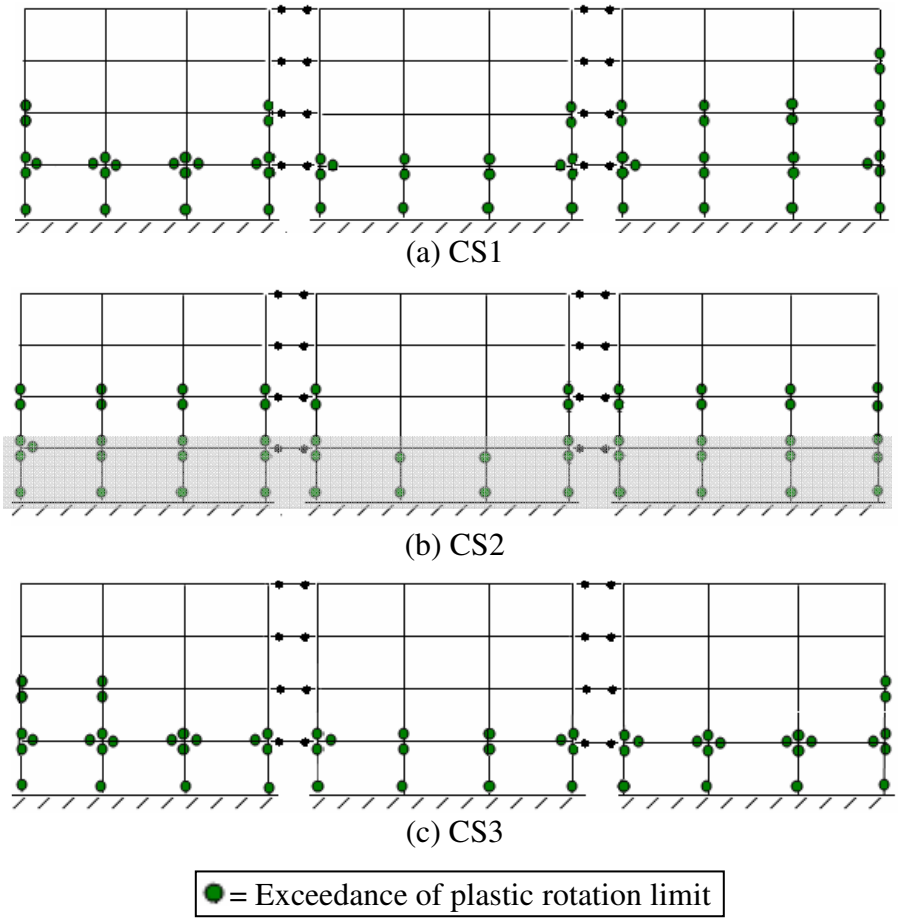

Fig. 5.11. Locations where CP plastic rotation limits are exceeded (N-S)

Table 5.14. FEMA 356 BSO evaluation for global and member-level performance

Case study	Global-level evaluation			Member-level evaluation		
	LS 10% in 50	CP 2% in 50	BSO	LS 10% in 50	CP 2% in 50	BSO
CS1	O.K.	O.K.	O.K.	O.K.	N.G.	N.G.
CS2	O.K.	N.G.	N.G.	N.G.	N.G.	N.G.
CS3	O.K.	O.K.	O.K.	O.K.	N.G.	N.G.

Key: O.K. = Case study meets performance objective
N.G. = Case study does not meet performance objective

6 FRAGILITY ANALYSIS

6.1 Introduction

6.1.1 Methodology

Fragility curves were developed to compare the vulnerability of the case study buildings for varying seismic intensities. The method outlined by Wen et al. (2004) and summarized in Section 2 was used to develop the fragility curves based on seismic demands, capacities, and their corresponding uncertainties.

In this study, the seismic demand was determined from the results of the dynamic analysis with 2% and 10% in 50 years Memphis, Tennessee, ground motions. The structural capacity was defined as the maximum interstory drift that a member or story can withstand without reaching a prescribed limit state. The qualitative performance levels used in this study are taken from the FEMA 356 performance objectives. Along with the Life Safety (LS) and Collapse Prevention (CP) performance levels from the earlier FEMA 356 evaluation, the fragility analysis also included the Immediate Occupancy (IO) performance level. The IO performance level is defined as very minimal damage such that the building is operational immediately after an earthquake. Quantitative limit states suggested by Wen et al. (2004) were also used to define additional structural capacity limits.

The following equation was used to develop the fragility relationships (Wen et al. 2004):

$$P(LS \mid S_a) = 1 - \Phi\left(\frac{\lambda_{CL} + \lambda_{D|S_a}}{\sqrt{\beta_{D|S_a}{}^2 + \beta_{CL}{}^2 + \beta_M{}^2}}\right) \tag{6.1}$$

where:

$P(LS \mid S_a)$ = Probability of exceeding a limit state given the spectral acceleration at the fundamental period of the building

Φ = Standard normal cumulative distribution function

λ_{CL} = ln(median drift capacity for a particular limit state), where drift capacity is expressed as a percentage of the story height

λ_{D/S_a} = ln(calculated median demand drift given the spectral acceleration), where demand drift is determined from a fitted power law equation

β_{D/S_a} = Uncertainty associated with the fitted power law equation used to estimate demand drift = $\sqrt{\ln(1+s^2)}$

β_{CL} = Uncertainty associated with the drift capacity criteria, taken as 0.3 for this study (Wen et al. 2004)

β_M = Uncertainty associated with analytical modeling of the structure, taken as 0.3 for this study (Wen et al. 2004)

s^2 = Square of the standard error = $\dfrac{\sum\left[\ln(Y_i)-\ln(Y_p)\right]^2}{n-2}$

Y_i, Y_p = Observed demand drift and power law predicted demand drift, respectively, given the spectral acceleration

n = Number of sample data points for demand

6.1.2 Additional Ground Motions

To cover a broader range of seismic demand, the results from an additional twenty ground motions for Memphis, Tennessee, developed by Wen and Wu (2000) for 2% and 10% probabilities of exceedance in 50 years, were used to define the demand relationships. Tables 6.1 and 6.2 give the details of these ground motions, and spectral accelerations with five percent damping are shown in Fig. 6.1 for each suite. The same method by Trifunac and Brady (1975) was used to truncate the ground motions to 95 percent of the total energy imparted (see Section 4.3). The acceleration time histories are given in Appendix A.

Table 6.1. 10% in 50 years ground motions (Wen and Wu 2000)

Ground motion	PGA (g)	Duration (s)	Duration of 95% energy (s)	Body-wave magnitude	Focal depth (mi.)	Epicentral distance from Memphis (mi.)
475_01wu	0.059	41.0	22.2	6.3	3.2	75
475_02wu	0.075	41.0	19.7	6.4	4.2	36
475_03wu	0.070	41.0	17.5	6.8	11.2	78
475_04wu	0.068	41.0	23.4	6.8	1.3	57
475_05wu	0.108	41.0	14.9	6.2	16.8	66
475_06wu	0.054	150	48.9	6.2	2.0	26
475_07wu	0.070	41.0	20.3	6.5	7.1	37
475_08wu	0.088	20.5	12.4	6.5	14.9	80
475_09wu	0.093	20.5	10.2	6.3	5.9	103
475_10wu	0.064	41.0	18.5	6.8	5.4	22

Table 6.2. 2% in 50 years ground motions (Wen and Wu 2000)

Ground motion	PGA (g)	Duration (s)	Duration of 95% energy (s)	Body-wave magnitude	Focal depth (mi.)	Epicentral distance from Memphis (mi.)
2475_01wu	0.439	150	29.2	8.0	15.9	92
2475_02wu	0.333	150	23.5	8.0	21.1	116
2475_03wu	0.360	150	23.7	8.0	15.9	101
2475_04wu	0.323	150	52.8	8.0	5.7	106
2475_05wu	0.476	150	36.2	8.0	5.7	61
2475_06wu	0.416	150	37.1	8.0	10.8	73
2475_07wu	0.365	150	24.8	8.0	10.8	74
2475_08wu	0.292	150	20.9	8.0	5.7	91
2475_09wu	0.335	150	26.0	8.0	5.7	106
2475_10wu	0.412	150	22.2	8.0	10.8	117

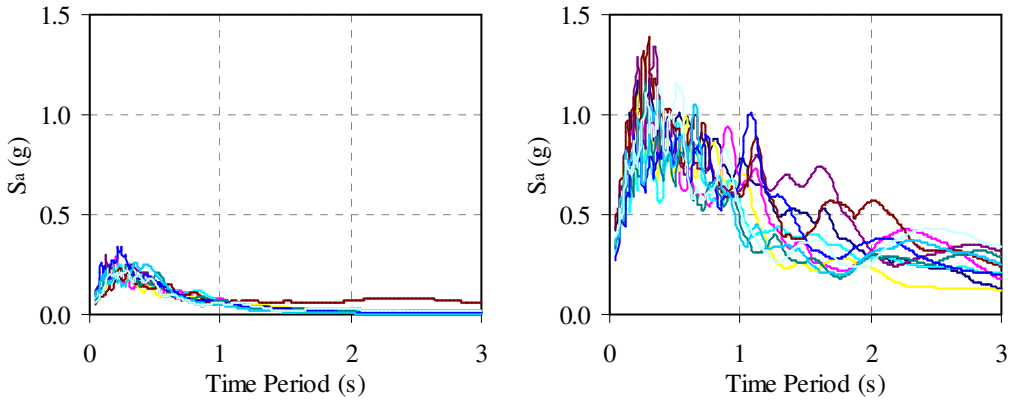

(a) 10% in 50 years (b) 2% in 50 years

Fig. 6.1. Spectral accelerations for Wen and Wu ground motions

6.2 Qualitative Limits

6.2.1 Global-level

The global drift values (see Table 6.3) from the FEMA 356 evaluation were used to define the median drift capacity, λ_{CL}, used in developing global fragility curves for the case study buildings. For the SMF case studies, CS1 and CS3, the global interstory drift values of 1%, 2%, and 4% were used for the IO, LS, and CP performance levels, respectively. Because the FEMA global drift values are more appropriate for buildings properly detailed for seismic loading, Ramamoorthy et al. (2006) suggested using reduced interstory drift values of 0.5%, 1%, and 2% for IO, LS, and CP for buildings with insufficient section detailing for ductility. These reduced drift values, which were based on the FEMA 356 member-level rotation values, were used in the CS2 global analysis. This is discussed in more detail in Section 5.

To determine the demand relationship, the maximum interstory drift results from the twenty Rix and Fernandez motions and the twenty Wen and Wu motions were plotted versus the spectral acceleration corresponding to the fundamental period of the building for five percent damping. The ZEUS-NL fundamental periods using cracked section properties for the E-W and N-S directions in Tables 5.1 and 5.2 were used to

determine the spectral accelerations corresponding to each ground motion record. A power law equation was fitted to the forty data points for each case study and direction. Maximum interstory drifts were used for the controlling story for each ground motion record in the global fragility analysis. These interstory drifts can be found in Appendix B. The best fit power equations for the global fragilities are shown in Fig. 6.2 for the E-W direction and Fig. 6.3 for the N-S direction.

Table 6.3. Global interstory drift limits

Structural performance level	Drift (%)		
	CS1	CS2	CS3
Immediate Occupancy (IO)	1	0.5	1
Life Safety (LS)	2	1	2
Collapse Prevention (CP)	4	2	4

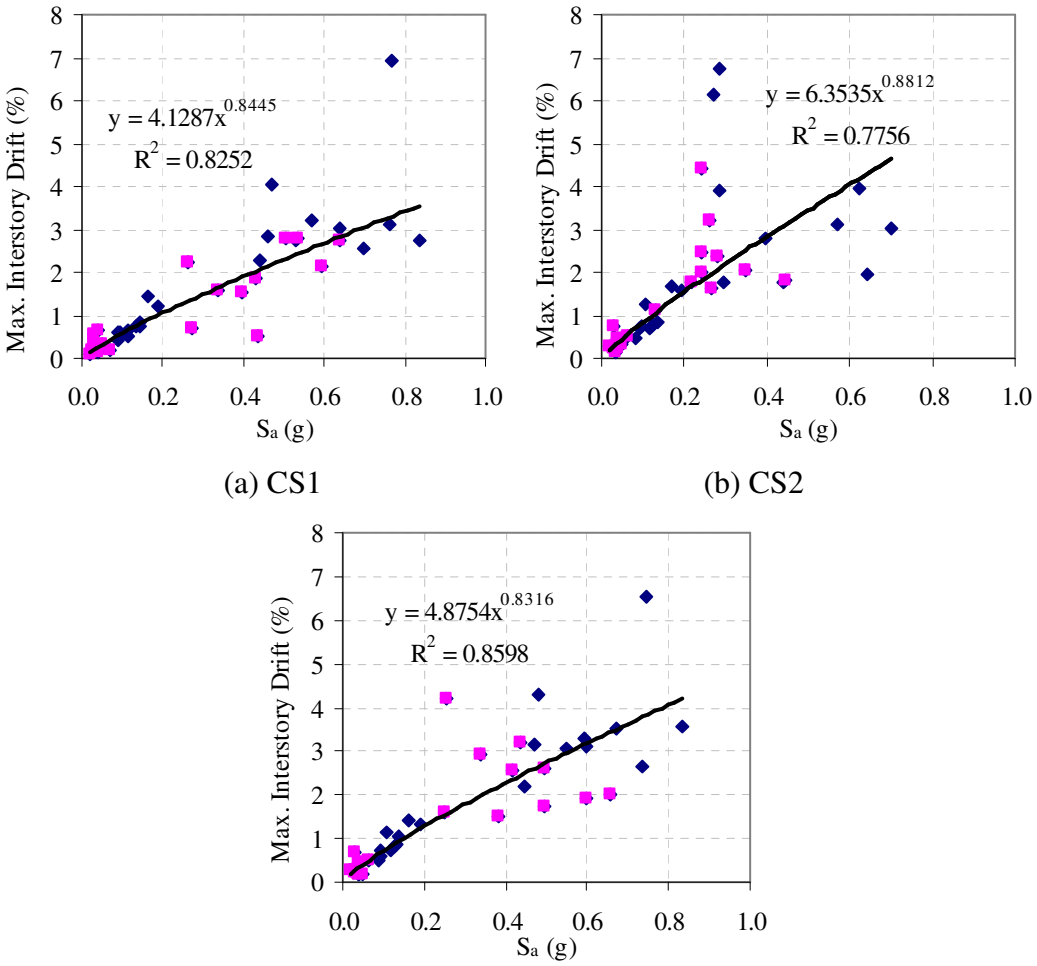

Fig. 6.2. Development of global power law equations (E-W)

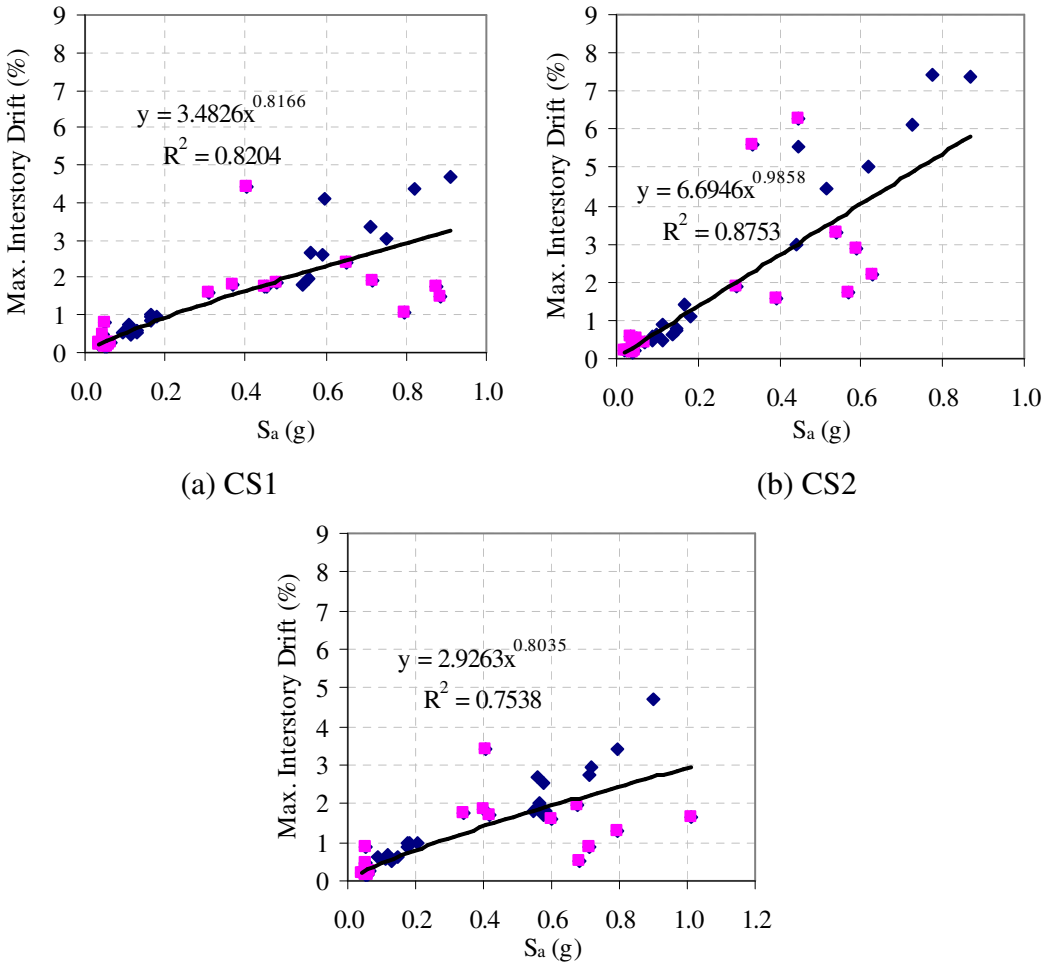

Fig. 6.3. Development of global power law equations (N-S)

Several adjustments were needed for the 2% in 50 years response history analysis results in both the E-W and N-S directions for CS2. As with the Rix-Fernandez ground motions, model instability in the E-W CS2 model stopped the analysis before the 2% in 50 years Wen and Wu ground motions ran completely. To address this, spectral accelerations corresponding to the segment of the ground motion that actually completed were plotted versus the corresponding CS2 maximum interstory drifts from the same analysis as shown in Fig. 6.2. The adjusted shortened spectral accelerations for the CS2 E-W direction are shown in Tables 6.4 and 6.5 along with the full ground motion

spectral accelerations for comparison. Only one 2% in 50 years ground motion fully completed, and the remaining ground motions completed 30 to 95 percent of the original duration. Such adjustments were not needed in the N-S direction.

Table 6.4. Reduced 2% in 50 years Wen and Wu motions (CS2 E-W model)

Ground motion	Completed time (s)	Total time (s)	Percent complete	Shortened S_a (g)	Complete S_a (g)
475_01wu	11.65	29.20	39.9	0.132	0.493
475_02wu	19.59	23.44	83.6	0.243	0.395
475_03wu	22.16	23.68	93.6	0.240	0.240
475_04wu	12.68	52.76	24.0	0.240	0.434
475_05wu	15.34	36.20	42.4	0.280	0.676
475_06wu	18.01	37.10	48.5	0.445	0.444
475_07wu	16.25	24.80	65.5	0.267	0.355
475_08wu	15.91	20.90	76.1	0.347	0.592
475_09wu	14.93	26.00	57.4	0.218	0.338
475_10wu	13.41	22.20	60.4	0.241	0.259

Table 6.5. Reduced 2% in 50 years Rix-Fernandez motions (CS2 E-W model)

Ground motion	Completed time (s)	Total time (s)	Percent complete	Shortened S_a (g)	Complete S_a (g)
2475_01wu	46.20	46.20	100.0	0.545	0.550
2475_02wu	34.52	45.32	76.2	0.256	0.672
2475_03wu	48.22	51.97	92.8	0.591	0.591
2475_04wu	46.16	72.62	63.6	0.267	0.743
2475_05wu	66.34	67.14	98.8	0.282	0.596
2475_06wu	47.21	65.67	71.9	0.737	0.737
2475_07wu	34.04	51.54	66.0	0.445	0.445
2475_08wu	32.05	49.40	64.9	0.397	0.832
2475_09wu	16.15	35.05	46.1	0.295	0.472
2475_10wu	15.56	36.81	42.3	0.282	0.481

In addition, the CS2 story mechanism in the N-S direction for the 2% in 50 years motions caused excessive first story drifts in the ZEUS-NL analysis that were out of the

range of reasonable structural performance. For the fitted power equation relationship, a cutoff drift of 8% was selected as a reasonable upper bound for the IMF CS2 structure. Three first story drifts between 9 and 26 percent for the Rix-Fernandez motions and two first story drifts of 10 and 28 percent for the Wen and Wu motions were deemed unreasonable and were not included for the demand relationship for the fragility curves. These measures were taken to use only quality data for the fragility relationships. The CS2 data adjustments were also included in the fitted power law equations for the member-level fragility analysis.

The global fragility curves for the IO, LS, and CP performance levels are shown in Figs. 6.4 and 6.5. The effect of the type of lateral system on the seismic fragility is evident for each performance level and is most pronounced for CP performance. The probabilities of exceeding the CP performance level for the SMF case studies are approximately half that of CS2 for a given spectral acceleration. Although the CS1 and CS3 curve values are similar, CS1 has slightly lower probabilities of exceeding each performance level in the E-W direction but slightly higher in the N-S direction than CS3 due to the member configuration in each direction.

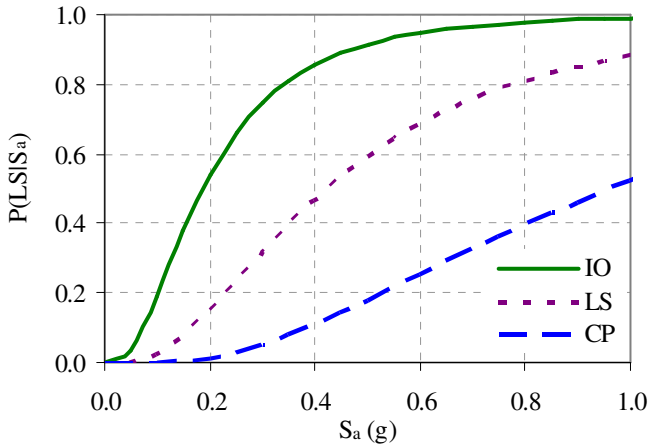

(a) CS1

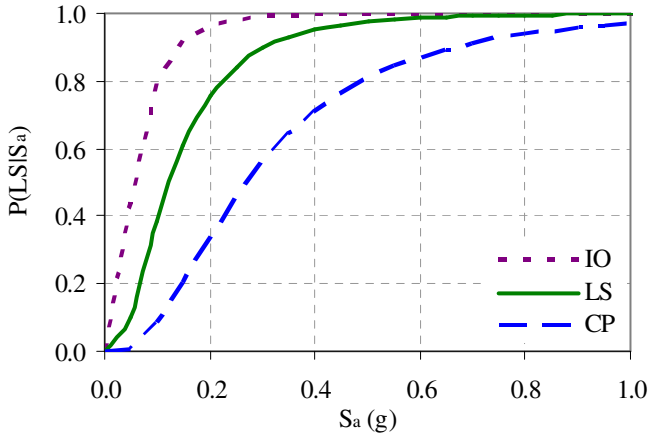

(b) CS2

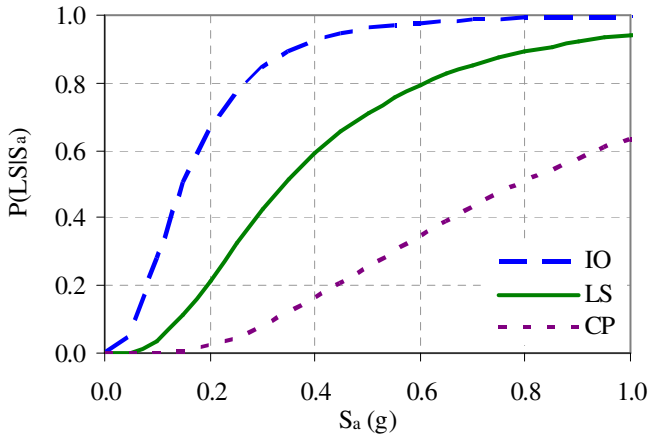

(c) CS3

Fig. 6.4. Global level fragility curves (E-W)

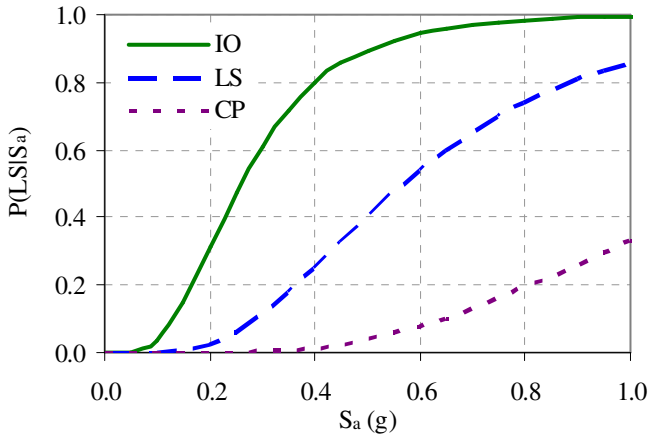

(a) CS1

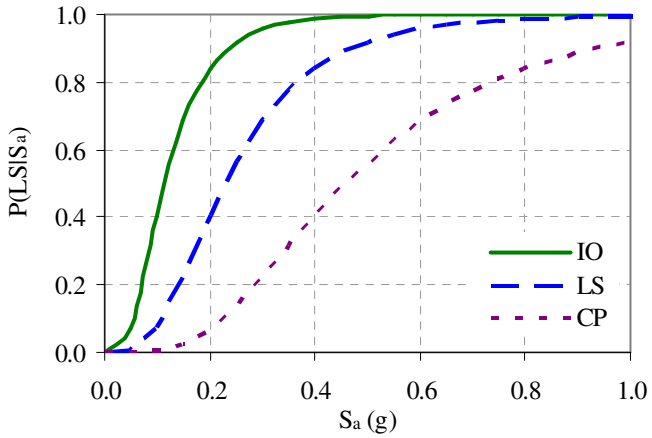

(b) CS2

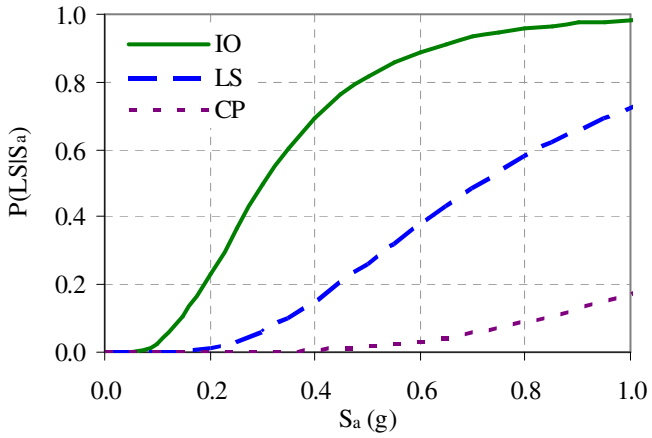

(c) CS3

Fig. 6.5. Global level fragility curves (N-S)

6.2.2 Member-level

Member-level fragility analyses for the case study buildings were conducted using qualitative interstory drift limits based on the plastic rotation performance limits provided in FEMA 356. The median capacity drift limits were set at the drifts where the IO, LS, and CP member-level FEMA 356 plastic rotation limits were exceeded in a push-over analysis for the critical story. Two different push-over patterns were used: a vertical distribution pattern based on the fundamental mode shape (resembling an inverted triangle) and a critical story push-over pattern introduced by Dooley and Bracci (2001). The modal vertical distribution is explained in Section 5. In the critical story push-over, a lateral force is applied to one story, and the story directly below is restrained for all but vertical translation. The critical second story push-over is shown in Fig. 6.6, along with an example of the fundamental mode pattern.

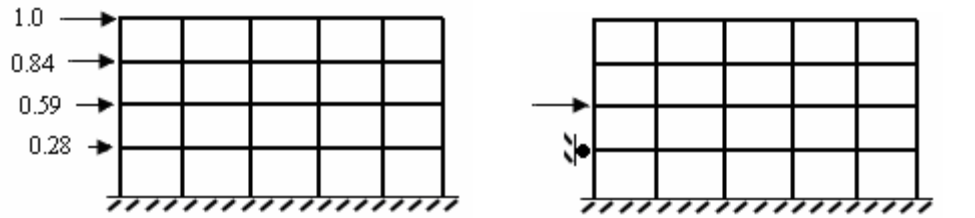

(a) Modal (inverted triangular) loading (b) Critical second story response

Fig. 6.6. Example loading patterns for member-level push-over analysis

Interstory drift limits based on the member-level analyses are shown in Tables 6.6 and 6.7. The critical response (CR) push-over produced larger drift limits than the modal (MP) push-over for the median drift capacity. Based on the FEMA 356 limits, the CS2 IO and LS drifts limits were identical, and the CS2 LS and CP drift limits were significantly smaller than CS1 and CS3.

Table 6.6. Qualitative member-level interstory drift limits (E-W)

Case study	MP push-over drift limit (%)			CR push-over drift limit (%)		
	IO	LS	CP	IO	LS	CP
CS1	0.46	1.20	1.44	0.92	2.47	3.26
CS2	0.52	0.52	0.60	0.89	0.89	1.07
CS3	0.49	0.93	1.18	1.08	2.62	3.38

Table 6.7. Qualitative member-level interstory drift limits (N-S)

Case study	MP push-over drift limit (%)			CR push-over drift limit (%)		
	IO	LS	CP	IO	LS	CP
CS1	0.49	1.68	1.98	1.01	2.48	3.20
CS2	0.46	0.46	0.56	0.82	0.82	1.04
CS3	0.51	1.43	2.23	1.07	2.47	3.14

The push-over curves used to determine the member-level limits based on the triangular load pattern are shown in Figs. 6.7 and 6.8 for the E-W and N-S directions. First story drifts controlled for each of the case studies. Figs. 6.9 and 6.10 show the performance level drift limits for the critical response push-overs. In the critical response push-over, the second story was critical for CS1 and CS3 in both the N-S and E-W direction, and the first story was critical for CS2. The difference in the drift limits for moment frames with and without special seismic detailing can be seen in the member-level push-over curves. For the CS2 IMF, the rotation limits correspond to lower drifts than for CS1 with an SMF.

The fitted power law equations to describe the relationship between demand and spectral acceleration, discussed for the global level analysis, are shown in Figs. 6.11 and 6.12 for the modal push-over analysis. Instead of the maximum interstory drift for any story as in the global drift demand, only the first story maximum interstory drifts corresponding to the story push-over curves are used in the member-level drift demand. In the cases where the second story push-over controlled for the critical response analysis, the second story maximum interstory drifts were used.

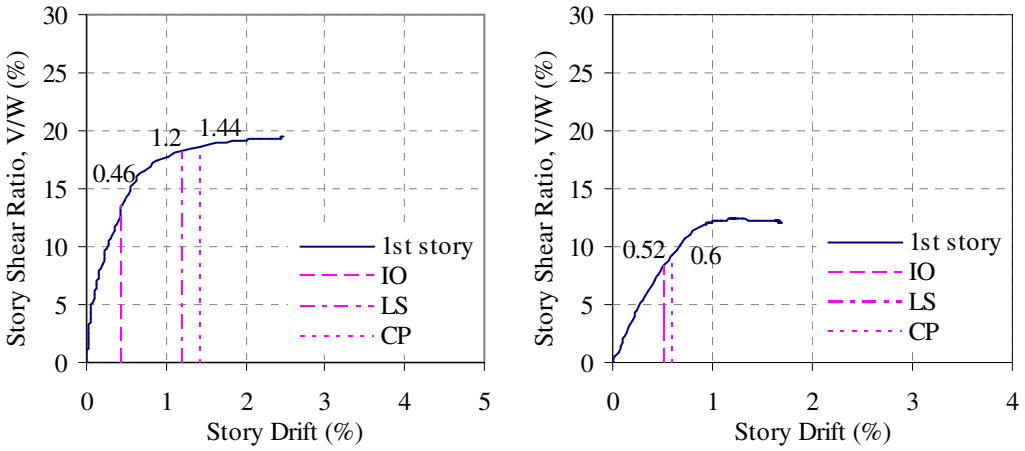

(a) CS1

(b) CS2

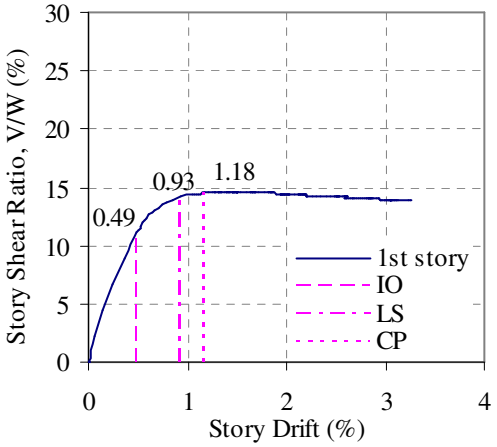

(c) CS3

Fig. 6.7. Modal push-over curves and member-level limits (E-W)

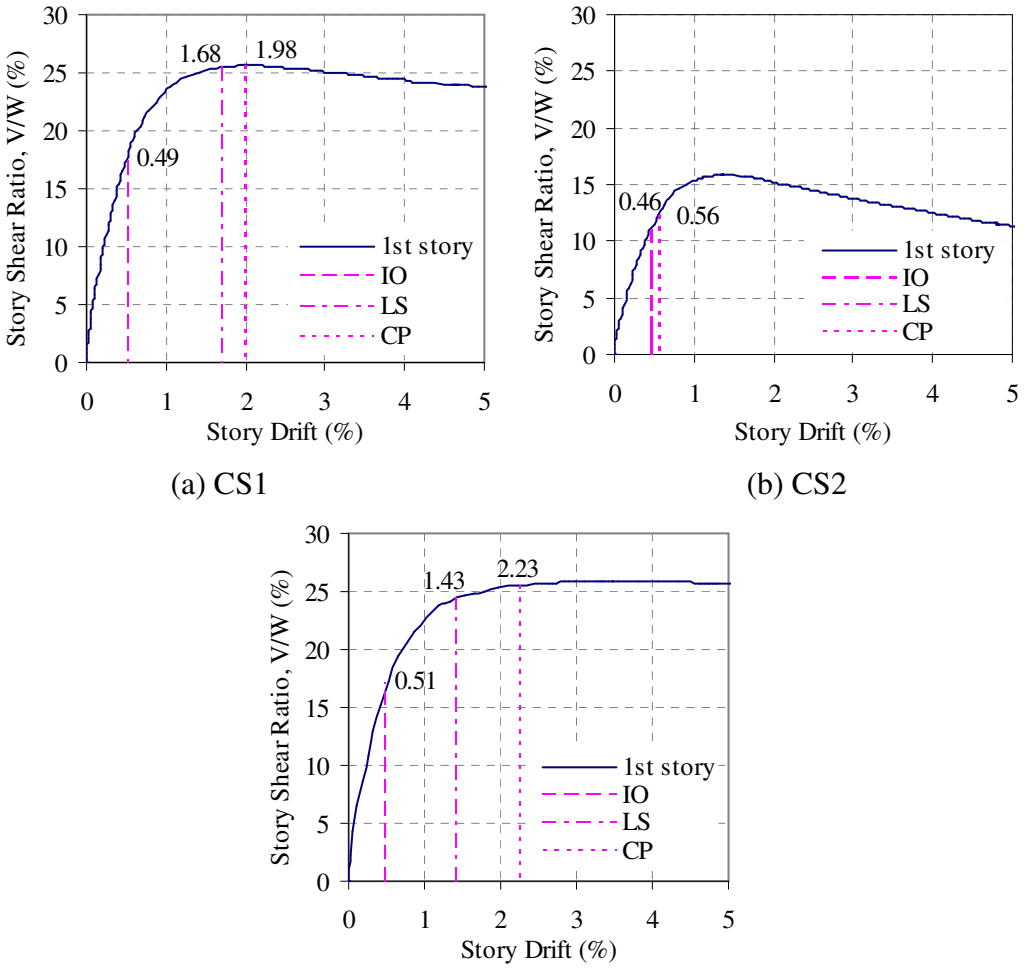

(a) CS1 (b) CS2

(c) CS3

Fig. 6.8. Modal push-over curves and member-level limits (N-S)

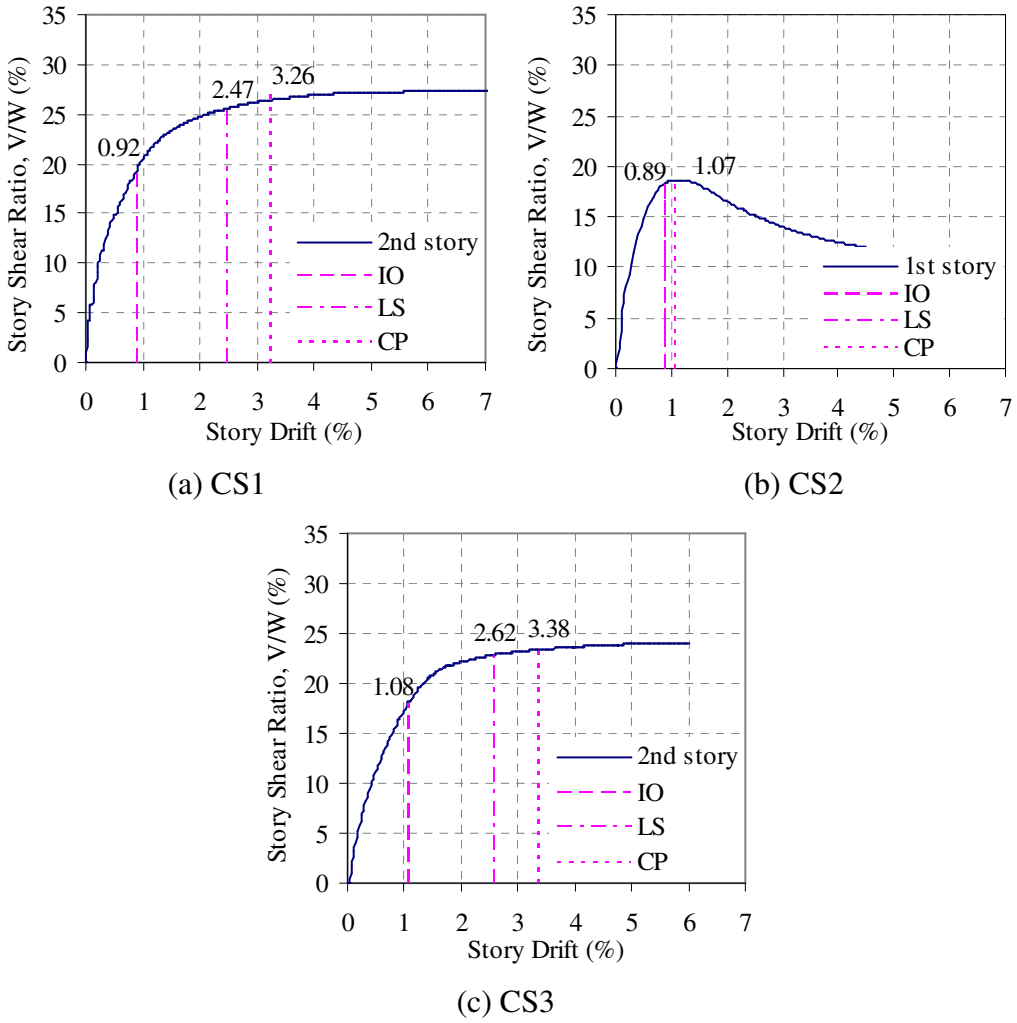

Fig. 6.9. Critical response push-over curves and member-level limits (E-W)

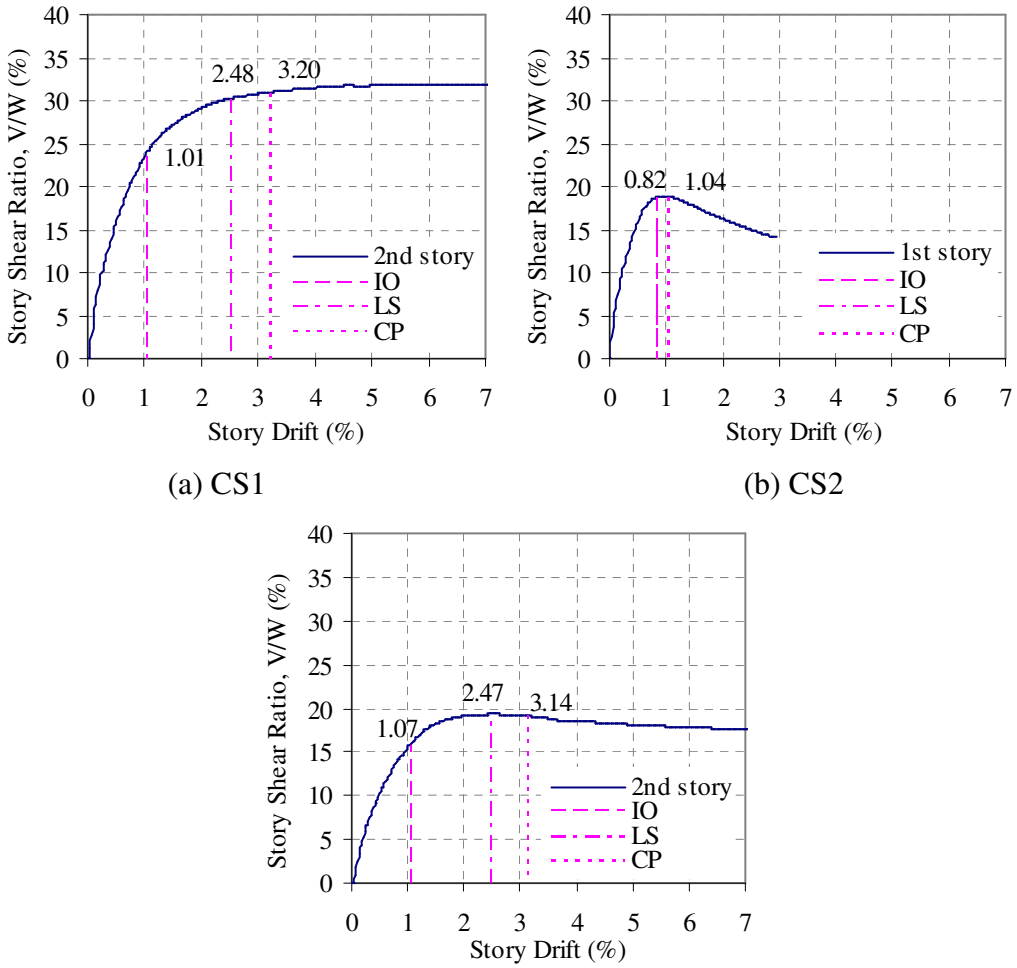

(a) CS1 (b) CS2

(c) CS3

Fig. 6.10. Critical response push-over curves and member-level limits (N-S)

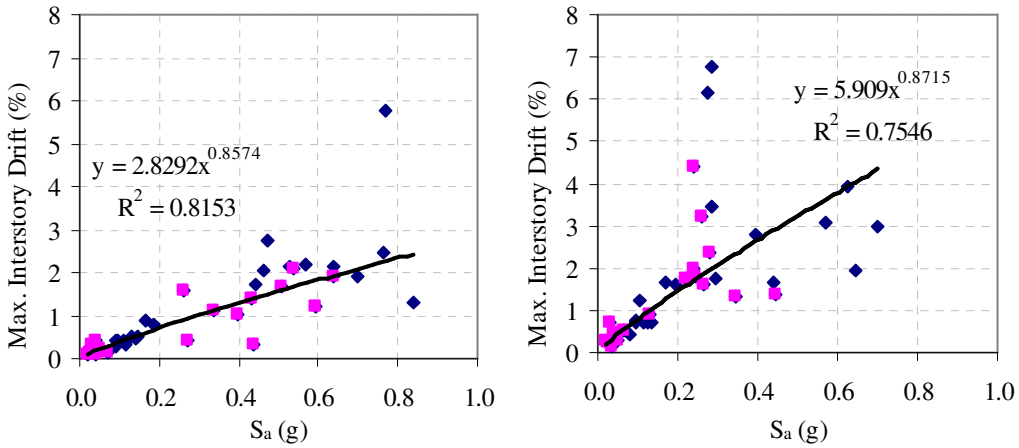

(a) CS1 (b) CS2

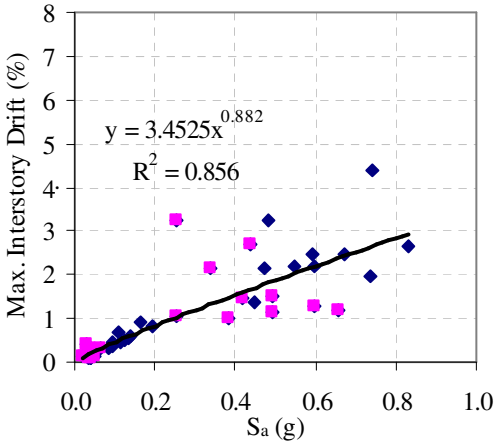

(c) CS3

Fig. 6.11. Development of member-level power law equations (E-W)

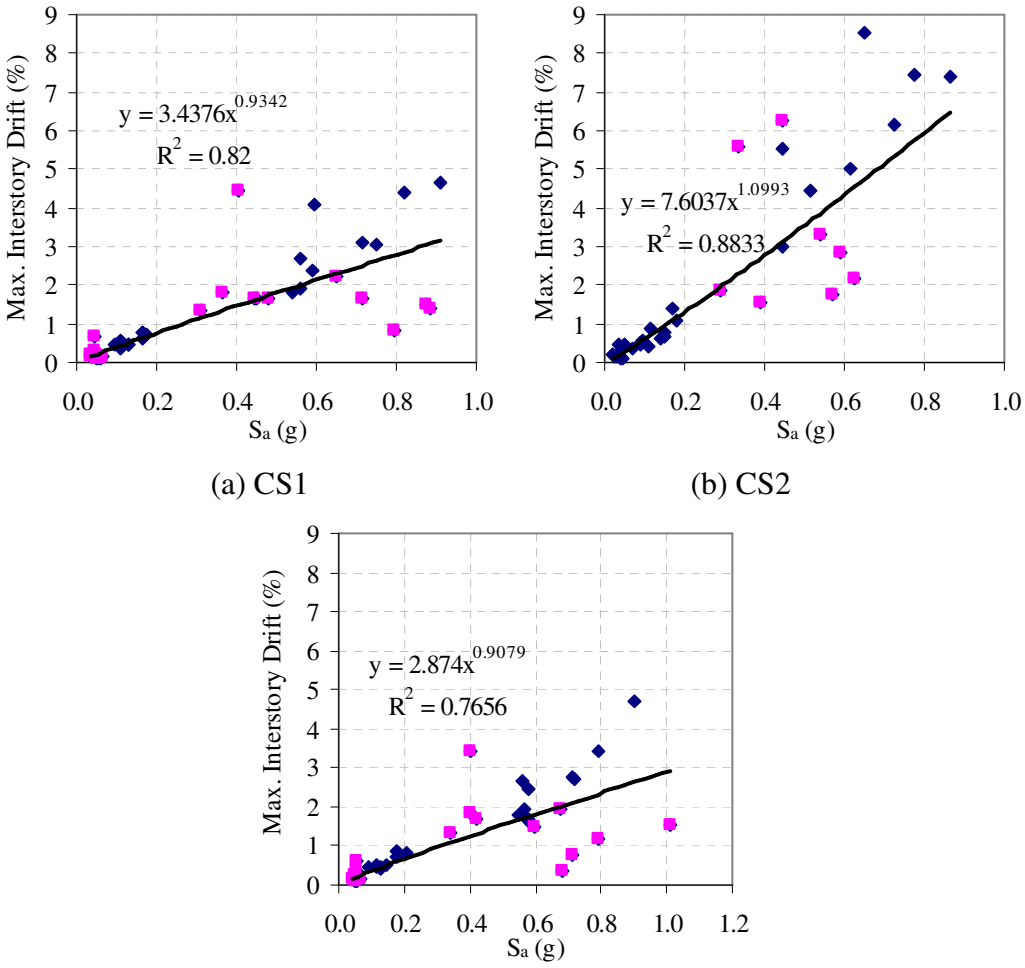

Fig. 6.12. Development of member-level power law equations (N-S)

The uncertainty parameters in Eq. (6.1) are given in Table 6.8 for the global level (GL), modal load pattern (MP) and critical response (CR) member-level fragility curves. The uncertainty parameters associated with estimating the capacity and modeling the structure (β_{CL} and β_{M}) were estimated as 0.3 based on the values Wen et al. (2004) used in developing fragility curves for RC frame members. The uncertainty associated with the demand relationship, β_{D/S_a} , was calculated for each set of data and ranged from 0.3787 to 0.5097.

Table 6.8. Uncertainty parameters for developing the fragility curves

Case study	Parameter	E-W direction			N-S direction		
		GL	MP	CR	GL	MP	CR
CS1	s^2	0.2048	0.2259	0.2096	0.1844	0.2421	0.1915
	β_{D/S_a}	0.4316	0.4573	0.4362	0.4114	0.4656	0.4186
	β_{CL}	0.3	0.3	0.3	0.3	0.3	0.3
	β_M	0.3	0.3	0.3	0.3	0.3	0.3
CS2	s^2	0.2319	0.2549	0.2549	0.1898	0.2164	0.2164
	β_{D/S_a}	0.4567	0.4765	0.4765	0.4169	0.4426	0.4426
	β_{CL}	0.3	0.3	0.3	0.3	0.3	0.3
	β_M	0.3	0.3	0.3	0.3	0.3	0.3
CS3	s^2	0.1542	0.1789	0.1561	0.2480	0.2967	0.2371
	β_{D/S_a}	0.3787	0.4056	0.3809	0.4707	0.5097	0.4613
	β_{CL}	0.3	0.3	0.3	0.3	0.3	0.3
	β_M	0.3	0.3	0.3	0.3	0.3	0.3

The fragility curves for the member-level fragility analysis are shown in Figs. 6.13 and 6.14 for the modal push-over and in Figs. 6.15 and 6.16 for the critical response push-over analysis. The member-level limits are considered to be more accurate than the global limits, and the probabilities of exceedance are higher based on for the member-level limits from the modal push-over analysis. The critical response fragility curves more closely resemble the global level fragility curves, as the interstory drift limits based on the critical response push-over analysis are closer to the global drift limits.

For most of the case studies, the LS and CP curves were closer together than the IO fragility curves, especially for the critical response loading pattern. With the same FEMA 356 rotation drift limits for CS2, the IO and LS fragility curves were identical. For all fragility curve sets, the IMF CS2 has the largest fragility values.

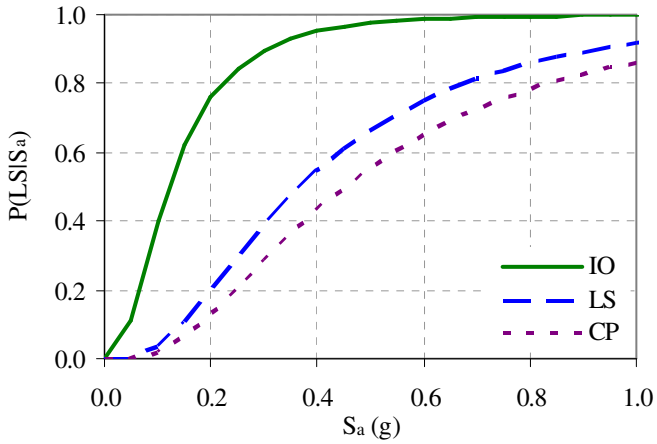

(a) CS1

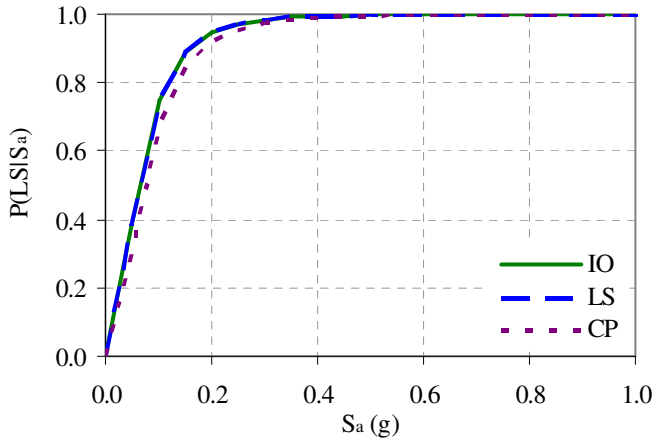

(b) CS2

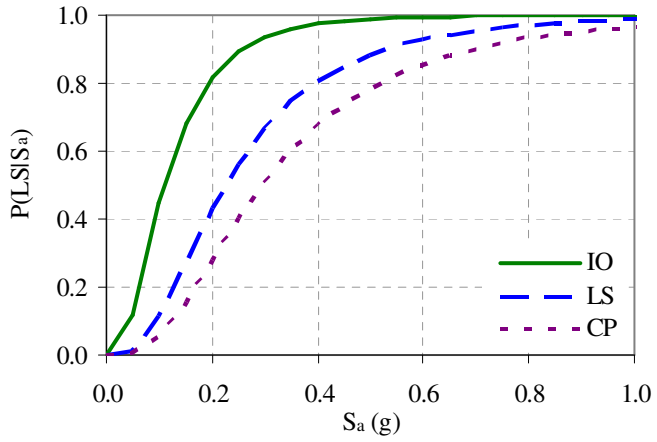

(c) CS3

Fig. 6.13. Modal pattern member-level fragility curves (E-W)

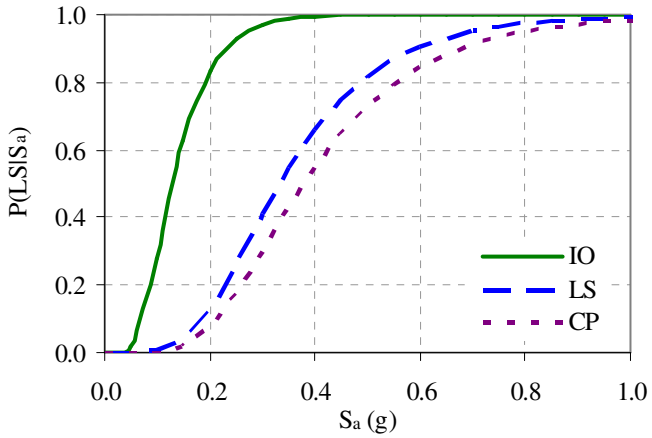

(a) CS1

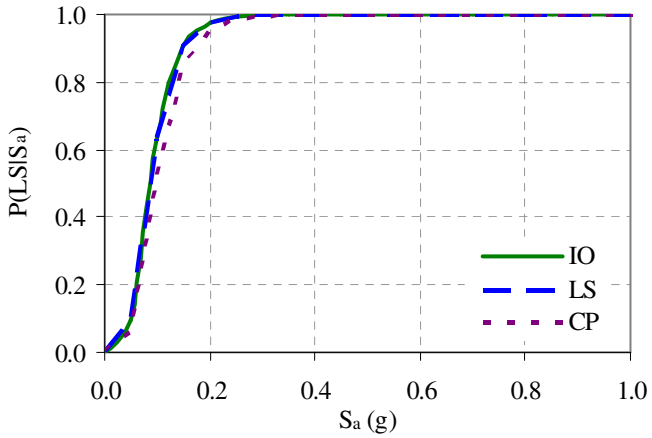

(b) CS2

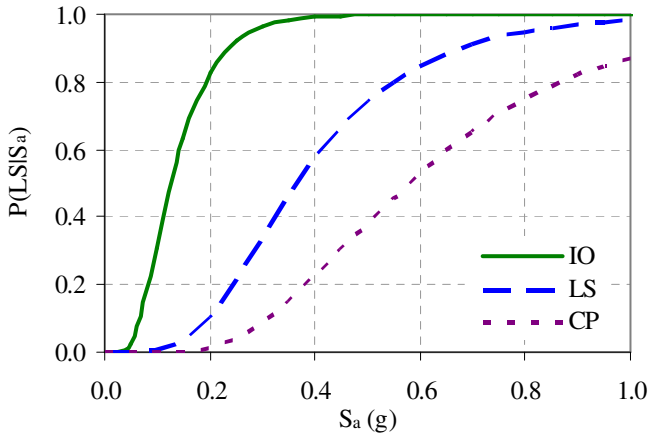

(c) CS3

Fig. 6.14. Modal pattern member-level fragility curves (N-S)

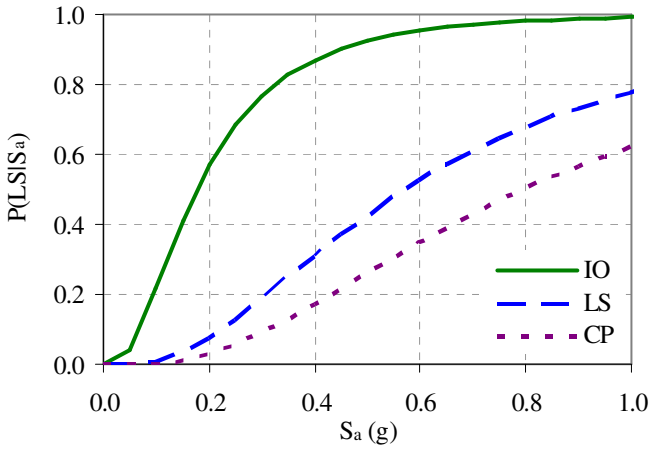

(a) CS1

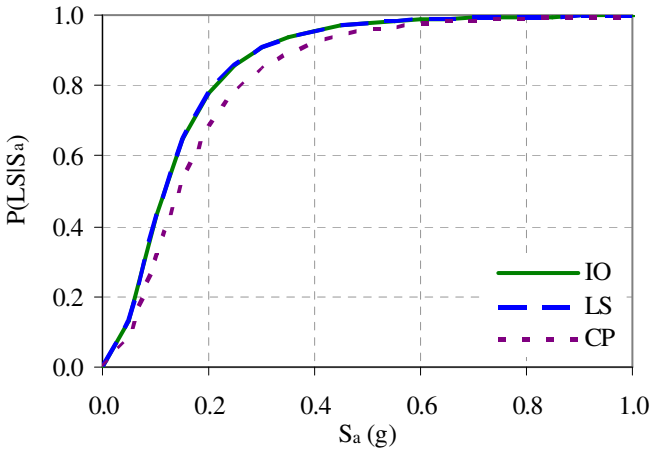

(b) CS2

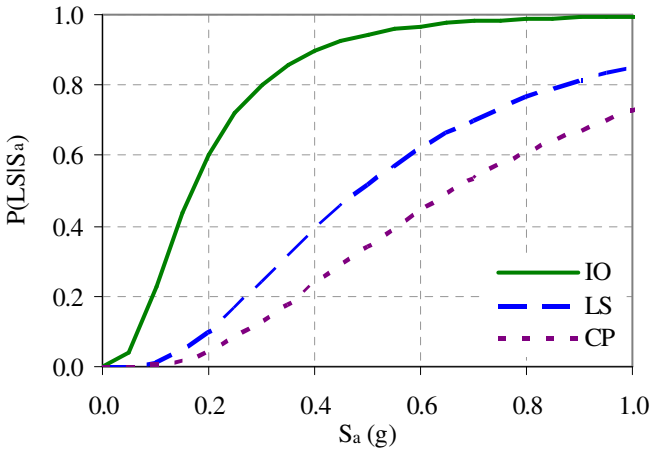

(c) CS3

Fig. 6.15. Critical response member-level fragility curves (E-W)

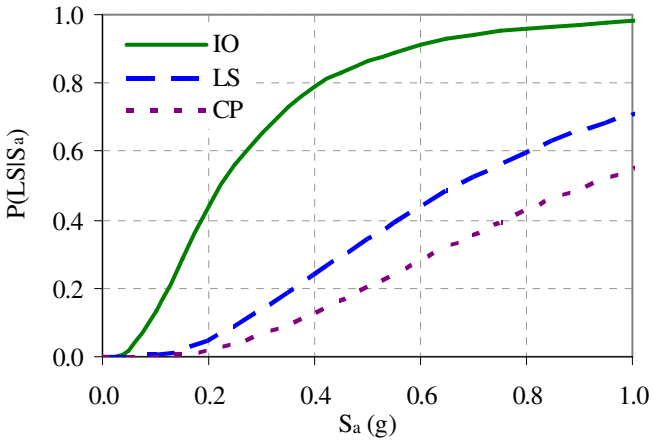

(a) CS1

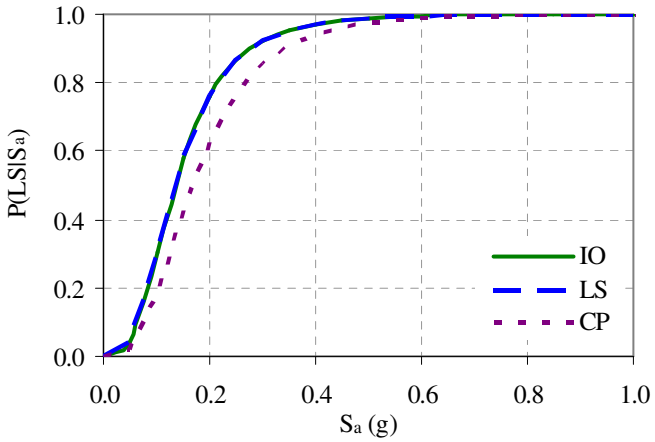

(b) CS2

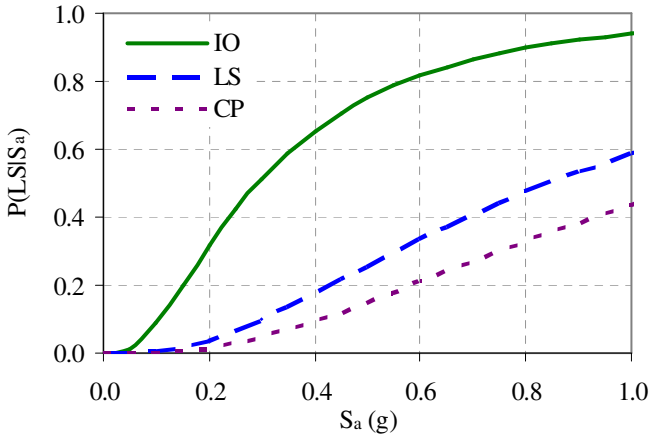

(c) CS3

Fig. 6.16. Critical response member-level fragility curves (N-S)

6.2.3 Numerical Comparison

The probabilities of exceeding the LS and CP performance levels were compared for the global level (GL), triangular push-over member-level (MP), and critical response (CR) fragilities in Tables 6.9 through 6.12. For each case study, the probability of exceeding the limit state for the median spectral acceleration (S_a) corresponding to each building's fundamental period for each of the Rix-Fernandez (RF) and Wen and Wu (WW) sets of motions was computed.

Table 6.9. Probability of exceeding LS for 10% in 50 years Rix-Fernandez motions

Modeling direction	Case study	Median S_a (g)	P(LS|S_a)		
			GL	MP	CR
E-W	CS1	0.1295	0.05	0.07	0.02
	CS2	0.1263	0.52	0.84	0.56
	CS3	0.1378	0.09	0.23	0.03
N-S	CS1	0.1228	0.03	0.04	0.01
	CS2	0.1188	0.37	0.81	0.42
	CS3	0.1206	0.02	0.03	0.01

Table 6.10. Probability of exceeding LS 10% in 50 years Wen and Wu motions

Modeling direction	Case study	Median S_a (g)	P(LS|S_a)		
			GL	MP	CR
E-W	CS1	0.0487	0.00	0.00	0.00
	CS2	0.0406	0.06	0.29	0.08
	CS3	0.0538	0.00	0.02	0.00
N-S	CS1	0.0393	0.00	0.00	0.00
	CS2	0.0353	0.01	0.10	0.01
	CS3	0.0375	0.00	0.00	0.00

Table 6.11. Probability of exceeding CP for 2% in 50 years Rix-Fernandez motions

Modeling direction	Case study	Median S_a (g)	P(CP|S_a)		
			GL	MP	CR
E-W	CS1	0.6024	0.26	0.65	0.20
	CS2	0.6141	0.88	1.00	0.98
	CS3	0.5939	0.34	0.74	0.43
N-S	CS1	0.5942	0.17	0.65	0.25
	CS2	0.6324	0.90	1.00	0.99
	CS3	0.5791	0.12	0.41	0.23

Table 6.12. Probability of exceeding CP for 2% in 50 years Wen and Wu motions

Modeling direction	Case study	Median S_a (g)	P(CP|S_a)		
			GL	MP	CR
E-W	CS1	0.4339	0.13	0.47	0.35
	CS2	0.4148	0.73	0.99	0.97
	CS3	0.4282	0.19	0.58	0.28
N-S	CS1	0.5652	0.15	0.63	0.28
	CS2	0.4343	0.74	1.00	0.95
	CS3	0.6360	0.14	0.36	0.20

The GL and CR probabilities were both lower than the MP probabilities as dictated by the corresponding capacity limits. The RF motions generally produced higher spectral accelerations for the building fundamental periods and corresponding higher probabilities of exceedance than the WW motions, with the exception of CS3 in the N-S direction. The probabilities of exceeding the performance levels were higher in the E-W direction, determined to be the more vulnerable direction in the analysis and evaluation discussed in Section 5.

The probabilities of exceeding the LS performance level for the 10% in 50 years RF motions for CS2 were large, ranging from 52 to 84 percent for the qualitative fragility analysis. Comparatively, the probabilities of exceeding the LS performance level were between 2 and 7 percent for CS1 and 1 and 23 percent for CS3 for the RF

motions. The probabilities for exceeding the LS performance level for the 10% in 50 years WW motions were much lower.

For the 2% in 50 years RF motions, the probabilities of exceeding the CP performance level were between 88 and 100 percent for CS2. These values were lower for CS1 and CS3 for exceeding the CP performance level (26 to 65 percent probability and a 34 to 74 percent probability, respectively). These ranges were similar for the WW motions.

6.3 Quantitative Limits

In addition to the FEMA 356 drift limits, quantitative interstory drift limits based on the member behavior were also used to define the drift capacity. The two limits used in this study were suggested by Wen et al. (2004):

1) First Yield (FY) – Interstory drift at which a member first begins to yield under applied lateral loading
2) Plastic Mechanism Initiation (PMI) – Interstory drift at which a story mechanism or an overall beam sidesway mechanism initiates under applied lateral loading

The interstory drift limits at which FY and PMI initiate are given in Table 6.13 and Figs. 6.17 and 6.18 for each case study. These drift limits were determined using the inverted triangular load pattern from the member-level fragility analysis. This pattern for the first story was determined to provide the critical drifts from the member-level analysis. Yielding for FY was determined when the moment curvature of the section reached a yield plateau. PMI was reached when all the columns or beams in story yielded at the member ends. These terms are discussed in more detail in Section 2.

Table 6.13. Quantitative interstory drift limits

Case study	Drift limit (%)			
	E-W direction		N-S direction	
	FY	PMI	FY	PMI
CS1	0.36	1.55	0.36	1.18
CS2	0.53	1.98	0.41	1.41
CS3	0.55	1.51	0.38	1.32

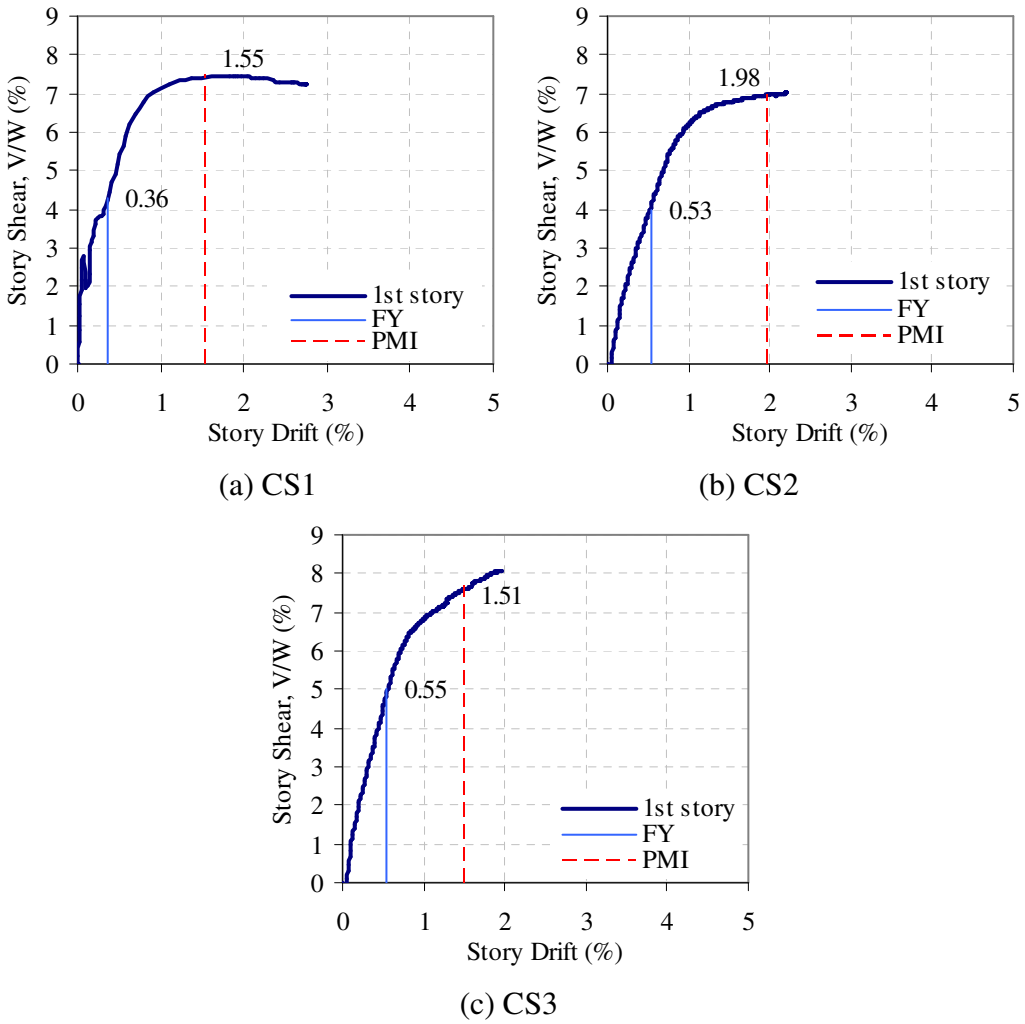

Fig. 6.17. Triangular push-over curves and quantitative limits (E-W)

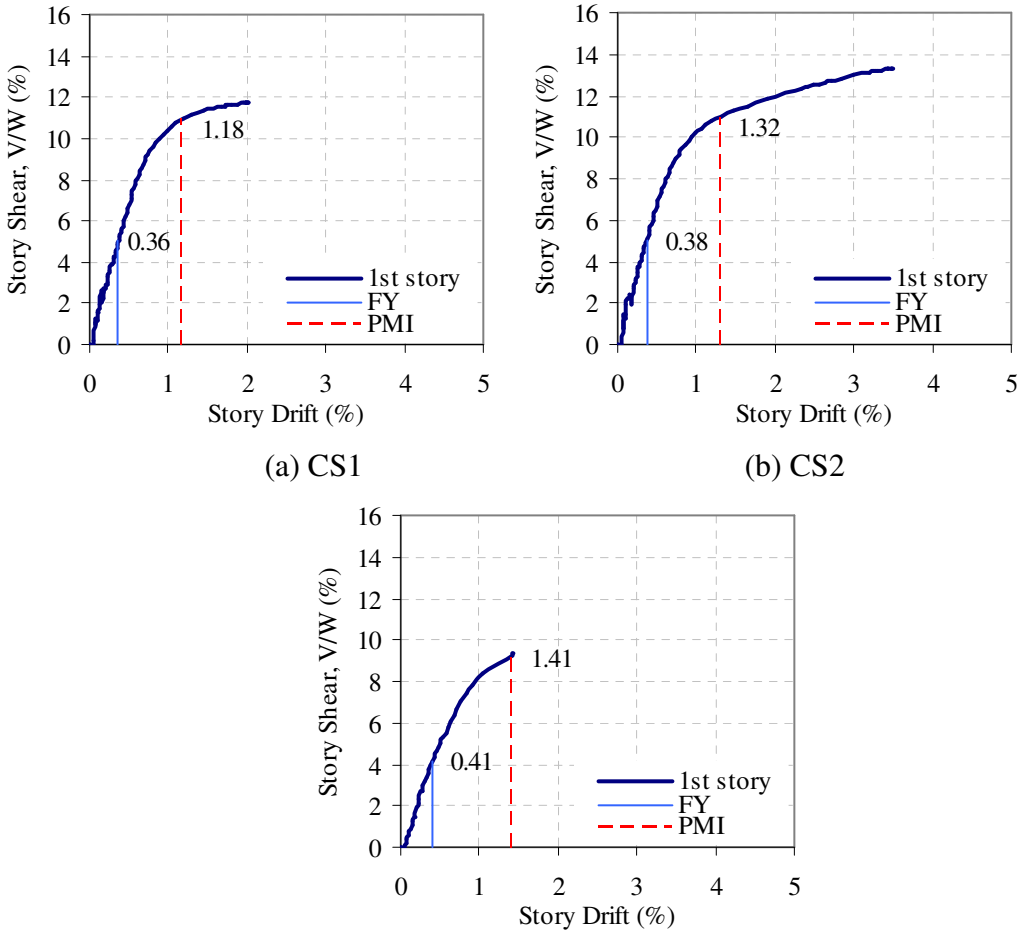

Fig. 6.18. Triangular push-over curves and quantitative limits (N-S)

Fig. 6.19 shows the locations of inelastic rotation at the PMI performance level in the E-W direction. For CS2 and CS3, the exterior frame did not fully yield before the ultimate capacities of the wide-module joists in the interior frames were reached. For these two cases, the PMI limit state was recorded at the drift where each of the interior wide-module joists exceeded their capacities. The inelastic rotation locations corresponding to PMI for CS2 and CS3 are very similar.

The locations of inelastic rotation at the PMI limit state for the N-S model are shown in Fig. 6.20. The effects of the different beam-column strength ratios can be observed in the initiation of the plastic mechanism. For CS2, with a column-to-beam

strength ratio of 0.8, almost all the story hinging occurred at the columns. CS1 and CS3 had column-to-beam strength ratios greater than 1.4, and the beams yielded before the columns in many of the bays.

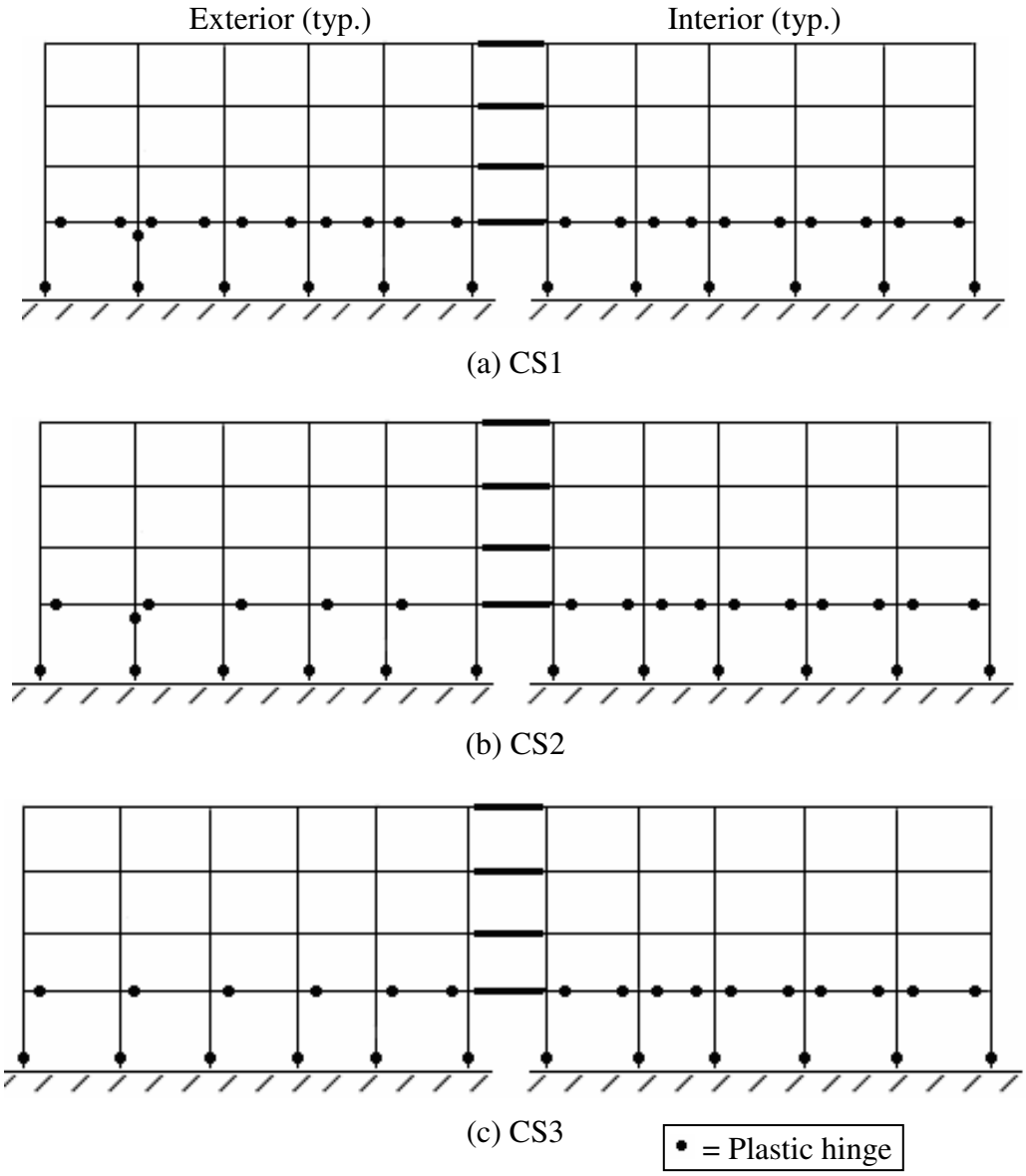

Fig. 6.19. Locations of inelastic rotation at PMI for triangular push-over (E-W)

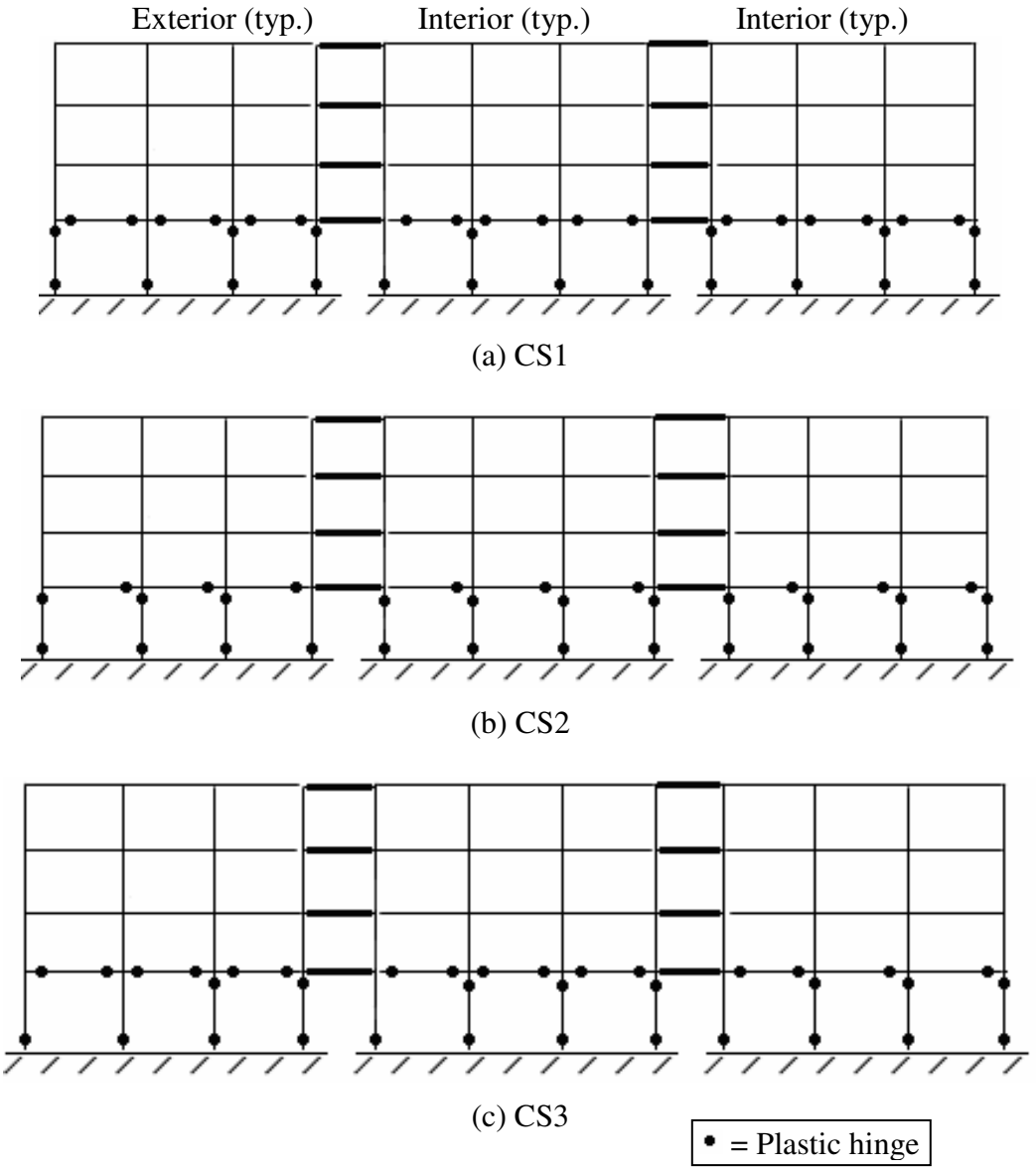

Fig. 6.20. Locations of inelastic rotation at PMI for triangular push-over (N-S)

The fragility curves corresponding to the quantitative FY and PMI limit states are shown in Figs. 6.21 and 6.22. As in the qualitative analysis, CS2 had the highest probability of exceeding both limit states for both model directions. For the E-W direction, CS3 showed the lowest probability of exceeding the FY limit state, while CS1 showed the lowest probability of exceeding the PMI limit state. For the N-S direction, CS1 showed the lowest probabilities of exceeding both FY and PMI.

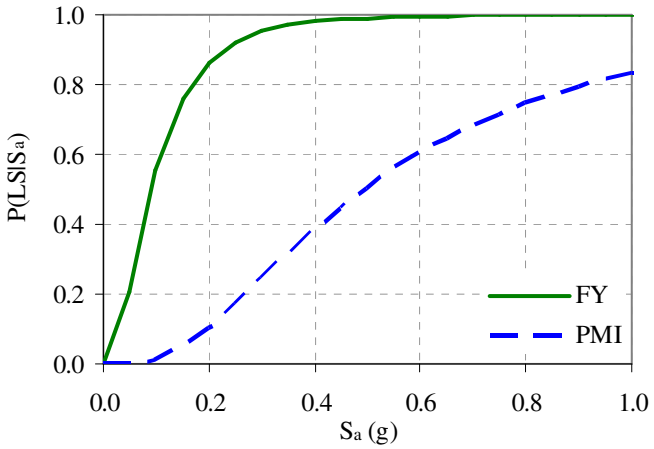

(a) CS1

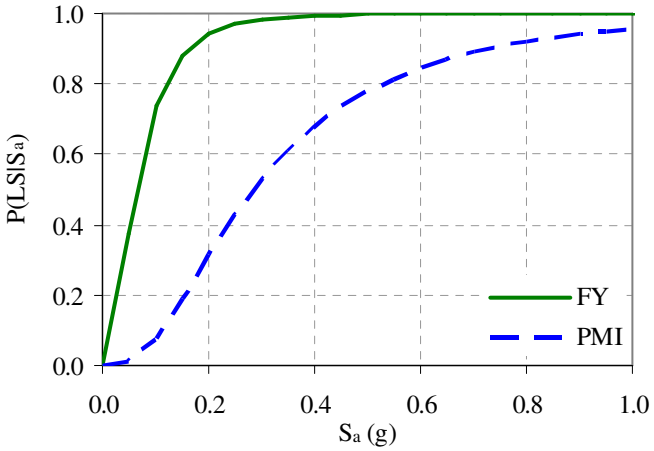

(b) CS2

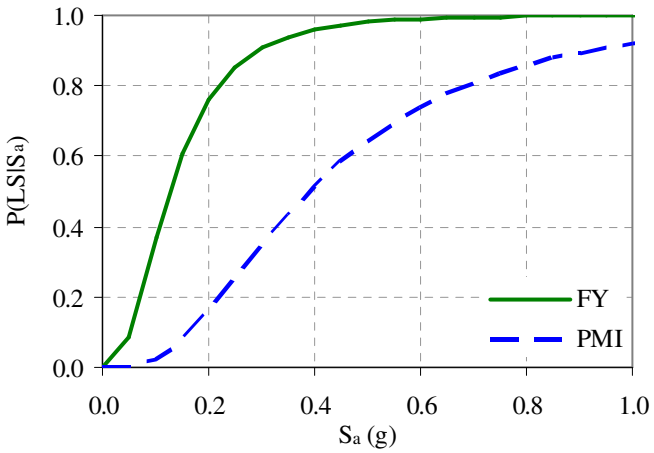

(c) CS3

Fig. 6.21. Quantitative fragility curves (E-W)

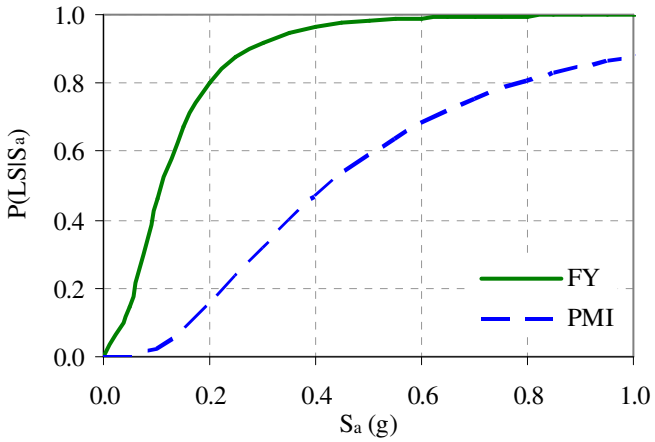

(a) CS1

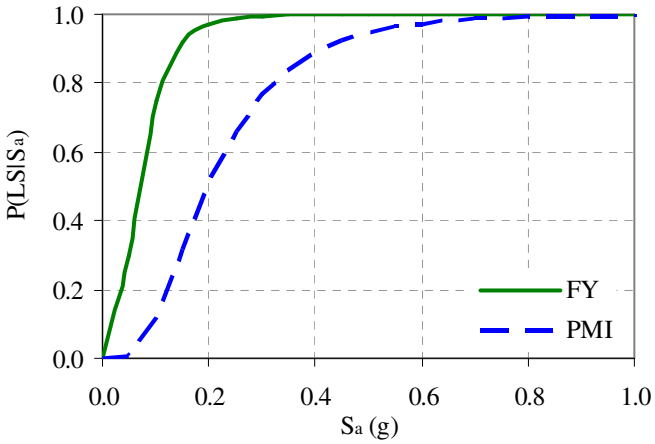

(b) CS2

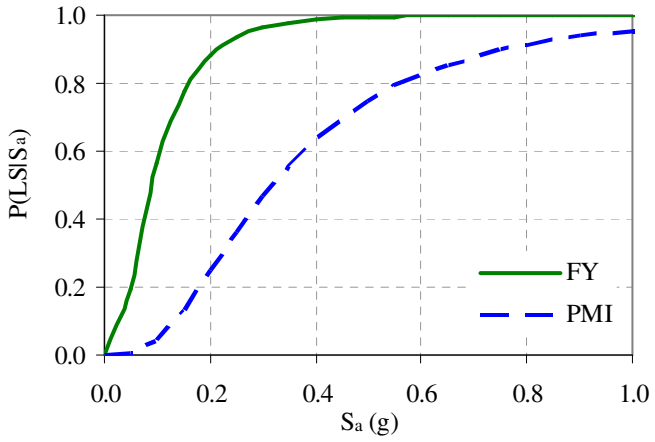

(c) CS3

Fig. 6.22. Quantitative fragility curves (N-S)

6.4 Selection of Default Fragility Curves

6.4.1 General

A default set of fragility curves was determined from the four sets of fragility curves developed from the FEMA 356 and quantitative limits for implementation into loss estimation software, such as MAEviz developed by the MAE Center (2006). Three performance levels were selected from the FEMA 356 and quantitative fragility curves, defined generically as Performance Level 1 (PL1), PL2, and PL3. Based on work by Bai et al. (2007), damage states are defined based on these performance levels, as shown in Fig. 6.23. The four damage states are classified as insignificant (I), moderate (M), heavy (H), and complete (C) damage.

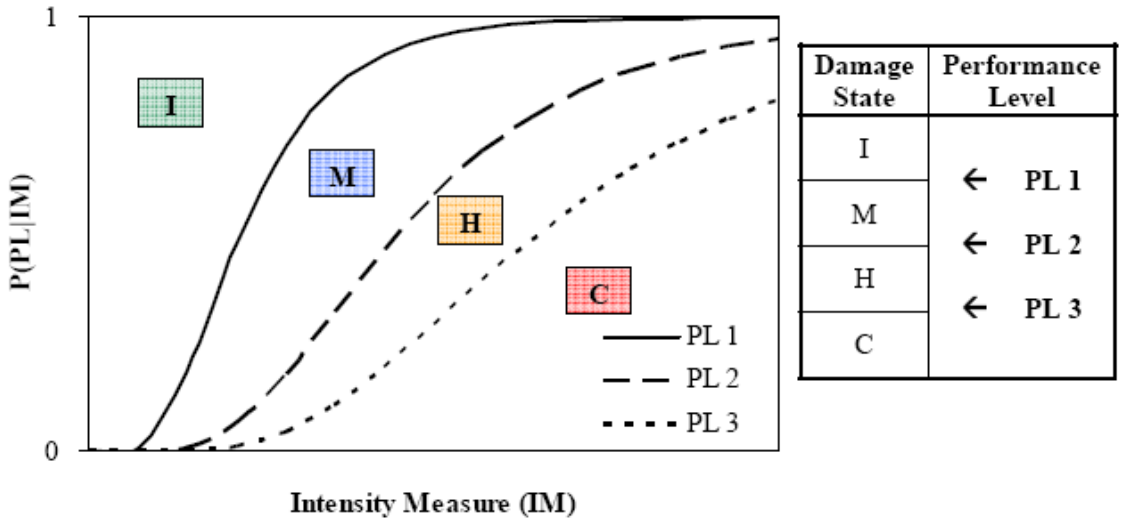

Fig. 6.23. Relationship between performance levels and damage states (Bai et al. 2007)

6.4.2 Default Fragility Curves

To define the generic performance levels for the default fragility curves for each case study, a combination of the member-level FEMA 356 performance levels and the quantitative limit states were used. The FEMA 356 member-level performance levels (IO, LS, and CP) using the modal push-over pattern (MP) were more specific to the

structural detailing and geometry than the global-level performance limits and more conservative than the critical response (CR) limits. However, for CS2 the IO and LS limits were the same for the MP limits; therefore, the CR limits were used for PL2. The quantitative limit state, PMI, was used as the third performance level in all of the case studies except of CS1 and CS3 in the N-S direction. The generic performance levels for each case study and direction are given in Table 6.14 along with the corresponding interstory drift limits.

Table 6.14. Performance levels and corresponding interstory drift (%) limits for default fragility curves

Direction	Case study	PL1	PL2	PL3
E-W	CS1	IO(MP) = 0.46	LS(MP) = 1.20	PMI = 1.55
	CS2	IO(MP) = 0.52	LS(CR) = 0.89	PMI = 1.98
	CS3	IO(MP) = 0.49	LS(MP) = 0.93	PMI = 1.51
N-S	CS1	IO(MP) = 0.49	LS(MP) = 1.68	CP(MP) = 1.98
	CS2	IO(MP) = 0.46	LS(CR) = 0.82	PMI = 1.41
	CS3	IO(MP) = 0.45	LS(MP) = 1.42	CP(MP) = 2.23

The generic performance levels are shown along with the remaining limit states for each case study in Figs. 6.24 through 6.35. The emphasized fragility curves in the first of two figures for each case study and direction correspond to those listed in Table 6.14, and the second figure shows the final performance levels with the corresponding damage states.

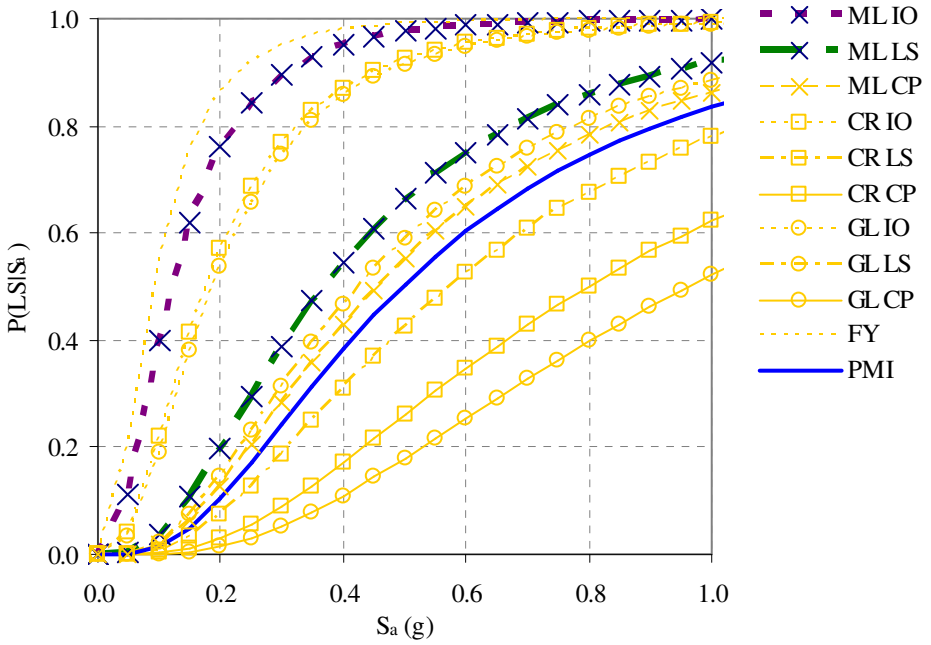

Fig. 6.24. Selection of default fragility curves for CS2 (E-W)

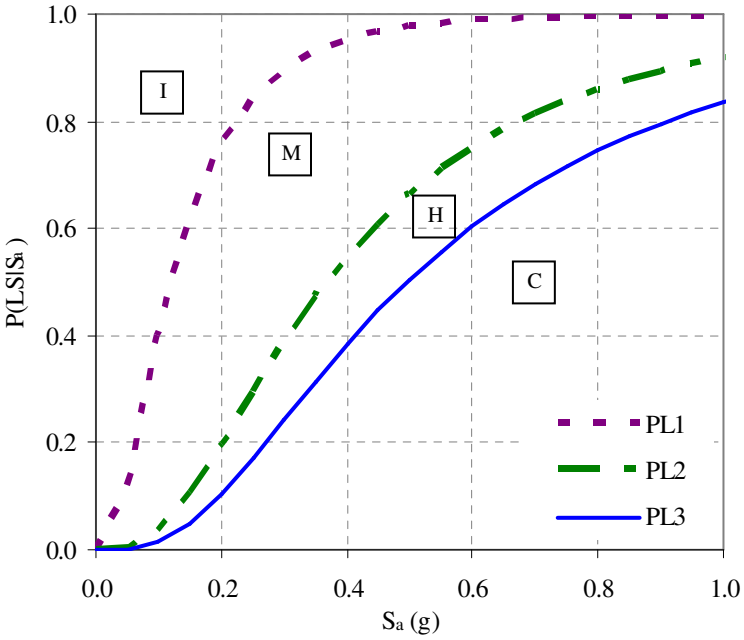

Fig. 6.25. Default fragility curves for CS1 (E-W)

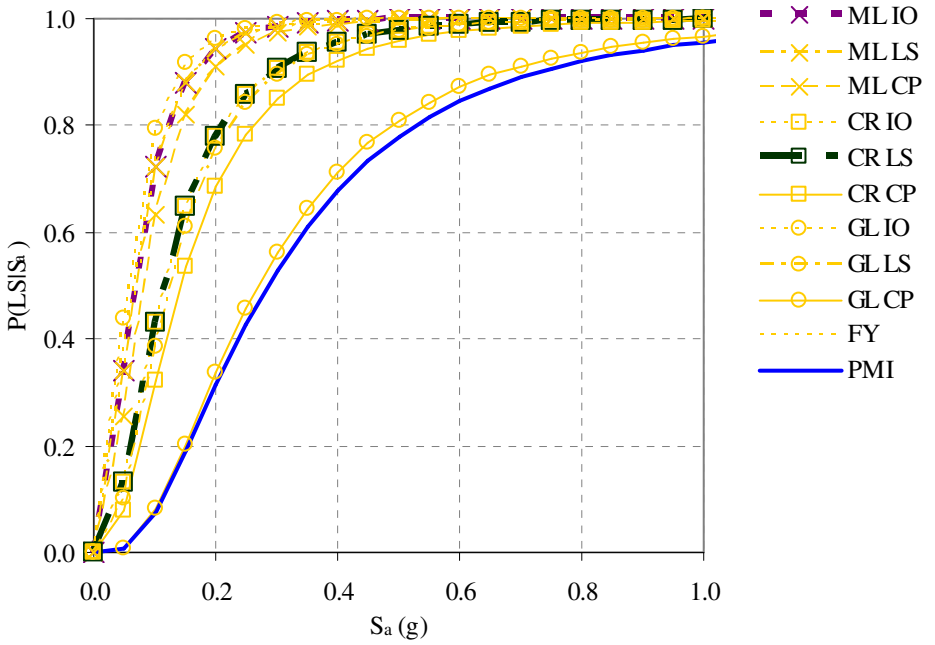

Fig. 6.26. Selection of default fragility curves for CS2 (E-W)

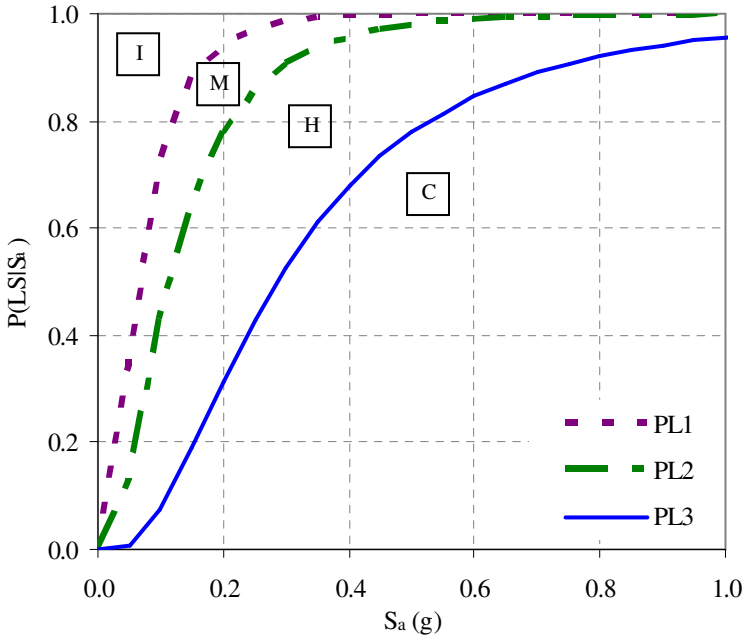

Fig. 6.27. Default fragility curves for CS2 (E-W)

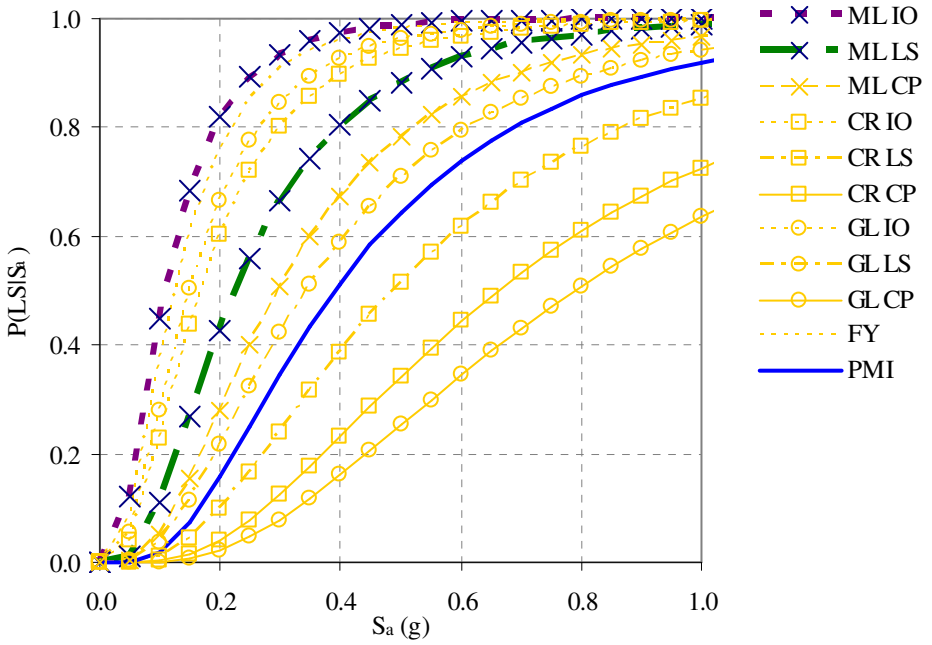

Fig. 6.28. Selection of default fragility curves for CS3 (E-W)

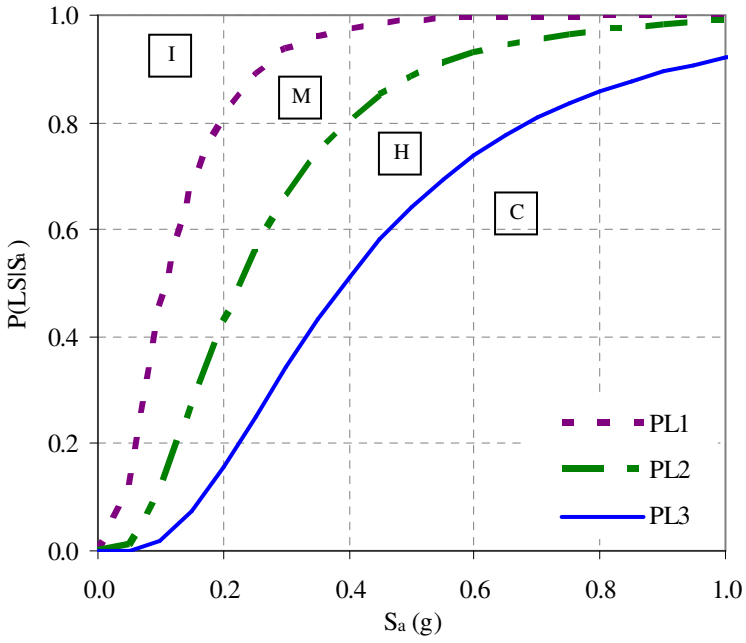

Fig. 6.29. Default fragility curves for CS3 (E-W)

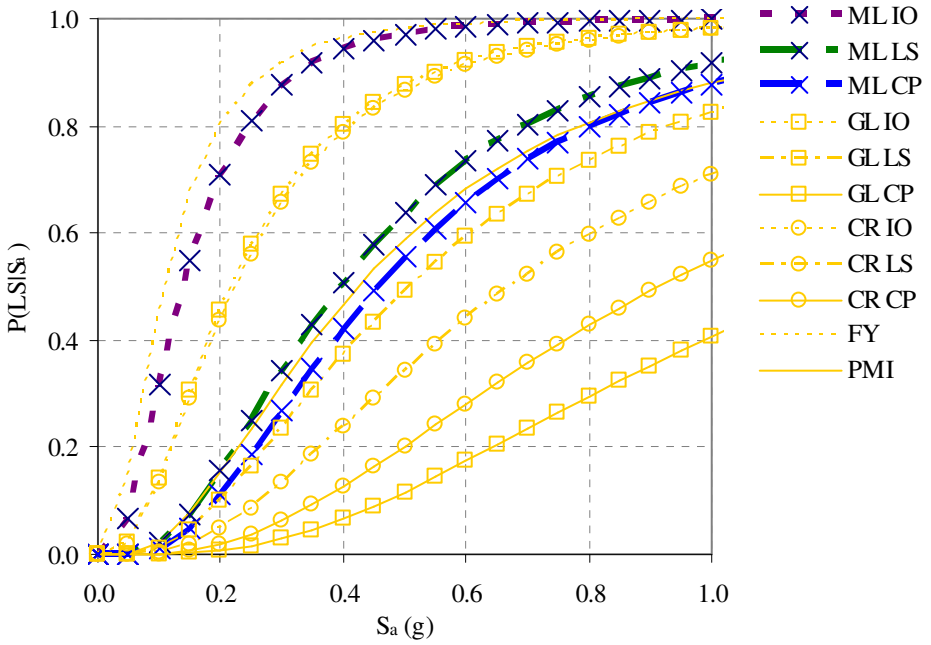

Fig. 6.30. Selection of default fragility curves for CS1 (N-S)

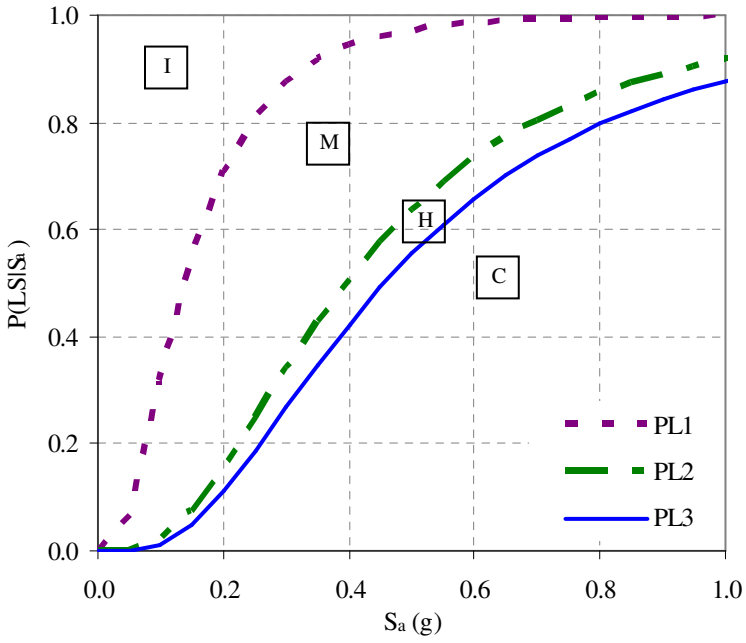

Fig. 6.31. Default fragility curves for CS1 (N-S)

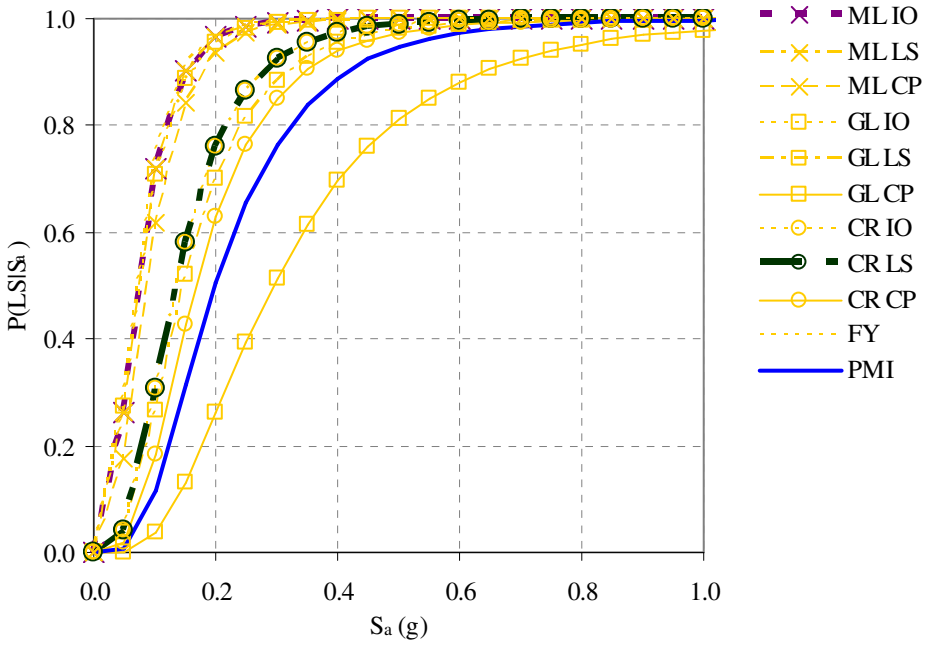

Fig. 6.32. Selection of default fragility curves for CS2 (N-S)

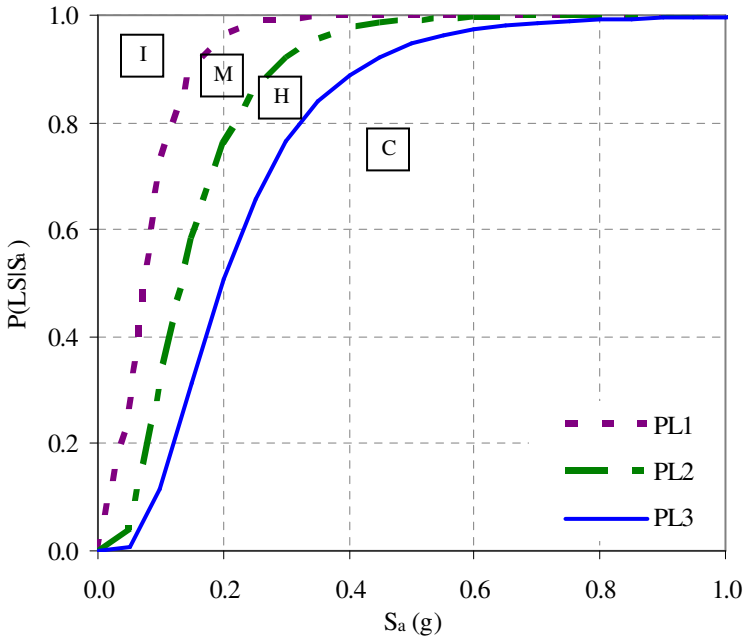

Fig. 6.33. Default fragility curves for CS2 (N-S)

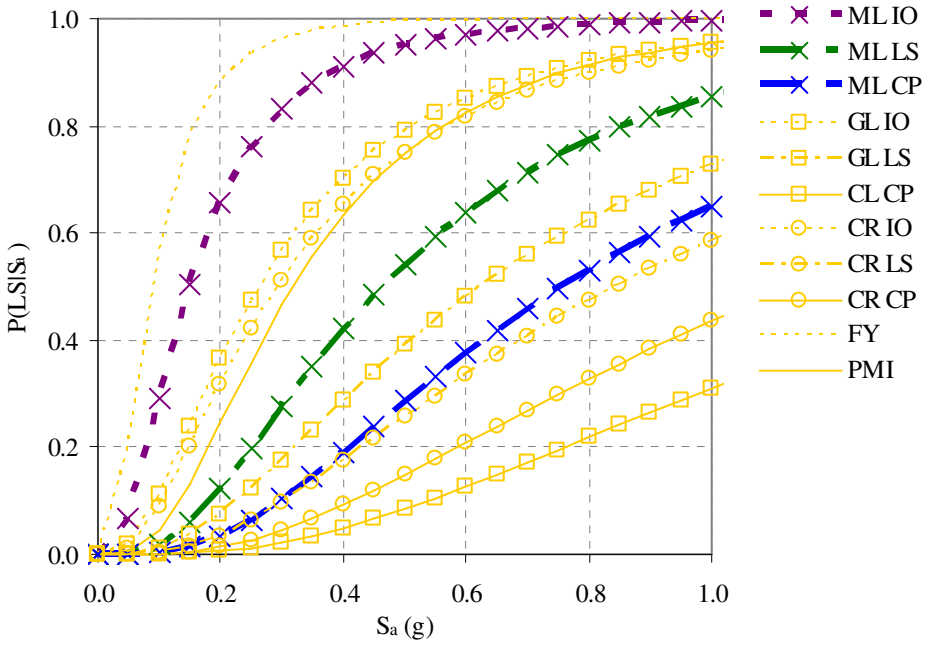

Fig. 6.34. Selection of default fragility curves for CS3 (N-S)

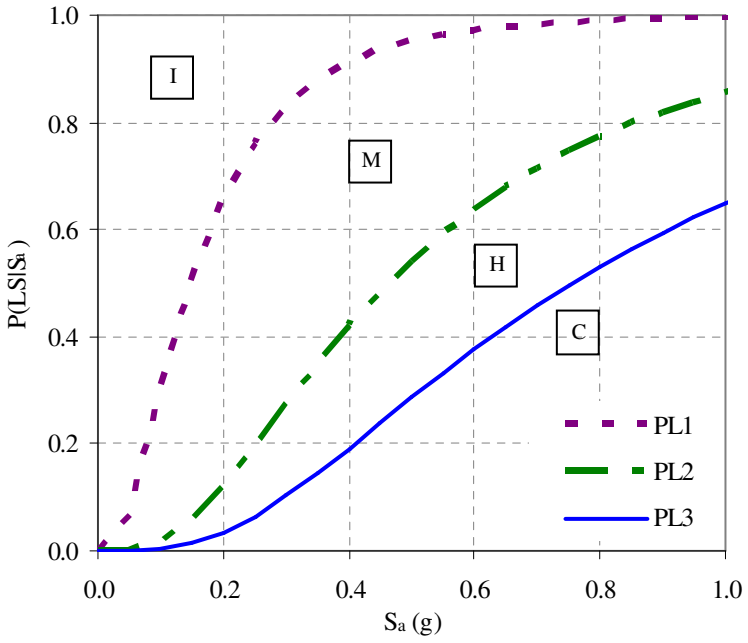

Fig. 6.35. Default fragility curves for CS3 (N-S)

6.4.3 MAEviz Implementation

MAEviz (MAE Center 2006) is a seismic risk assessment software, developed through a joint effort between the Mid-America Earthquake (MAE) Center and the National Center for Supercomputing Application (NCSA). The program uses enhanced graphics and user input options within the consequence-based risk management methodology to generate damage estimates based on extensive research and development of earthquake hazards and seismic performance. The goal of the program is to assist policy-makers and decision-makers in developing risk reduction strategies and implementing mitigation actions.

To simplify the fragility equations and reduce the number of parameters, Eq. (6.2) is used to implement the fragility relationships into MAEviz.

$$P(LS \mid S_a) = \Phi\left(\frac{\ln S_a - \lambda_C}{\beta_C}\right) \tag{6.2}$$

where:

$P(LS \mid S_a)$	=	Probability of exceeding a limit state given a spectral acceleration value
Φ	=	Standard normal cumulative distribution function
S_a	=	Spectral acceleration (g)
λ_C, β_C	=	Modification parameters

The original parameters used to describe the fragility curves [Eq. (6.1)] are different than those in used in the MAEviz simplified equation in Eq. (6.2). As a result, new fragility curves were fitted to the original fragility curve relationships to determine the parameters for the MAEviz fragility expressions, as shown in Fig. 6.36 for CS1 in the E-W direction. The parameters for the MAEviz expressions for each case study are given in Table 6.15.

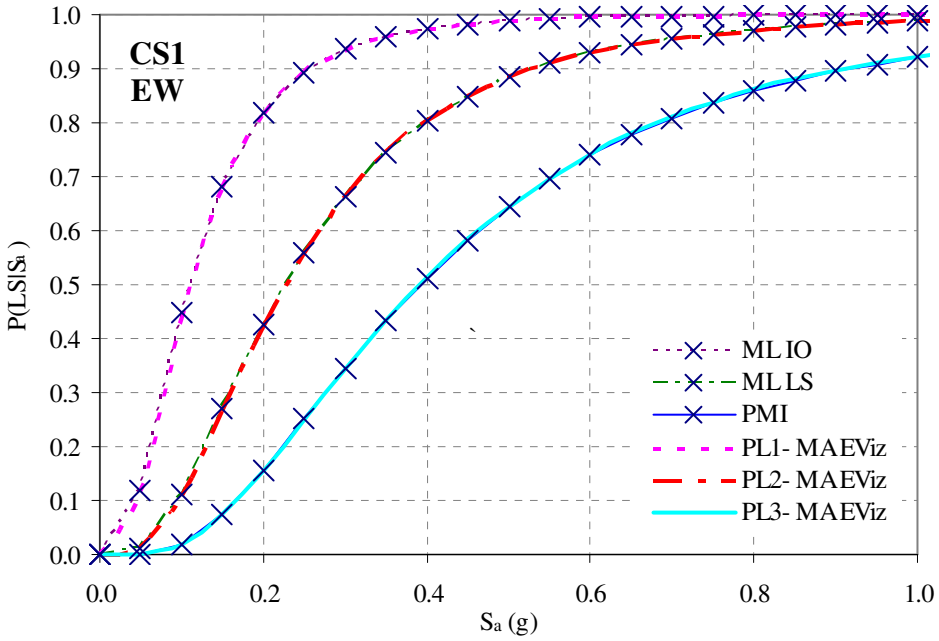

Fig. 6.36. Comparison of default fragility curves with MAEviz fragility expressions

For final implementation into MAEviz, the default fragility curves in Table 6.15 were further reduced to two sets of fragility curves for regional loss estimations. A low-rise IMF concrete building with wide-module joists, designed with the amended 2003 IBC or the 1999 SBC, is represented by the CS2 default fragility curves in the N-S direction. For CS2, the more conservative N-S direction was chosen for the IMF structure due to model stability problems in the E-W direction. The CS1 default fragility curves for the N-S direction are used to represent a low-rise SMF concrete building with joists designed for the 2003 IBC (without amendments). The CS1 default fragility curves showed close agreement between the E-W and N-S directions, with only slight differences for PL3.

Table 6.15. Fragility curve parameters for MAEviz

Direction	Case study	Limit state	λ_C	β_C
CS1	N-S	PL1	-2.11	0.72
		PL2	-1.00	
		PL3	-0.69	
	E-W	PL1	-2.00	0.68
		PL2	-0.93	
		PL3	-0.78	
CS2	N-S	PL1	-2.63	0.58
		PL2	-0.93	
		PL3	-0.78	
	E-W	PL1	-2.70	0.725
		PL2	-2.16	
		PL3	-1.23	
CS3	N-S	PL1	-1.89	0.73
		PL2	-0.78	
		PL3	-0.28	
	E-W	PL1	-2.20	0.66
		PL2	-1.48	
		PL3	-0.94	

7 SUMMARY, CONCLUSIONS AND RECOMMENDATIONS

7.1 Summary

The objective of this study was to evaluate the seismic performance of a four-story reinforced concrete (RC) moment frame designed according to the provisions of three building codes of significance in the Central United States. Case Study 1 (CS1) was designed with the 2003 *International Building Code* (IBC) (ICC 2003) and had a design base shear of 7.2% *W*, while CS2 designed with the 2003 IBC with local amended seismic provisions (City of Memphis and Shelby County 2005) had a design base shear of 3.8% *W*. The design base shear for CS3 was 4.2% *W* using the 1999 *Standard Building Code* (SBC) (SBCCI).

Higher design accelerations classified CS1 and CS3 as Seismic Design Category (SDC) D, requiring a special moment frame (SMF) lateral system. CS2 was classified as SDC C, permitting the use of an intermediate moment frame (IMF). It should be noted that the SBC design was just above the cut-off for SDC D and could qualify as SDC C for slightly different conditions. The lateral system type had the largest influence on the seismic performance of the case study structures. Another critical factor was the number of moment frames required in each direction. In the long (E-W) direction, higher drift demands and redundancy provisions required moment frames along each column line for CS1, while CS2 and CS3 were only required to have exterior lateral frames.

Static push-over and dynamic analyses with synthetic ground motions developed for 2% and 10% probabilities of exceedance in 50 years for Memphis, Tennessee, were used in the performance evaluation. The performance difference between lateral systems is most evident in the N-S (short) direction, for which the same number of moment frames is used for each case study. The N-S push-over analysis showed that the SMF buildings had approximately 1.5 times the strength capacity and ductility of the IMF building. Furthermore, for the 2% in 50 years ground motions, the CS2 model became

unstable when the capacities of the wide-module joists were exceeded in the more vulnerable E-W direction, and a first story mechanism formed in the N-S model.

In the FEMA 356 global interstory drift evaluation, each case study met LS performance for the 10% in 50 years motions. CS1 and CS3 satisfied CP performance for the 2% in 50 years motions, but first story drifts in CS2 resulting from the story mechanism exceeded the CP performance level for the 2% in 50 years hazard. For the more detailed member-level evaluation based on plastic rotation limits, CS2 was the only case study that did not meet LS performance for the 10% in 50 years motions. None of the case studies satisfied the CP performance level for the 2% in 50 years event. The median maximum column plastic rotations of the SMF case studies for the 2% in 50 years event were a maximum of two times the CP rotation limits in a few locations, as compared to as much as 18 times the CP limits for the CS2 columns. The exceedance of the plastic rotation limits by the SMFs may indicate that the FEMA 356 limits for RC frame members are quite conservative. However, it is recognized that the 2% in 50 years Memphis motions have significant spectral acceleration values.

The Basic Safety Objective (BSO) in FEMA 356 reflects the general seismic design code philosophy to accomplish two limited performance objectives: (1) to resist higher probability of occurrence earthquakes (10% probability of exceedance in 50 years) without loss of life (Life Safety or LS); and (2) to withstand lower probability earthquakes (2% probability of exceedance in 50 years) without collapse (Collapse Prevention or CP). CS1 and CS3 met the BSO for the global drift evaluation, but the second performance objective was not met for the more detailed member-level evaluation. CS2 did not meet either of the BSO performance objectives.

7.2 Conclusions

This study shows the expected demands and resulting damage for a Central U.S. RC frame building designed according to the building codes currently adopted in Memphis, Tennessee. These building codes are also applicable in other parts of the Central U.S., and the structure type considered is relatively common. The following conclusions were drawn for this study:

1. The comparative performance evaluation of the three case study designs underscores the importance of the lateral system type (seismic detailing) in the seismic performance. Even with relatively different design base shears, the IBC and SBC designs with special moment frames (SMFs) met the same FEMA 356 performance objectives. In contrast, the intermediate moment frame (IMF) designed with the IBC with local seismic amendments exhibited lower performance and did not meet either Life Safety (LS) for 10% in 50 years or Collapse Prevention (CP) performance for 2% in 50 years for the member-level evaluation. Differences in the structural performance of each lateral resisting system were also evident in the nonlinear analysis responses and the fragility curves.
2. Redundancy provisions and higher drift demands also impacted the performance of the case studies, but to a lesser extent than the lateral system type. The 2003 IBC was the only building code that included redundancy provisions for the redistribution of lateral forces, which can restrict the moment frame layout. The higher design drift demands associated with the higher design base shears influenced the column sizes.
3. The maximum interstory drifts for each case study for the 10% probability of exceedance in 50 years event were similar and within suggested LS global interstory drift values. However, the fragility curves show that there is still a considerable probability of exceeding the LS performance level for the amended IBC designed building for the 10% in 50 years ground motion based on the member-level evaluation. Conversely, the probabilities of exceeding the LS performance level for the SMF case studies were very low for the same hazard level.
4. For the 2% in 50 years hazard, the case study structure designed with the 2003 IBC with local Memphis seismic amendments (CS2) has a significant probability of exceeding the CP performance level. The CS2 building model became unstable when the wide-module joist capacities were exceeded in the more

vulnerable long (E-W) direction under the 2% in 50 years motions, and a story mechanism formed in the short (N-S) direction with predicted first story drifts of greater than 7%.

5. For the 2% in 50 years Memphis motions, the case study buildings designed as SMFs showed substantially better performance than the IMF building based on the nonlinear analysis and FEMA 356 performance evaluation.
6. FEMA 356 member-level CP plastic rotation limits for RC frames were exceeded by the case studies designed for the most up-to-date seismic code (IBC 2003) for the 2% in 50 years motions, which may indicate that these limits are conservative.
7. The differences in the fragility curves for the special and intermediate moment frame buildings show the importance of knowing the type of lateral system when selecting fragility curves to predict the probabilities of exceeding limits states for a given earthquake intensity.

7.3 Recommendations for Future Research

The work in this study was limited to a four-story concrete moment frame building with a wide-module joist floor system. The case study performance was dependent on the structural layout; therefore, the performance would vary for different types of structural configurations such as irregular structures and structures with a greater or lesser number of stories. Some recommendations for complementary research are listed below.

1. Investigating different structural types and configurations using the same methodology would broaden the scope of determining the impact of current building code seismic provisions in the Central U.S. Additional structural types might include special and intermediate steel moment frames, taller RC frames, or RC shear wall systems.
2. The building site for this study was located in downtown Memphis, which has some of the largest seismic design values in the Memphis area. As mentioned previously, slightly lower seismic design values in the 1999 SBC design would

classify the case study structure as Seismic Design Category C, requiring less seismic detailing, and would significantly affect the performance. Running a similar analysis with an intermediate moment frame for the 1999 SBC design instead of a special moment frame to determine the effect on the performance might be useful.

3. This study utilized synthetic ground motions developed for the Memphis area. To apply this study to a larger region, ground motions for other vulnerable areas in the New Madrid Seismic Zone could also be investigated.
4. A more in-depth cost assessment for the special and intermediate moment frame buildings would be useful in determining practical cost-benefit ratios of designing for improved seismic performance.

REFERENCES

Abrams, D. P., and Shinozuka, M., ed. (1997). "Loss assessment of Memphis buildings." *Technical Report NCEER-97-0018.* National Center for Earthquake Engineering Research, Buffalo, NY.

ACI Committee 318. (1995). *Building Code Requirements for Reinforced Concrete (ACI 318-95)*, American Concrete Institute, Detroit, MI.

ACI Committee 318. (2002). *Building Code Requirements for Reinforced Concrete (ACI 318-02)*, American Concrete Institute, Farmington, MI.

AISC. (2005). *Steel Construction Manual*, American Institute of Steel Construction, Inc., Chicago, IL.

ASCE. (1995). *ASCE Minimum Design Loads for Buildings and Other Structures (ASCE 7-95)*, American Society of Civil Engineers, Washington, DC.

ASCE. (2000). *Prestandard and Commentary for the Seismic Rehabilitation of Buildings (FEMA 356)*, American Society of Civil Engineers, Washington, DC.

ASCE. (2002). *ASCE Minimum Design Loads for Buildings and Other Structures (ASCE 7-02)*, American Society of Civil Engineers, Washington, DC.

Bai, J. W., Hueste, M. B., and Gardoni, P. (2007) "Assessment of the expected seismic structural losses for buildings in Mid-America." submitted to *Journal of Structural Engineering*.

Beavers, J. (2002). "A review of seismic hazard description in US design codes and procedures." *Progress of Structural Engineering Materials*, 4, 46-63.

BSSC. (1992). *NEHRP Recommended Provisions for the Development of Seismic Regulations for New Buildings, Part 1: (Provisions) and Part II: (Commentary)*, Building Seismic Safety Council, Washington, DC.

BSSC. (1998). *NEHRP Recommended Provisions for Seismic Regulations for New Buildings and Other Structures, Part 1: (Provisions) and Part II: (Commentary)*, Building Seismic Safety Council, Washington, DC.

BSSC. (2004). *NEHRP Recommended Provisions for Seismic Regulations of New Buildings and Other Structures Part 1: Provisions (FEMA 450),* Building Seismic Safety Council, Washington, DC.

City of Memphis and Shelby County. (2005). "Appendix L- Alternate Seismic Protection Calculations and Procedures." Memphis and Shelby County 2005 Joint Building Code Local Amendments, Memphis, TN.

Cornell, C. A., Jalayer, F., Hamburger, R. O., and Foutch, D. A. (2002). "Probabilistic basis for the 2000 SAC Federal Emergency Management Agency steel moment frame guidelines." *Journal of Structural Engineering*, 128(4), 526-533.

CSI. (2002). *An Introduction to ETABS: Version 8*, Computers and Structures, Inc., Berkeley, CA.

CUSEC. (2007). "New Madrid Seismic Zone." Central United States Earthquake Consortium, <http://www.cusec.org/S_zones/NMSZ/nmsz_home.htm> (Nov. 12, 2007).

Dooley, K. L., and Bracci J. M. (2001). "Seismic evaluation of column-to-beam strength ratios in reinforced concrete frames." *ACI Structural Journal*, 98(6), 843-851.

Dowty, S., and Ghosh, S. K. (2002). "IBC structural provisions: A better alternative." *Building Standards*, 12-16.

Elnashai, A. S., Papanikolaou, V. and Lee, D.H. (2002). *ZEUS-NL User Manual*, Mid-America Earthquake Center, University of Illinois at Urbana-Champaign.

Erberik, M. A., and Elnashai, A.S. (2004). "Fragility analysis of flat-slab structures." *Engineering Structures*, 26, 937–948.

FEMA. (1985). "An Assessment of Damage and Casualties for Six Cities in the Central United States Resulting from Earthquakes in the New Madrid Seismic Zones." Prepared under contract EMK-C-0057 (CUSEPP), Federal Emergency Management Agency, Washington, DC.

Fernández, J., and Rix, G. (2006). "Soil attenuation relationships and seismic hazard analyses in the Upper Mississippi Embayment." Eighth U.S. National Conference on Earthquake Engineering 8NCEE, San Francisco, CA.

Francis, S., and Stone, J. (1998). "The International Building Code and its impact on wood-frame design and construction." *1998 ASAE Annual International Meeting*, Orlando, FL.

French, S., and Muthukumar, S. (2004). "Shelby County Inventory Database." Mid-America Earthquake Center, University of Illinois at Urbana-Champaign.

Hamburger, R., and Kircher, C. (2000). "Recent developments in seismic design: Methodologies and codes." *Earthquake Spectra*, 16(1), vii-xiii.

Hayes, J. R., Woodson, S. C., Pekelnicky, R. G., Poland, C. D., Corely, W. G., and Sozen, M. (2005). "Can strengthening for earthquake improve blast and progressive collapse resistance?" *Journal of Structural Engineering*, 131(8), 1157-1177.

Holmes, W. (2000). "The 1997 NEHRP recommended provisions for seismic regulations for new buildings and other structures." *Earthquake Spectra*, 16(1), 101-114.

Hueste, M. B., and Bai, J. W. (2007). "Seismic retrofit of a reinforced concrete flat-slab structure: Part I- seismic performance evaluation." *Engineering Structures*, 29(6), 1165-1177.

Hwang, H. H. M., and Huo, J-R. (1997). "A method for earthquake motion-damage relationships with application to reinforced concrete frames." Loss-Assessment of Memphis buildings. *Technical Report NCEER 97-0008*, National Center for Earthquake Engineering Research, Buffalo, NY.

ICC. (2003). *International Building Code (IBC 2003)*, International Code Council, Falls Church, VA.

Jeong, S. H., and Elnashai, A. S. (2005). "Analytical assessment of an irregular RC frame for full scale 3D pseudo-dynamic testing Part I: Analytical model verification." *Journal of Earthquake Engineering* 9(1), 95-128.

Kalkan, E., and Kunnath, S. (2006). "Assessment of current nonlinear static procedures for seismic evaluation of buildings." *Engineering Structures*, 29, 305-316.

Karayannis, C. G., Izzuddin, B. A. and Elnashai, A. S. (1994). "Application of adaptive analysis to reinforced concrete frames." *Journal of Structural Engineering*, 120(10), 2935-2957.

Kinali, K., and Ellingwood, B.R. (2007). "Seismic fragility assessment of steel frames for consequence-based engineering: A case study for Memphis, TN." *Engineering Structures*, 29(6), 1115-1127.

Krawinkler, H., and Seneviratna, G. D. P. K. (1998). "Pros and cons of a pushover analysis of seismic performance evaluation." *Engineering Structures*, 20(4-6), 452-464.

Leyendecker, E. V., Hunt, R. J., Frankel, A. D., and Rukstales, K. S. (2000). "Development of maximum considered earthquake ground motion maps." *Earthquake Spectra*, 16(1), 21-40.

Mander, J. B., Priestley, J.N., and Park, R. (1988). "Observed stress-strain behavior of confined concrete." *Journal of Structural Engineering*, 114(8), 1827-1849.

Mid-America Earthquake Center. (2006). "Earthquake Risk Assessment Using MAEviz." University of Illinois at Urbana-Champaign.

Mwafy, A. M., and Elnashai, A. S. (2001). "Static pushover versus dynamic collapse analysis of RC buildings." *Engineering Structures*, 23(5), 407-424.

Pezeshk, S. (2004). "Site specific considerations in seismic design." West Tennessee Structural Engineer's Association, Memphis, Tennessee. <http://www.ce.memphis.edu/WTNSEA/Site%20Specific%20Considerations%20in%20Seismic-for%20web%20page.pdf> (Oct. 2, 2006).

Ramamoorthy, S., Gardoni, P., and Bracci, J. (2006). "Probabilistic demand models and fragility curves for reinforced concrete frame." *Journal of Structural Engineering*, 132(10), 1563-1572.

Rix, G. J., and Fernandez, J.A. (2006). "Probabilistic ground motions for selected cities in the Upper Mississippi Embayment." Georgia Tech, <http://www.ce.gatech.edu/~geosys/soil_dynamics/research/groundmotionsembay/> (Apr. 6, 2006).

Romero, S., and Rix, G. (2001). "Regional variation in near surface shear wave velocity in the Greater Memphis area." *Engineering Geology*, 62, 137-158.

RS Means. (2007). *Building Construction Cost Data 65th Annual Edition*, R.S. Means Construction Publishers & Consultants, Kingston, MA.

Sadjadi, R., Kianoush, M.R., and Talebi, S. (2007). "Seismic performance of reinforced concrete moment resisting frames." *Engineering Structures*, in press.

SBCCI. (1999). *Standard Building Code (SBC)*, Southern Building Code Congress International, Birmingham, AL.

Singhal, A., and Kiremidjian, A. S. (1997). "A method for earthquake motion-damage relationships with application to reinforced concrete frames." *Technical Report NCEER 97-0008.* National Center for Earthquake Engineering Research, Buffalo, NY.

Street, R. L., and Nuttli, O. W. (1990). "The great central Mississippi valley earthquakes of 1811-1812." University of Kentucky, Lexington.

Trifunac, M. D., and Brady, A.G. (1975). "A study on the duration of strong earthquake ground motion." *Bulletin of the Seismological Society of America*, 65(3), 581-626.

Wen, T. K., and Wu, C. L. (2000). "Generation of ground motions for Mid-America cities." Mid-America Earthquake (MAE) Center <http:/mae.ce.uiuc.edu/newsite/research/rr-1/gmotions/index.html> (27 Jan. 2000).

Wen, T. K., Ellingwood, B. R., and Bracci, J. M. (2004). "Vulnerability functions." Mid-America Earthquake Center, University of Illinois at Urbana-Champaign.

Wen, Y. K., Ellingwood, B.R., Veneziano, D. and Bracci, J.M. (2003). "Uncertainity Modeling in Earthquake Engineering." Mid-America Earthquake (MAE) Center Project FD-2 Report, Urbana, IL.

APPENDIX A GROUND MOTION TIME HISTORIES

The acceleration time histories for both the Rix and Fernandez ground motion records (see Section 4.3) and the Wen and Wu ground motions records (see Section 6.1.2) are provided. The vertical dotted line denotes the time step at which 95 percent of the earthquake energy is imparted, discussed in Section 4.3.

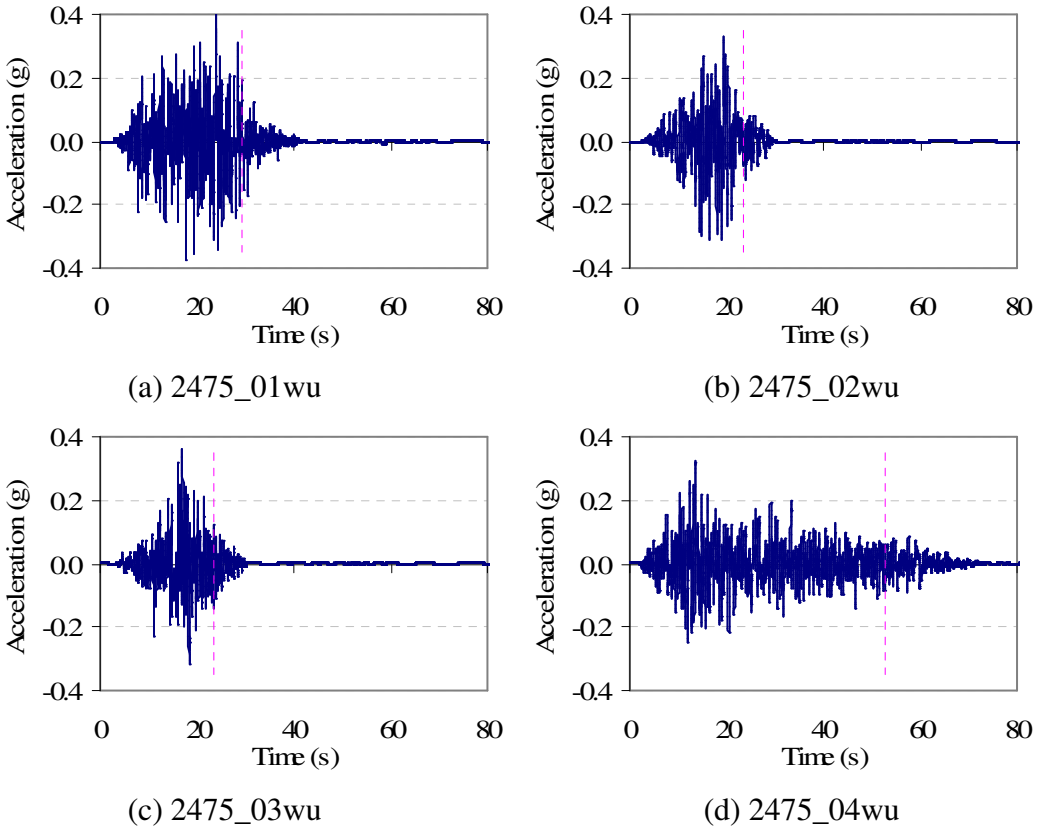

(a) 2475_01wu (b) 2475_02wu

(c) 2475_03wu (d) 2475_04wu

Fig. A.1. Acceleration time histories for 2% in 50 years Wen and Wu motions

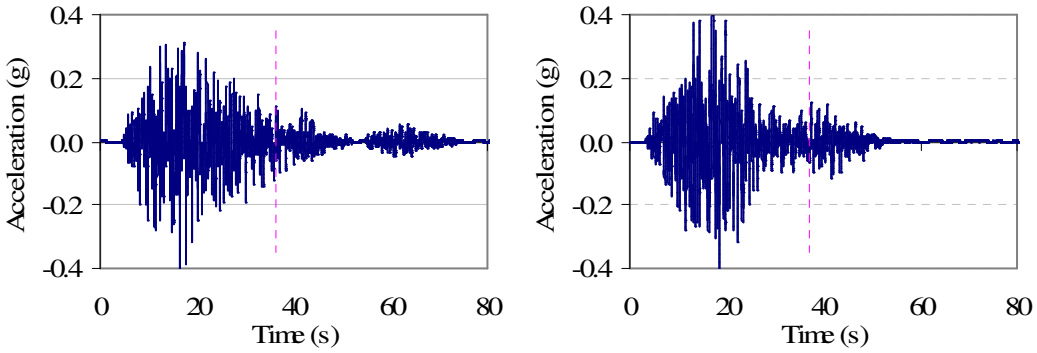

(e) 2475_05wu

(f) 2475_06wu

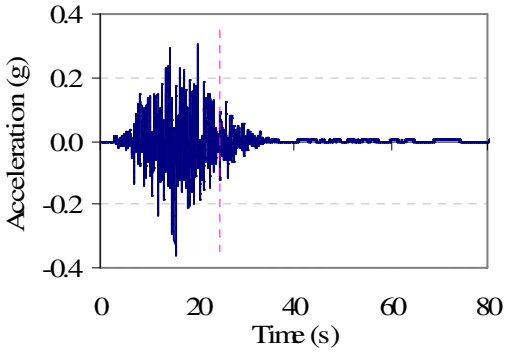

(g) 2475_07wu

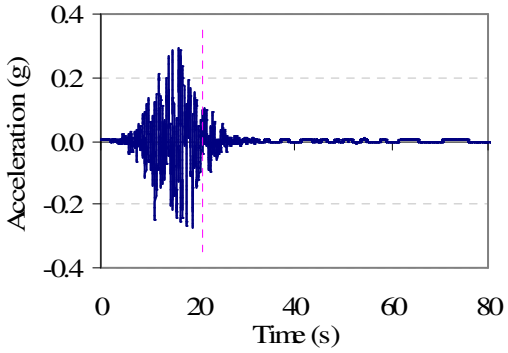

(h) 2475_08wu

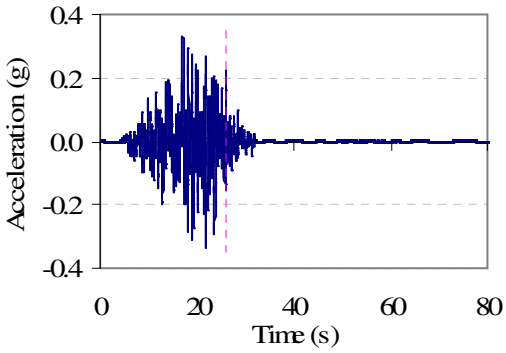

(i) 2475_09wu

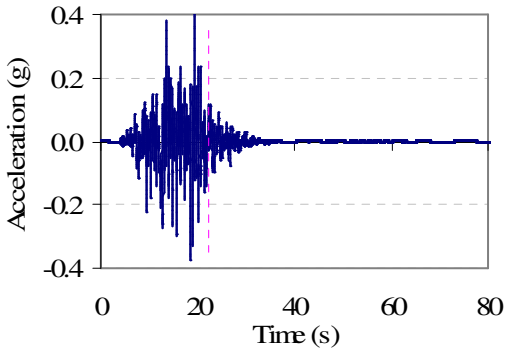

(j) 2475_010wu

Fig. A.1. Continued.

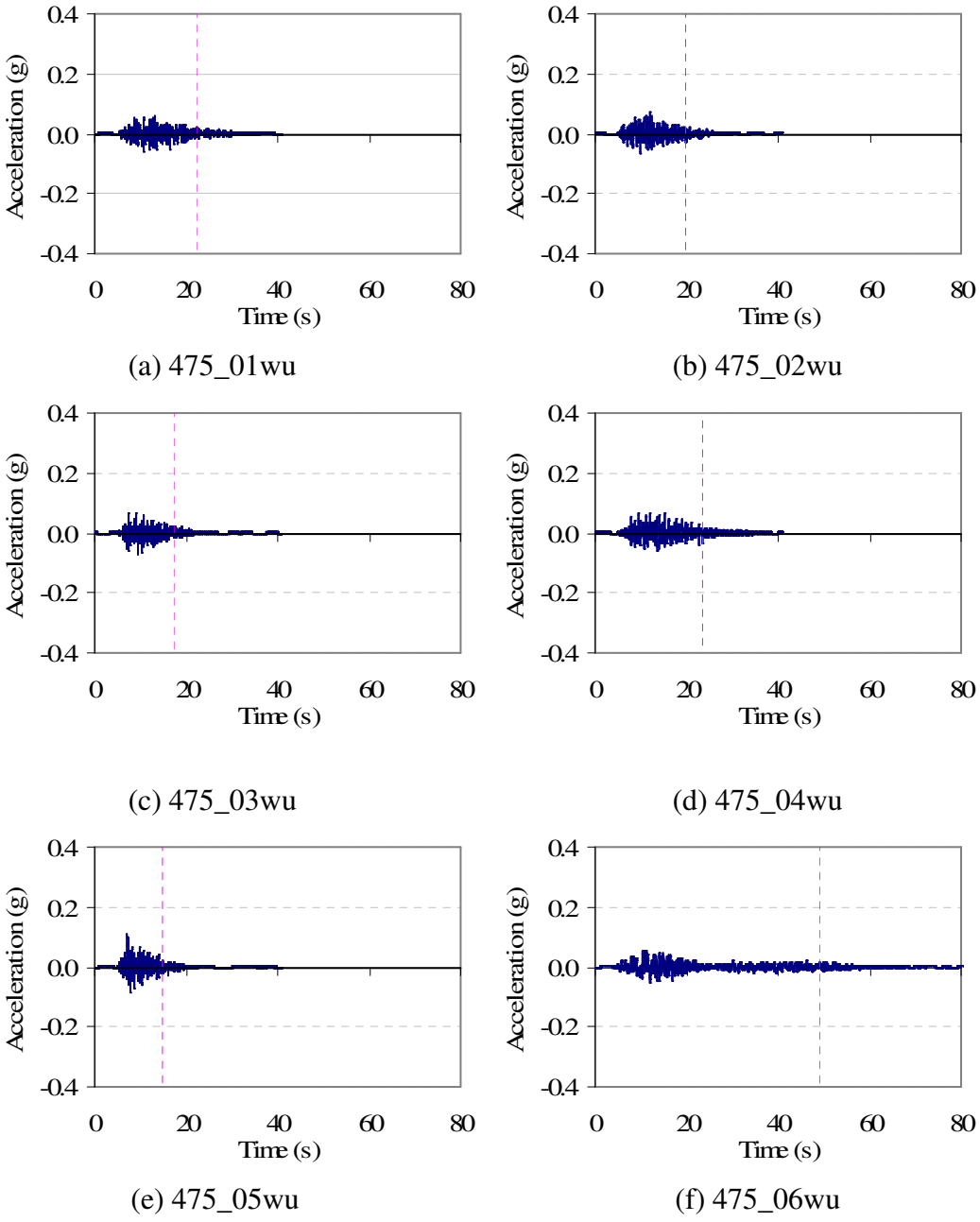

Fig. A.2. Acceleration time histories for 10% in 50 years Wen and Wu motions

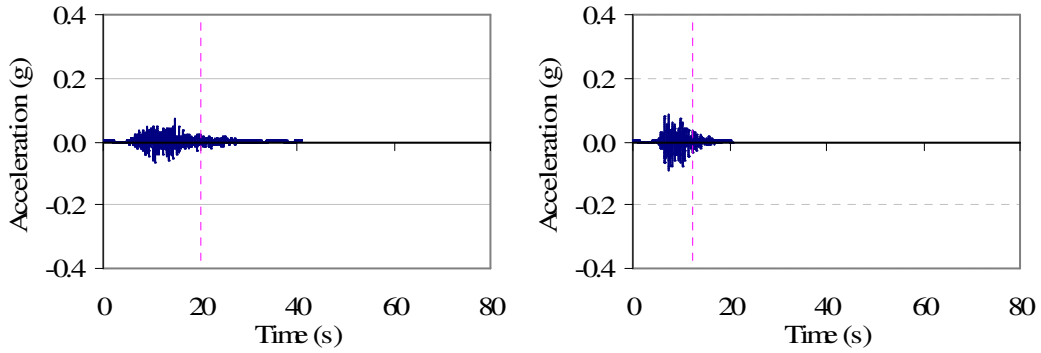

(g) 475_07wu

(h) 475_08wu

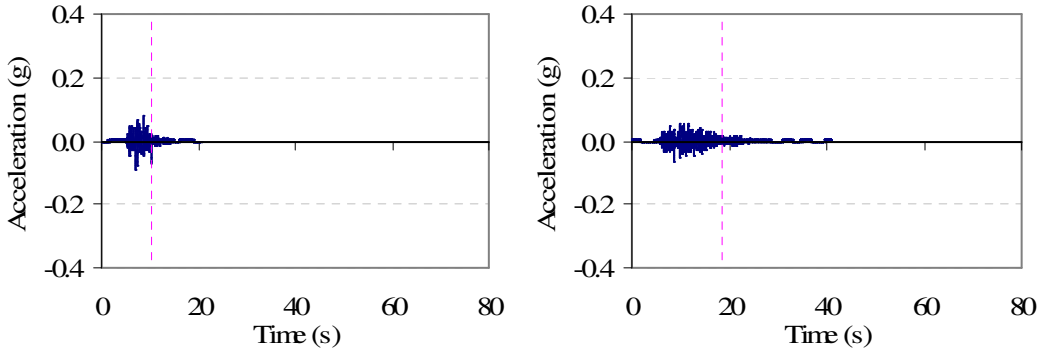

(i) 475_09wu

(j) 475_010wu

Fig. A.2. Continued.

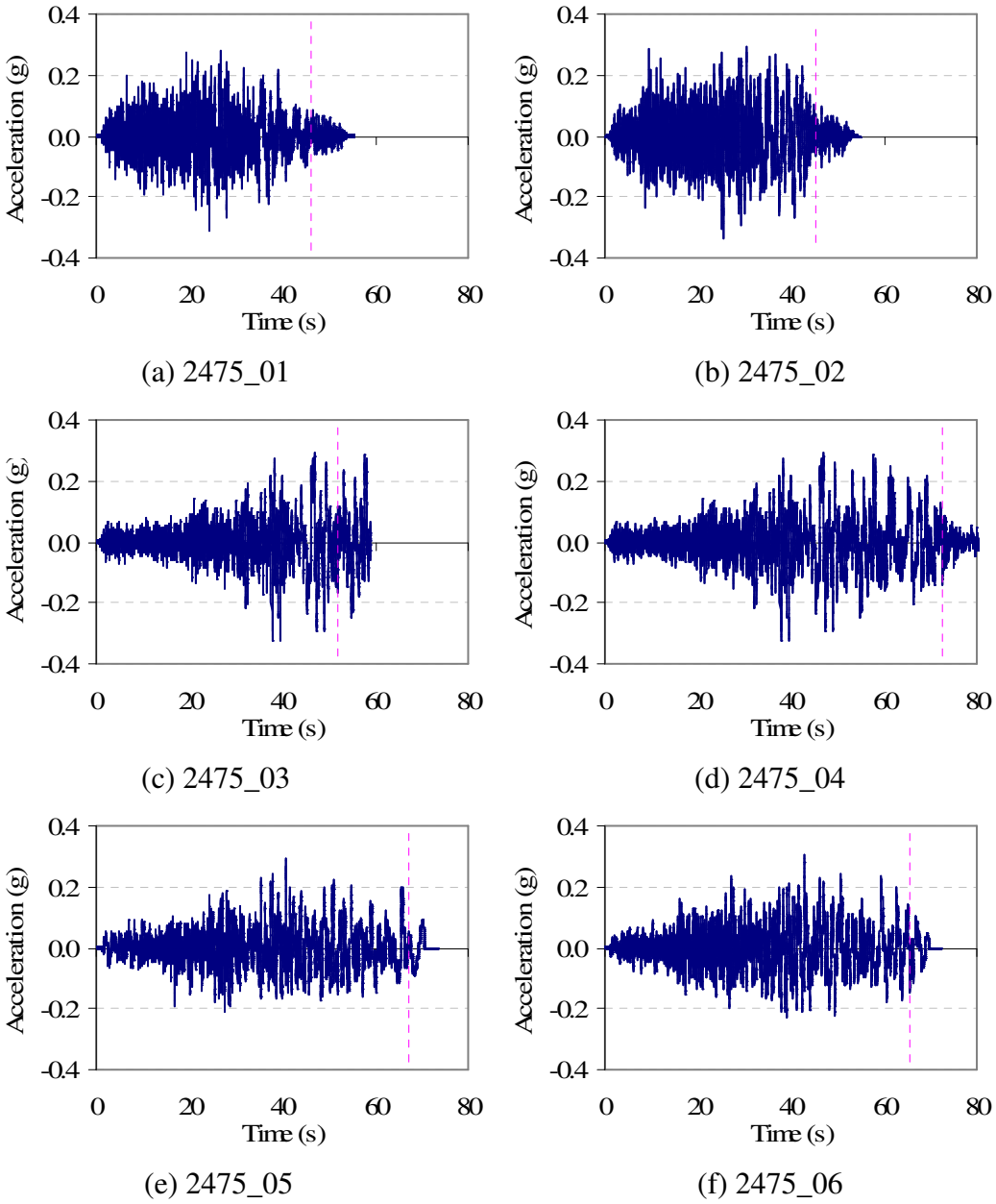

Fig. A.3. Acceleration time histories for 2% in 50 years Rix and Fernandez motions

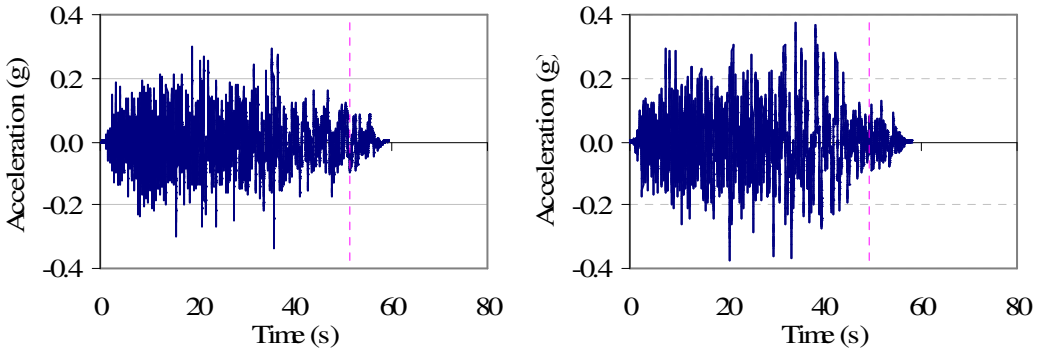

(g) 2475_07

(h) 2475_08

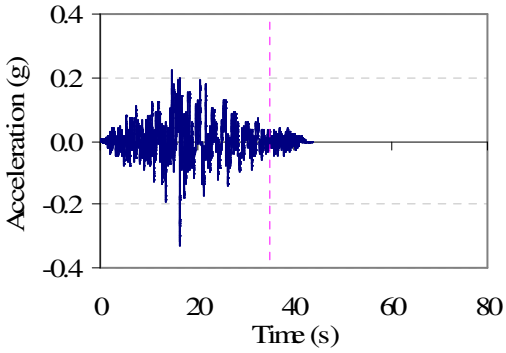

(i) 2475_09

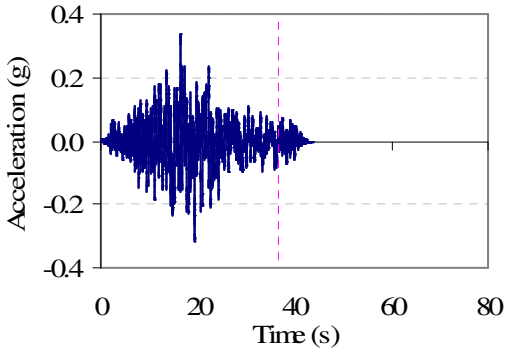

(j) 2475_010

Fig. A.3. Continued.

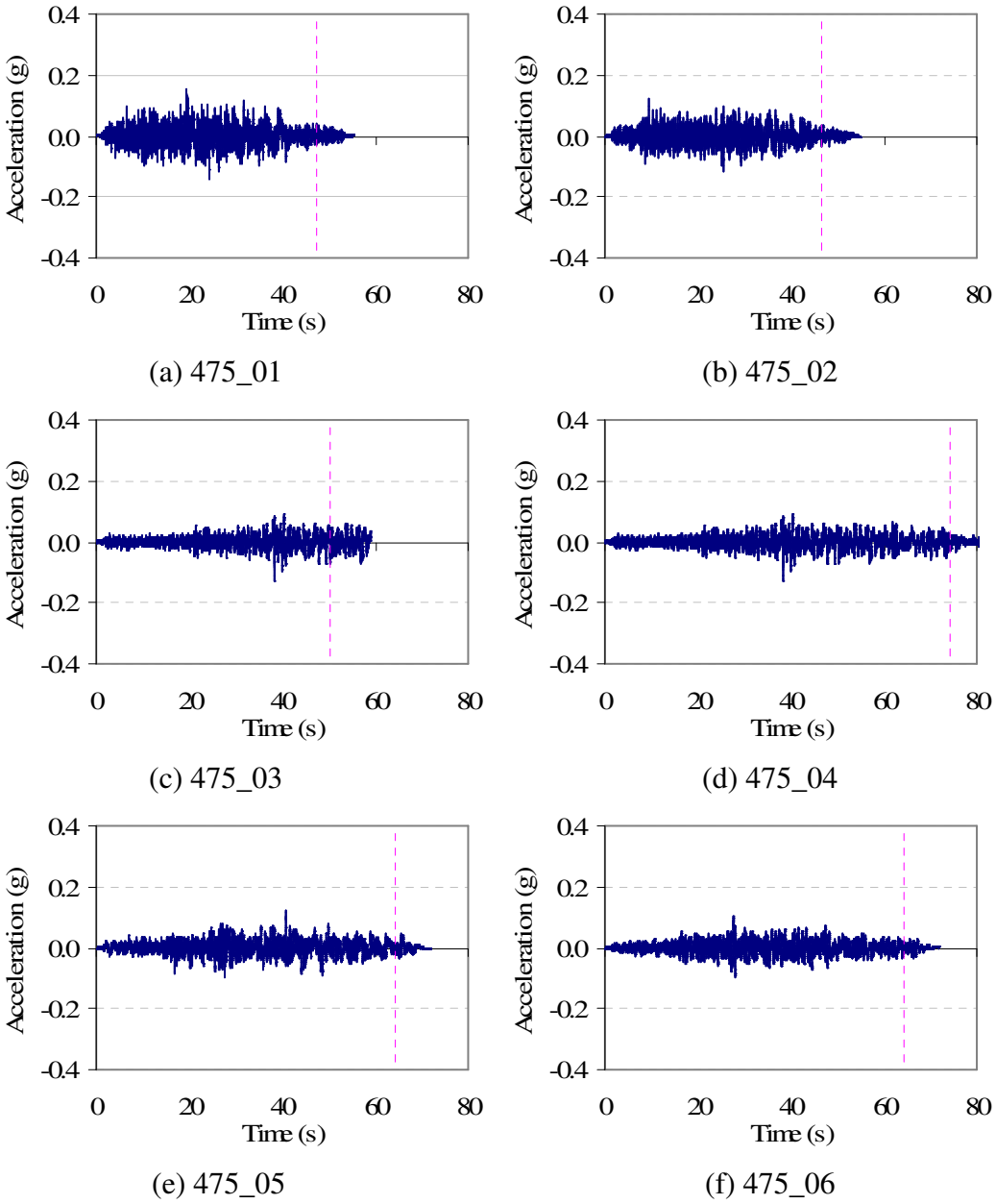

Fig. A.4. Acceleration time histories for 10% in 50 years Rix and Fernandez motions

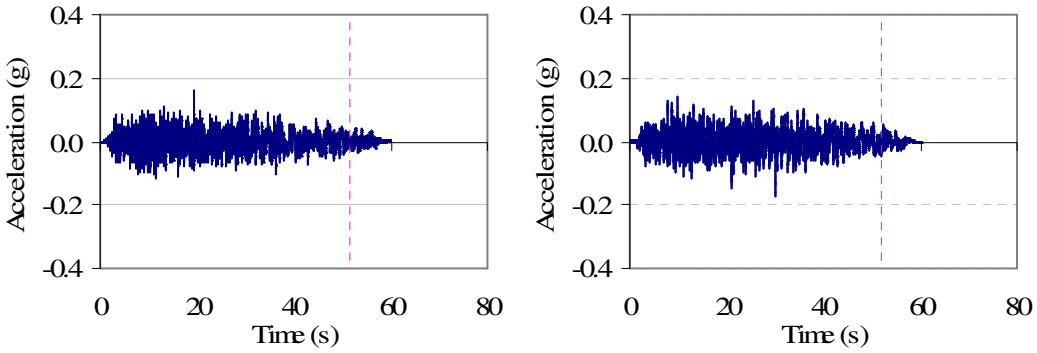

(g) 475_07

(h) 475_08

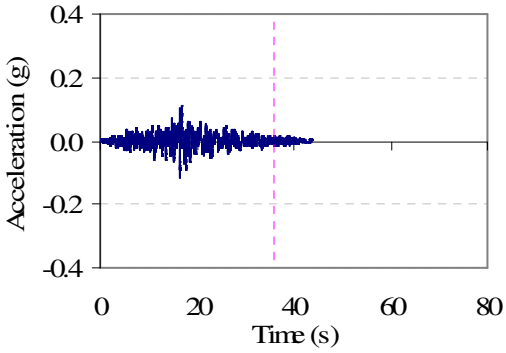

(i) 475_09

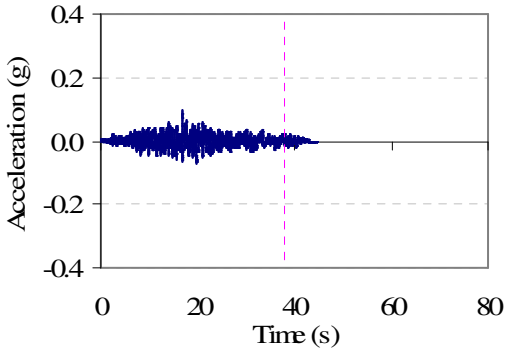

(j) 475_010

Fig. A.4. Continued.

APPENDIX B MAXIMUM INTERSTORY DRIFTS

The maximum interstory drifts for both the 10% and 2% in 50 years hazards for each case study for the Rix and Fernandez and the Wen and Wu ground motion records are provided. The median maximum drifts are provided for each case in bold.

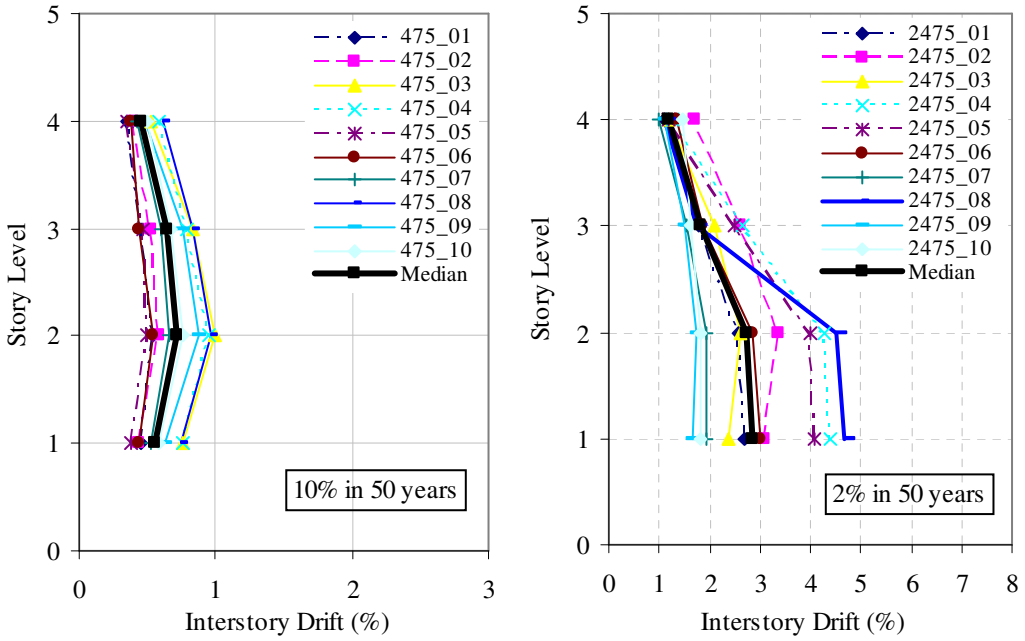

(a) CS1

Fig. B.1. N-S maximum interstory drifts (Rix and Fernandez motions)

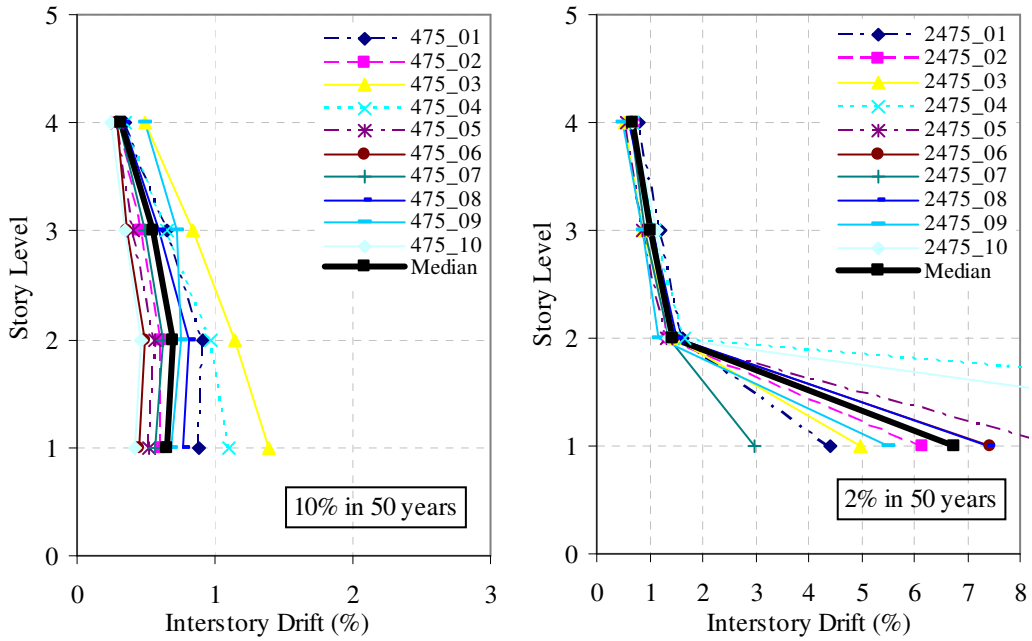

(b) CS2

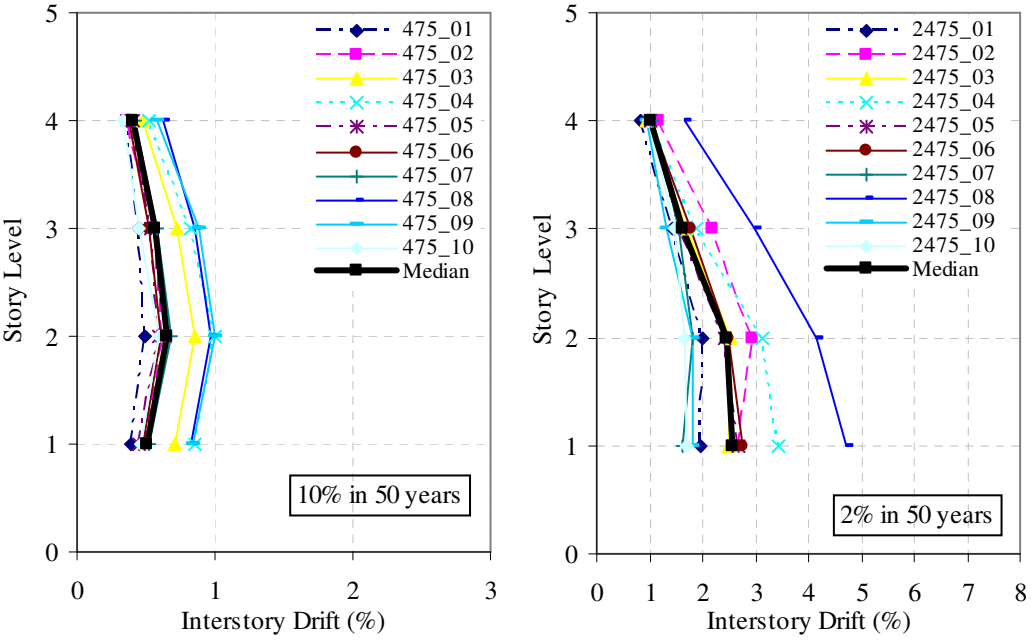

(c) CS3

Fig. B.1. Continued.

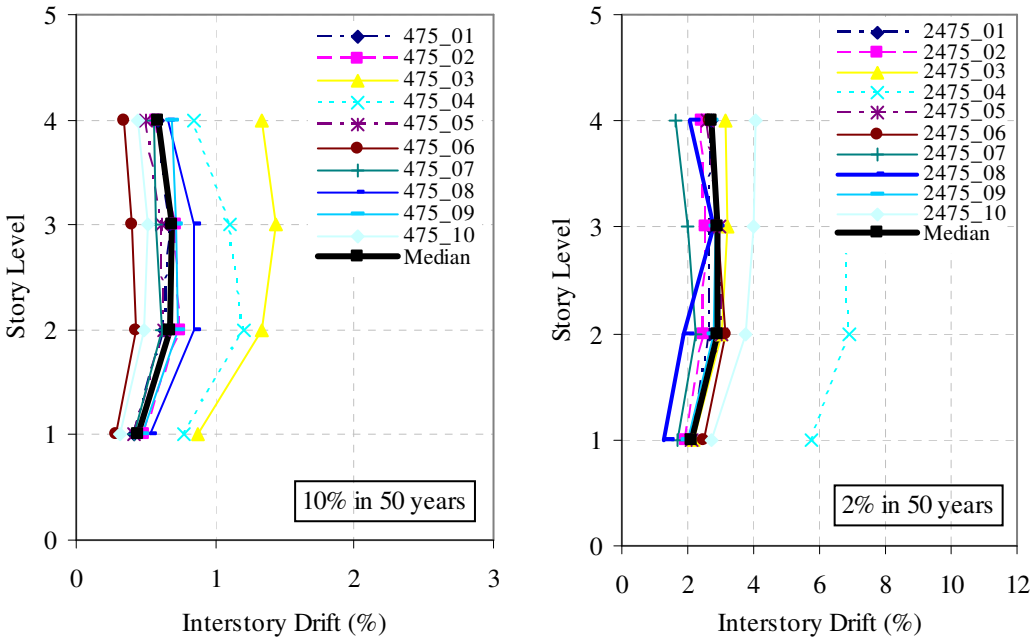

(a) CS1

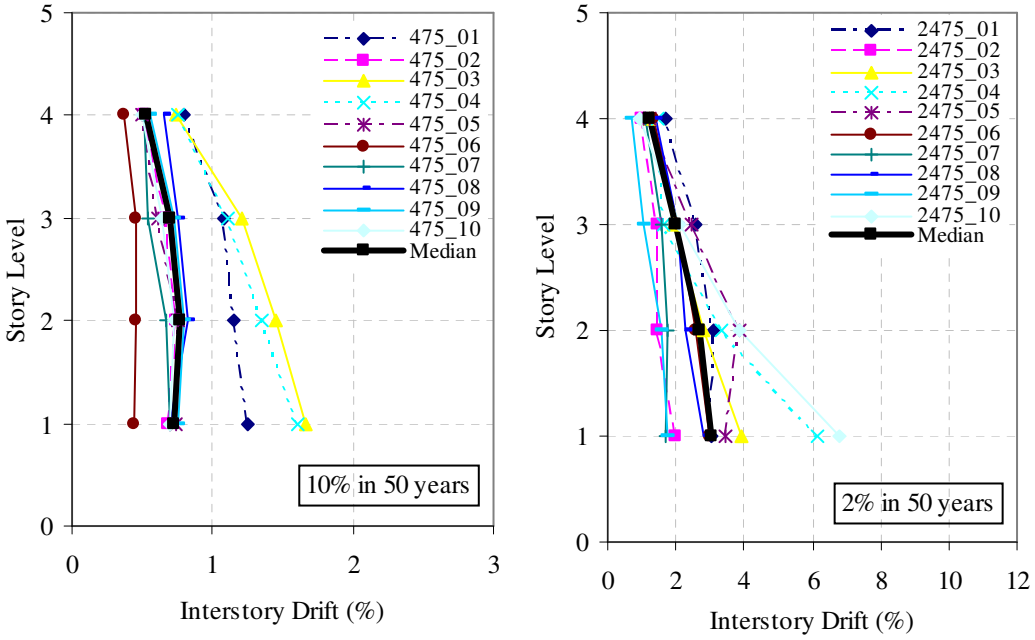

(b) CS2

Fig. B.2. E-W maximum interstory drifts (Rix and Fernandez motions)

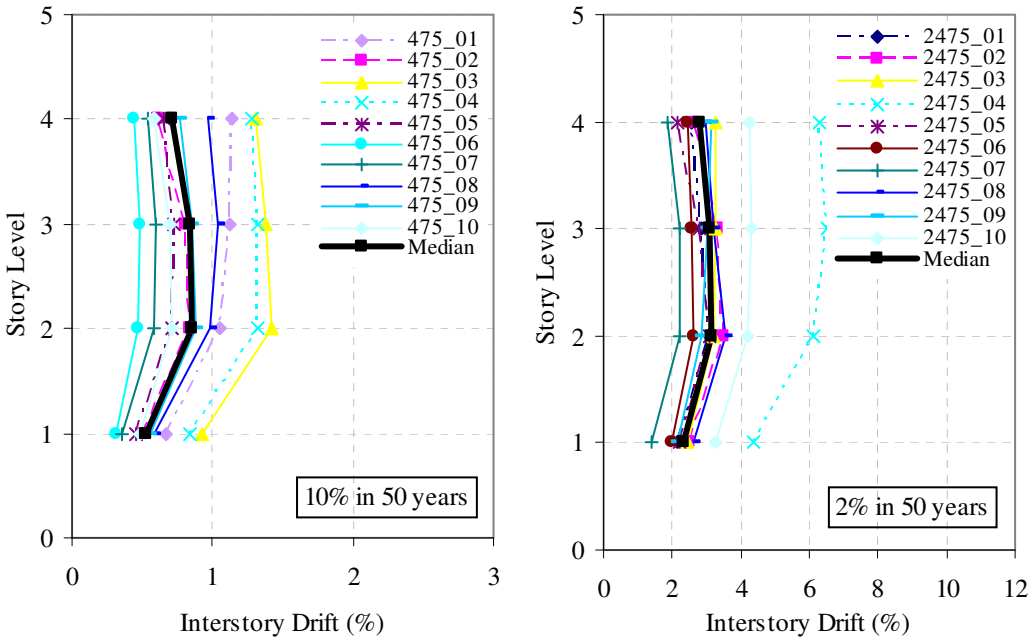

(c) CS3

Fig. B.2. Continued.

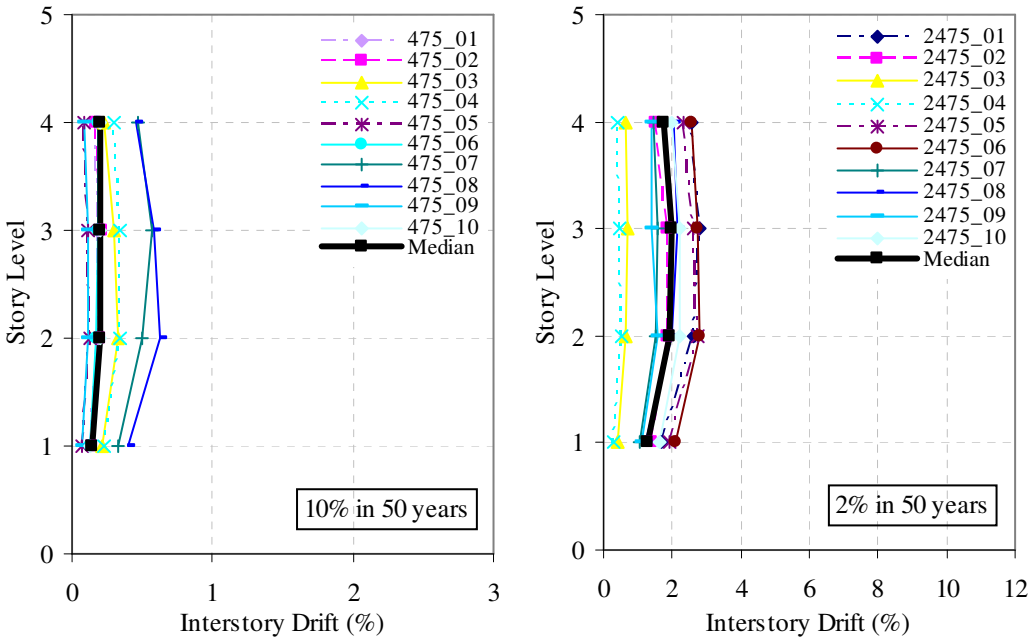

(a) CS1

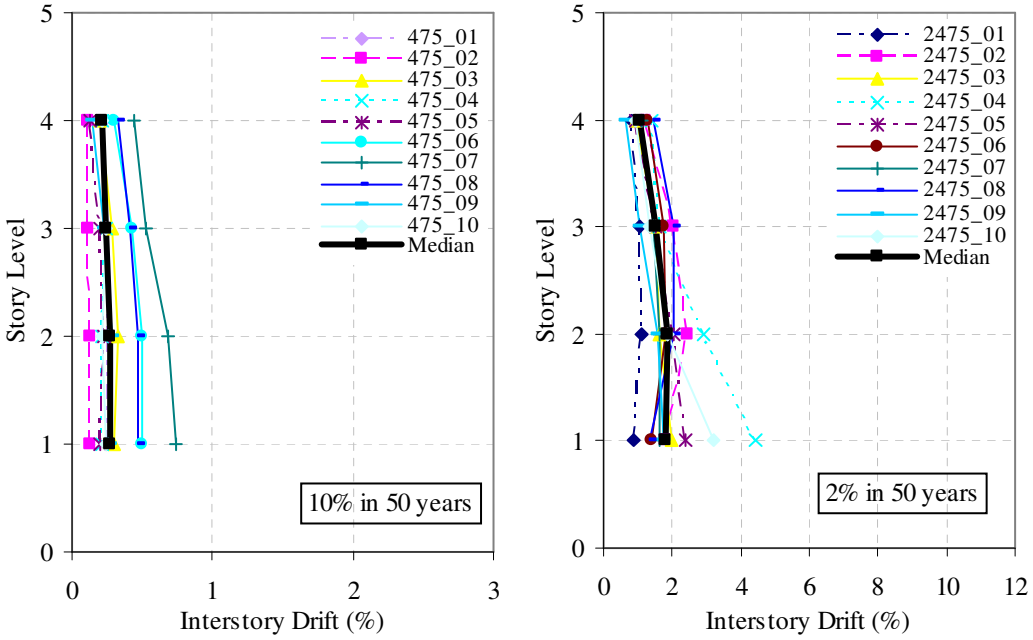

(b) CS2

Fig. B.3. E-W maximum interstory drifts (Wen and Wu motions)

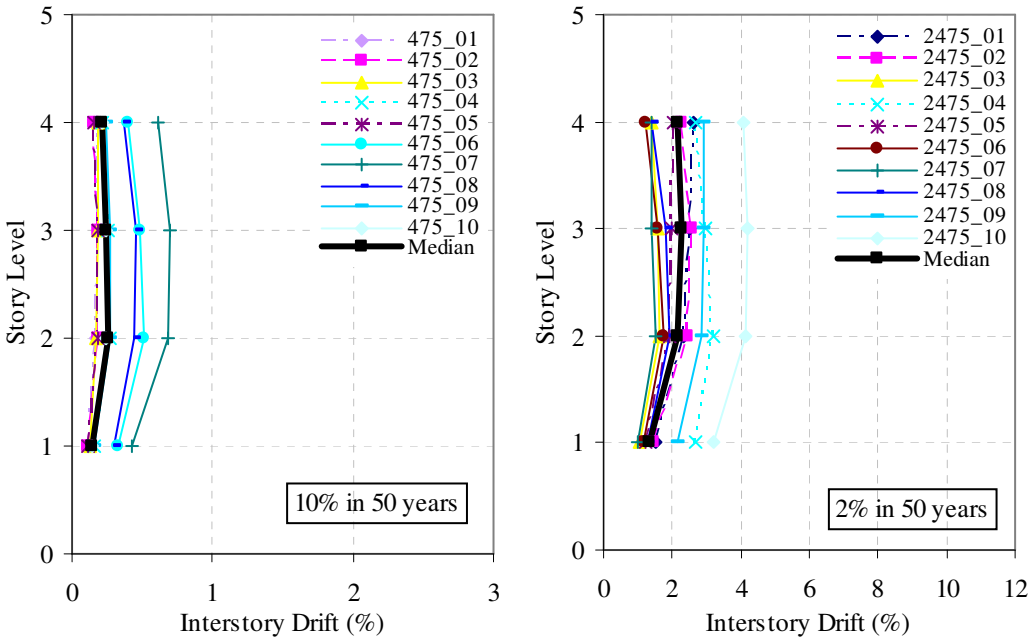

(c) CS3

Fig. B.3. Continued.

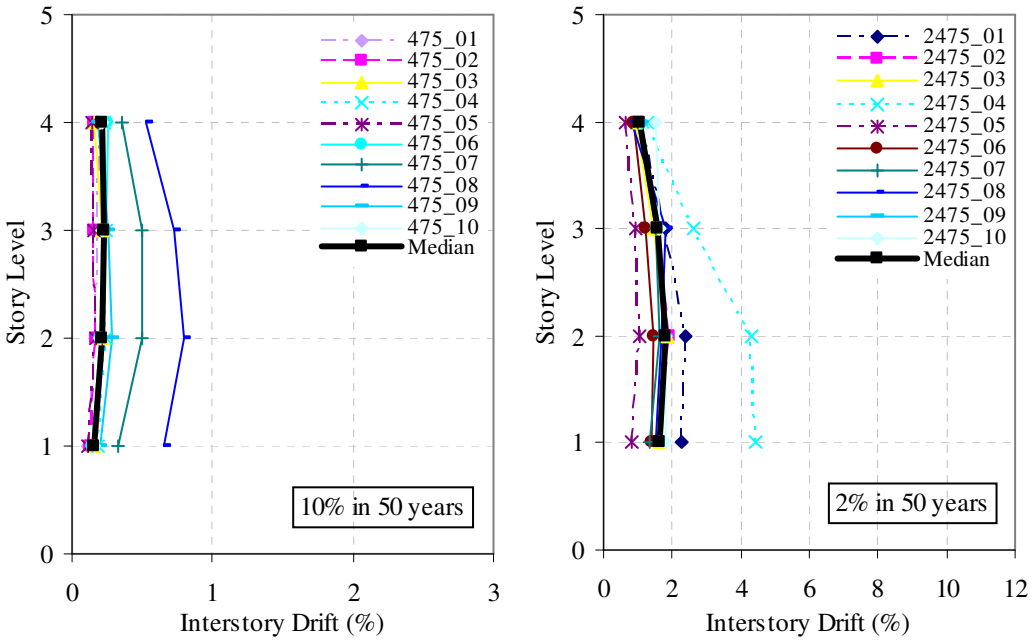

(a) CS1

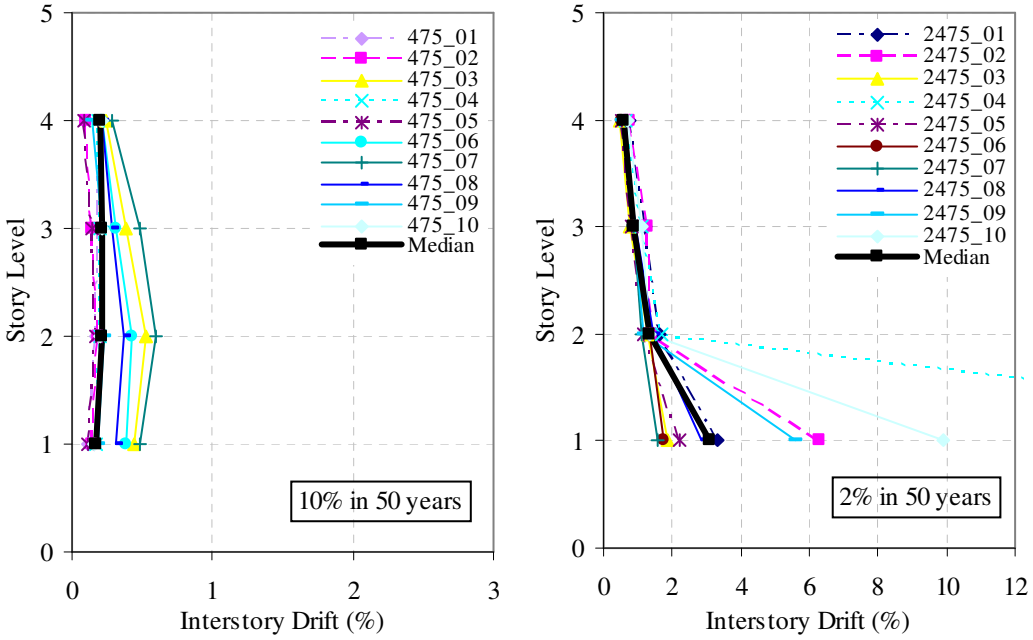

(b) CS2

Fig. B.4. N-S maximum interstory drifts (Wen and Wu motions)

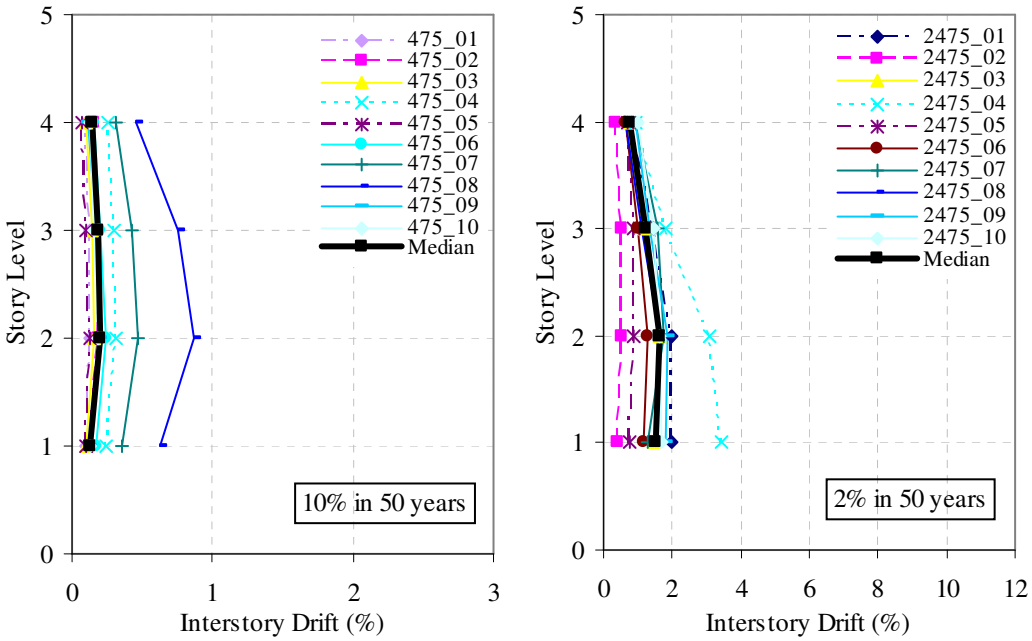

(c) CS3

Fig. B.4. Continued.

VITA

Name: Erin Kueht

Address: Texas A&M University
3136 TAMU
College Station, TX 77843-3136

Email
Address: ldgbest@hotmail.com

Student
Organizations: Structural Engineering Association of Texas, Texas A&M student chapter
American Society of Civil Engineers, Texas A&M student chapter

Education: B.S., Texas A&M University, Civil Engineering, 2004
M.S., Texas A&M University, Civil Engineering, 2007